Swansea University

Surface Texture and Visual Appearance of Packaging Steel

by

STEPHEN JONES

Submitted to Swansea University in fulfilment of the requirements for the Degree of Doctor of Engineering

Summary

Growth in markets for which visual appearance is a critical function and increasing scrutiny given by their customers to the visual appearance of their product create a strong motivation for manufacturers of packaging steel to develop their knowledge about the visual appearance of their product. Understanding and controlling the visual appearance of their product would enable manufacturers of packaging steel to meet the demands of their customers and maintain an advantage over their competitors.

The surface texture of packaging steel influences the functional behaviour of the final coated product. The work presented in this thesis investigates the relationship between the surface texture and the visual appearance of packaging steel. Multi-scale analyses of un-coated and tinplate packaging steel are performed to determine the functional bandwidths of surface texture. Models are developed which enable multi-scale simulations of surface texture. This enables a description of the relationship between packaging steel surface texture and visual appearance from the manufacturing process through to the surface function. This information is then utilised to design novel surface textures that give enhanced control over packaging steel visual appearance.

Declarations and Statements

I declare that the work presented in this thesis has not previously been accepted in substance for any degree and is not being concurrently submitted in candidature for any degree.

I declare that this thesis is the result of my own investigations, except where otherwise stated and that other sources are acknowledged by footnotes giving explicit references and that a bibliography is appended.

I give consent for this thesis, if accepted, to be made available online in the University's Open Access Repository and for inter-library loan, and for the title and summary to be made available to outside organisations only after a five-year embargo period, due to commercial sensitivity of the work contained within.

I declare that the University's ethical procedures have been followed.

Stephen Jones

21/09/20

Contents

Acknowledgements

Thank you to my thesis supervisors, Dr. Eifion Jewell and Ir. Raymond Bröcking (dank u wel!). Your help and guidance have been invaluable. Thank you to D. J. Wentink for providing the MatLab code for the EDT model. Thank you to Gemma Finn-Lewis at Trostre for all your help and support collecting samples and everything else! Thanks Mum and Dad for your love and support. Thank you Louisa, for your love, encouragement, and for looking after Judah so I could get the thesis done! And most of all, thank you Jesus, I couldn't have made it without you.

List of Figures

List of Tables

Acronyms

SBT Shotblast texturing

EDT Electro-discharge texturing

EBT Electron beam texturing

ECT Electro-chromium texturing

LT Laser texturing

FFT Fast-Fourier Transform

PSD Power Spectral Density

ACF Auto-Correlation Function

Ra Profile mean roughness amplitude

Sa Areal mean roughness amplitude

Sq RMS roughness amplitude

Ssk Skewness

Sku Kurtosis

Sdq RMS slope

MSa Multiscale Sa

MSdq Multiscale Sdq

MAF Multiscale attenuation function

BRDF Bi-directional reflectivity distribution function

RDF Reflectivity distribution function

Chapter 1

Introduction

1.1 Packaging steel

Packaging steel is thin, coated steel used for a wide variety of packaging applications. It is used for food and beverage containers, aerosol containers, paint cans and closures for bottles or jars. This diversity of application is enabled by the versatility of packaging steel, as it performs well across several functions. Packaging steel is strong, formable, can be welded and is recyclable. This means that it can be shaped to the desire of the filler, can protect the contents for a long period of time and information can be printed on the outside of the packaging. The infinite recyclability of steel, along with the ease with which it can be separated from other bulk waste due to its magnetic properties, means that packaging steel meets requirements for sustainability and environmental friendliness. This broad functionality of packaging steel can be extended even further with the addition of a surface coating. These coatings include, but are not limited to, chrome-based coatings, polymer-based coatings, and tin coatings. These provide the packaging steel with corrosion resistance and improve its visual appearance.

Packaging steel coated with tin is known as tinplate. This thesis focuses on one aspect of tinplate surface functionality, namely visual appearance. In general, the visual appearance of materials has a disproportionate effect on the assignment of value to a product making it a function of special commercial interest [1]. Good visual appearance is vital for packaging products as a high-quality external surface implies a high-quality product within the package. This is especially true for the tinplate industry. This can be seen by considering the infant milk formula market as a case study.

1.1.1 Project drivers

Infant milk formula is usually packaged in cans made from tinplate. Figure 1.1 shows the growth in sales of infant formula across global regions. In 2013-14, there was large growth, particularly in Asia, driven by the growth in the relatively affluent middle class in developing Asian economies. The best example of this is China.

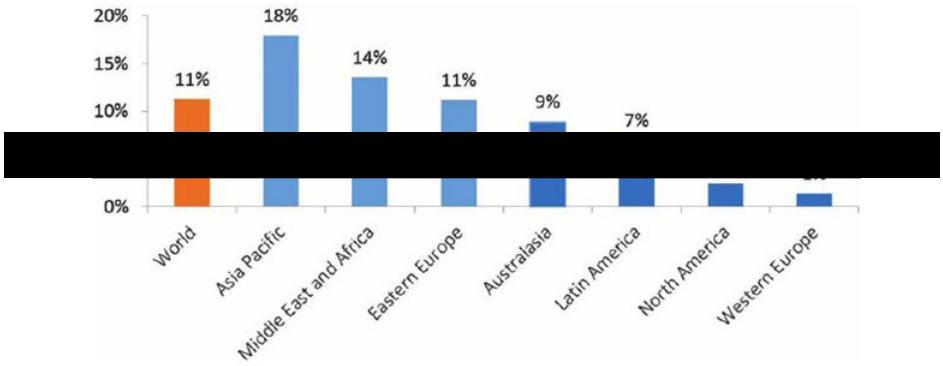

Figure 1.1: Global growth in sales of baby formula from 2013 - 2014 [3].

Figure 1.2 shows how valuable the infant formula market is in China alone, worth $26.7 billion in 2019, with further growth predicted. In 2008, tainted infant milk formula poisoned 300,000 babies in China, destroying consumer confidence in locally manufactured infant formula. This scandal means that foreign produced milk is seen as safer, higher quality and a mark of affluence. However, local companies are retaliating with lower prices and intelligent branding, meaning the high-value infant formula market is highly competitive [2]. Manufacturers of tinplate packaging steel, as well as their customers, are aware of these trends and desire to take advantage of them.

Figure 1.2: The projected growth in the Chinese infant formula market [2].

Advances in visual inspection technology are also contributing toward the increasing significance of visual appearance as a surface function of packaging steel. Customers of tinplate steel packaging products now have the metrological capabilities to establish visual appearance specifications, for example by citing specific gloss ranges that manufacturers of steel packaging are expected to adhere to. There is an increasing expectation of a higher level of consistency within a product range as well as a higher quality product. Customers also desire more involvement in the design and manufacture process so that the resultant product better meets their requirements.

To summarise, there are two trends currently active in the packaging steel industry:

1. Increasing value (and competitiveness) of markets for which visual appearance is a critical function.

2. Increasing scrutiny given by packaging manufacturers to the visual appearance of their products.

These trends create a strong motivation for manufacturers of packaging steel to develop their knowledge about the visual appearance of their products. Understanding and controlling the visual appearance of their products would enable manufacturers of packaging steel to meet the demands of their customers and maintain an advantage over their competitors.

1.2 Surface texture and visual appearance

In the previous section it was established that manufacturers of packaging steel have strong incentives to gain control over the visual appearance of their product. In this section, a pathway to intercept these trends is broadly described.

Throughout this thesis the terms "surface topography", "surface form" and "surface texture" are used as defined by Leach [5]. The surface topography of an object is defined as the full bandwidth of spatial wavelengths of that object. The surface form is the underlying shape of an object. The surface texture is the surface features that remain when the form has been removed from the overall topography.

It is well established that surface texture influences surface function [4–7]. This is also the case for visual appearance, although visual appearance as a surface function has been relatively neglected in research compared to fields such as tribology, coatings characterisation and fundamental metrology [8–13]. To understand and control the visual appearance of packaging steel, first the surface texture of packaging steel must be understood.

Surface metrology is the measurement and analysis of surfaces. Whitehouse describes surface metrology as having a dual purpose, as seen in Figure 1.3 [6]. A measurement of a surface can provide information about two regimes, one being the process that created the surface and the other being the function created by the surface. In other words, the two roles of industrial surface metrology are:

1. To help control the process.

2. To help optimise the function.

Therefore, to understand and control the visual appearance of packaging steel, relationships between three levels of metrology must be developed. On the first level is

Figure 1.3: The dual role of surface metrology [6].

the manufacturing process of packaging steel which in this case is all the processes that have an influence on the final texture of the steel strip. On the second level is the measurement, characterisation and analysis of the surface texture. On the third level is the measurement and characterisation of visual appearance. The challenge lies in establishing the relationship between these three levels. This can be seen in diagram form in Figure 1.4. This diagram provides a sketch of the work necessary to understand how the visual appearance of packaging steel created by the process, via the surface. The arrows between each of the domains represent gaps in knowledge that need to be filled.

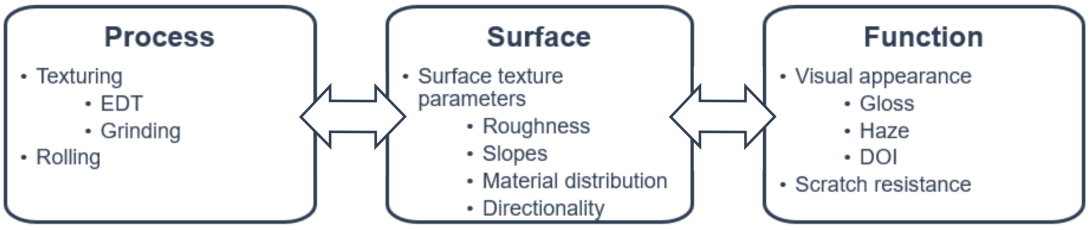

Figure 1.4: The three domains, and the relationships between them.

This lack of understanding of the relationships between the three domains exist because of a lack of appropriate methodology. To date in the packaging steel industry, visual appearance has been measured by subjective or relatively rudimentary techniques, and simple surface texture measurements do not sufficiently describe the final visual appearance, which is the ultimate aim of the customer.

In the packaging steel manufacturing process, surface finish is specified using a single parameter Ra, which is the mean amplitude of surface roughness. This parameter is used to determine if the surface texture of the final rolled strip is within certain tolerances. These tolerances are either set in the BS EN 10202 “Cold reduced tinmill products” standard, or agreed between the manufacturer and customer of a specific packaging steel product under the BS EN ISO 9001:8.3 framework for control of non-conforming product [14].

The Ra is measured using a stylus profilometer, with a cut-off of $0.8\mathrm{mm}$, across

the rolling direction of the strip, with the mean of 3 measurements being taken. (More information about surface metrology is given later in Chapter 2.) If the resultant value of Ra is within specification, the whole coil of material is deemed as acceptable and shipped to the customer.

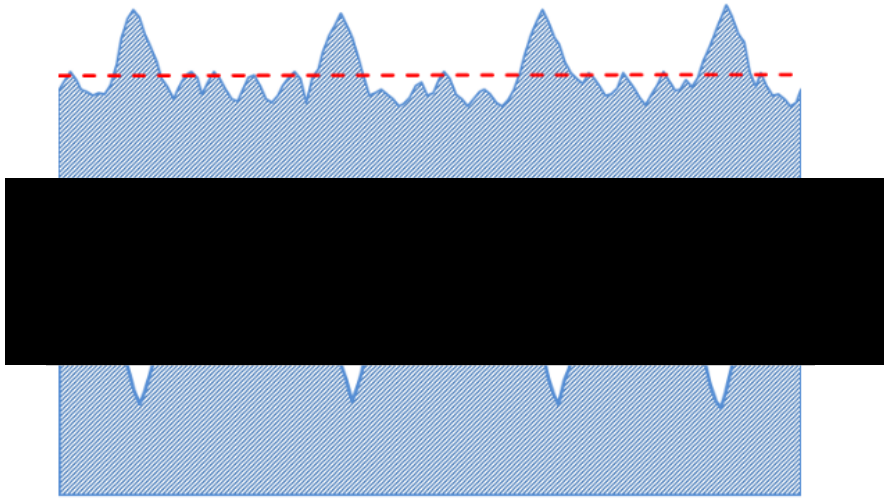

Figure 1.5: The above surfaces have the same mean amplitude of surface roughness Ra, even though they are very different, with one being the inversion of the other [15].

However, Figure 1.5 shows two surfaces with the same mean amplitude of surface roughness Ra. Although the two surfaces are very different, with one being the inverse of the other, the Ra parameter is the same for each of them. In other words, characterising these two surfaces with the Ra parameter would not distinguish between them. Considering the above described dual purpose of surface metrology, this means that a measurement of Ra on such surfaces would provide no information about either the manufacturing process or the function of the surface, even though one would expect that different processes were responsible for the creation of the different surface features, and that the function of the surfaces would differ. The numerical value of Ra does not provide any information regarding the surface shape, the spacing of surface features, nor of any irregularities present [16]. Considering Figure 1.4 in the light of this discussion, it can be seen that the current methods of surface metrology used in the steel packaging industry do not capture the relationship between the surface, the process, and the function.

In order to develop understanding of and gain control over the visual appearance, a first step must be to determine a characterisation of surface texture that provides more information about surface function than current methods. The next step would be to determine which process parameters influence these product parameters, and how they

are to be controlled.

1.3 Summary

To summarise, trends in the packaging industry give incentive to packaging steel manufacturers to control the visual appearance of their product. This is to be done via the intermediary step of controlling the surface texture of their product. The surface of a workpiece is the meeting point of the manufacturing process domain and the function domain. Surface metrology is oriented in two directions, toward the process domain to control the process and toward the function domain to control the function. The work described in this thesis aims to elucidate the relationship over three levels: from surface creation process to surface characteristics and from surface characteristics to surface function. This chapter has described the context to the work and the drivers resulting in a set of objectives to be achieved by this work, which are listed below.

1.3.1 Aims and objectives

- Determine the relationship between the manufacturing process and surface texture of packaging steel.
- Determine the relationship between the surface texture and visual appearance of packaging steel.
- Utilise discovered relationships to develop methods of controlling visual appearance of packaging steel.

Chapter 2

Literature Review

2.1 Overview

This literature review covers a broad range of topics. First the manufacturing process of tinplate is described, with extra attention being given to those stages of the process which are most pertinent for visual appearance. In this first section the creation of surface texture is covered. The second section then covers the measurement of surface texture. The collection, processing and analysis of the surface texture data is described. In the next section, the function of the surface is looked at, focussing on the visual appearance created by surface texture. In the final section, the multi-scale analysis of surface texture is presented. Techniques are described which enable the discovery of the "functional band-widths" of the surface texture. These are the spatial wavelengths of the surface which have greatest influence on surface function. The literature review ends with a summary and suggestions for how the insights uncovered by the literature review form the basis for the work carried out in this thesis.

2.2 Manufacturing process

2.2.1 Overview

This section of the thesis describes the manufacturing process of tinplate from the point the material enters the plant to the finished product. The focus is on the processes which are most pertinent for the visual appearance of tinplate.

Steel strip arrives from the steel making plant in large coils which must first be cleaned of the surface oxides which form during the steel making process. This is done in a process known as pickling in which the strip is immersed in acid and flexed to break up and remove the unwanted products. The strip is then cold rolled to reduce its thickness and make it more consistent along the length of the coil. After cold rolling, ductility is restored by annealing, in which the strip is heated to induce recrystallization. The strip then passes through one of two possible routes to adjust the final gauge of the product, the surface texture and some mechanical properties. The strip is either passed through a single reduction mill or the double reduction mill. Finally, the steel strip is electrolytically coated with tin and reflowed, before a passivation layer of chromium is added. The tinplate is then recoiled prior to delivery or cut into sheets according to the customer's specifications.

The processes most responsible for the visual appearance of the final product are rolling and coating. A brief overview of the early stages of the process will be given, followed by a detailed description of the rolling and coating processes.

Figure 2.1 shows an overview of the manufacturing process of tinplated packaging steel.

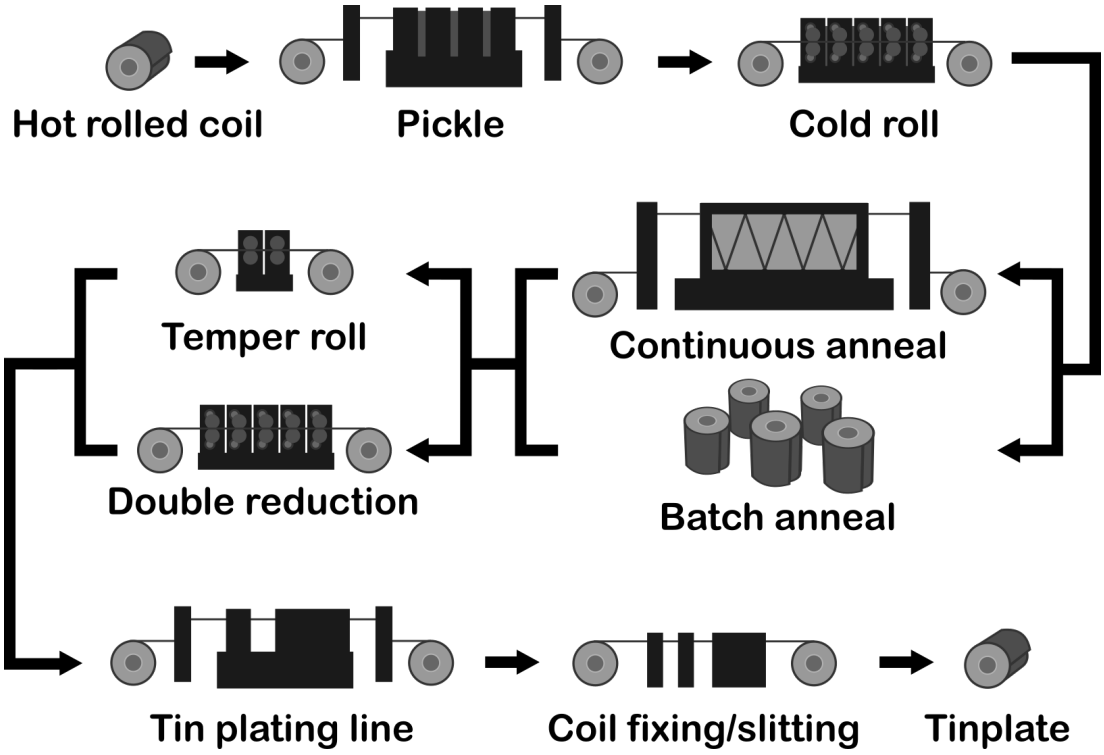

Figure 2.1: The manufacturing process of tinplated packaging steel.

2.2.2 Pickle

A discolouring oxide layer or scale is formed on the surface of steel during cooling after hot working processes. This must be removed before further processes such as cold rolling. Scale on the surface prohibits optimum adherence of coatings onto the surface of the steel substrate, causes poor performance in drawing operations and can result in several surface defects.

During pickling metal surfaces are chemically treated to remove undesirable impurities such as stains, contaminants, rust or scale. Removal of the scale is achieved by immersion of the strip into acid solution. The rate of pickling is affected by several variables, chief of which are acid concentration and bath temperature. The rate of pickling increases in direct proportion with the concentration of acid. The effect of temperature is even greater [17].

A poor pickle will lead to a poor surface finish due to defects such as rolled in

scale, sliver and other process related pickling quality issues, such as under-pickling, over-pickling, blistering and rusting.

2.2.3 Anneal

After the pickle, the strip is cold rolled. As a result of cold rolling the strength and hardness of the strip are increased but ductility is reduced. Annealing is a process whereby ductility is restored to the metal, with an associated loss of strength. In the annealing process, the temperature of the metal is increased to above its recrystallization temperature in a controlled manner.

Two processes for annealing are possible, continuous annealing and batch annealing. In batch annealing, the cold rolled steel is heated in coils. The coils are placed in a furnace and the temperature is raised to the soaking temperature. The coils remain in the furnace at this temperature for between 10 to 30 hours depending on the grade of steel required [18]. The continuous annealing process is split into three parts, the entry section, furnace section and exit section, with accumulators on entry and exit. On entry, the strip is cleaned. The heat treatment occurs in the furnace section and consists of rapid heating, followed by a short soaking time and rapid cooling, with the entire process taking between four to eight minutes. Continuous annealing offers several advantages over batch annealing, including more uniform properties, cleaner surfaces and shorter production times [19]. Batch anneal is preferred for low tempers and its very low ageing properties.

It is unclear what effect, if any, the annealing process has on the surface finish. Simao et al. investigated the surface texture transfer of work rolls onto strip [20]. They performed the same analyses on annealed and un-annealed steel coupons and could not detect any difference between the two. This indicates that annealing has no influence on surface texture and therefore has no influence on texture dependent visual appearance.

2.2.4 Rolling

Flat rolling is a well-established process having been in use for several centuries. The fundamental process has not changed since Leonardo da Vinci used it to roll lead in the 12th century AD [21]. Metal, in the form of sheets or coiled strip, is passed through one or more pairs of rollers to obtain a reduction in and uniformity of thickness. The

process is used in the manufacture of tinplate for exactly those reasons. A reduction in thickness means products can be made out of less material. Packaging steel is rolled twice to achieve the desired strip properties, such as gauge, strength and surface texture.

2.2.4.1 Initial cold roll

The strip is initially rolled between the pickling and annealing stages of manufacture. During this cold roll or cold reduction process the steel strip is passed through a set of rollers to produce a reduction of and consistency of thickness. Cold working of metal is defined as deformation of metal at temperature low compared to its melting point. Tensile strength, yield strength, and hardness are all increased, whereas plasticity, ability to deform, electrical conductivity and density all decrease.

Cold rolling takes place in multi-stand mills, normally with five-stand, four-high configurations although four- or six-stand are also used. The hot rolled, pickled, and oiled strip enters the stand at about 2.0 - 2.3 mm and is reduced to 0.16 - 0.28 mm which amounts to an 85 - 92% reduction in strip thickness [19]. Large amounts of heat are generated during the cold working process, which is extracted from the strip by a lubricating/cooling system. The lubricant is normally about 5% oil in water.

The amount of oil drawn into the roll bite and the initial surface roughness are the critical factors determining friction in the contact and surface finish of the product [22]. During rolling, surface smoothness increases, and appearance of the metal is improved. Surface finish is improved as asperities are flattened and pits consolidated.

2.2.4.2 Final cold roll

After annealing the strip is ready for a final roll before coating. The purpose of this final roll is to produce the desired surface finish, mechanical properties and final gauge. There are two routes available at this stage, either single reduction or double reduction. Double reduction is used when a higher strength tinplate is desired. This is achieved via a second cold reduction in place of the temper roll stage. The normal range of thickness reduction is about 30 - 40% but reductions of 10 - 50% are also possible. The strip is not annealed after the second cold roll meaning the material is substantially work hardened therefore stronger but less ductile. This process also leads to a significant directionality in the properties of the strip. As the material is made stronger,

products can be made from thinner material, leading to an increase in efficiency for the manufacturer. For example, the strip remain ductile enough for the production of can ends and bodies [18]. Final thickness can be as low as 0.12 mm, the typical range being 0.14 - 0.24 mm.

Single reduction, also known as temper rolling, differs from double reduction mainly in the level of reduction. The overall reduction during temper rolling is about 0.5 - 4%. Other differences are the use of lubricant and the number of stands in the mill. Temper rolling is a dry process and tends to be in a 2-stand mill. Visual appearance is more critical for the products produced by the single reduction route as these products are often sold into markets for which visual appearance is a critical function, such as the infant formula market described in Chapter 1. Therefore the work of this thesis will focus on that route.

2.2.5 Roll texturing

The texture of the work roll plays an important role in the rolling process for several reasons. Firstly, the friction and wear characteristics of the roll are in part determined by its surface texture. Secondly, the surface texture of the roll determines the surface texture of the strip. The inverse of the roll texture is imprinted into the strip. Concave features on the roll become convex features on the strip. For these reasons it is important to have control over the roll texture.

There are several roll texturing processes available to create the surface texture of a work roll. The most common and well-established of these is grinding. Shot-blast texturing (SBT) and electro-discharge texturing (EDT) are also well-established processes. Other processes which have a more recent history are laser-based texturing processes as well as electron beam texturing (EBT) and electrodeposited chromium texturing (TOPOCROM/ECT). This review will focus on grinding, shot-blasting and EDT as these are the most commonly used roll texturing process in the tinplate industry. Less conventional processes, such as laser texturing, will also be reviewed to assess their suitability for the creation of surface textures offering enhanced surface function.

The different surface texturing processes reviewed here each give a different texture on the work roll surface. The concept of the unit event can be used to describe surface texturing processes [6, 23]. Every surface texturing process can be characterised by

1. The unit event.

2. The distribution of multiple instances of that unit event on the surface.

The unit event is the effect that an individual element of the texturing process has on the surface by the addition, removal or relocation of surface material by mechanical, chemical and thermal mechanisms [23]. The unit event can be considered the "atom" of a texturing process, the indivisible element which together create the characteristics of the texturing process as a whole. The unit event determines the texture of the surface post-process therefore will determine the functional performance of the surface.

"The unit machining event, or simply the unit event, refers to the effect produced on the surface by the average element in the manufacturing process that is producing the surface, either by taking away material or by adding material to it in order to achieve a given texture, shape or dimension. The concept of a unit event is a fundamental link between manufacture and performance ."[10]

The unit event will not only alter the surface texture but will also alter the subsurface layer. This will have a dramatic effect on surface integrity and therefore surface functions such as wear. As visual appearance of metals does not depend on the sub surface layer these effects will not be considered in this thesis.

Another source of the difference between textures is the distribution of unit events. There are two general features of the distribution to be considered. The first is the relationship of unit events to one another on the surface. If there is no relationship between them, there is no order, and the resultant texture is stochastic. If there is some relationship between the points, for example if the unit events are distributed across a grid, the texture is deterministic. The other general feature of the distribution of unit events is directionality. If the relationship between unit events is not uniform across the lateral dimensions of the surface, then the texture will exhibit directionality. This is significant as a function which is texture-dependant will perform differently according to the directionality of the surface. For example, for ground textured rolled strip, there is a difference in texture and therefore function along and across the rolling direction.

2.2.5.1 Grinding

During a grinding process material is removed from a workpiece surface by the abrasive action of grains embedded on a wheel rotating at high speeds. Workpiece material

is removed by the abrasive grains as the wheel surface is forced into the workpiece surface.

Grinding has a long history and large scope of application as it is one of the simplest and least expensive processes for machining hard materials [24]. It is also highly versatile due to the wide range of possible wheel abrasive types, shapes, sizes and speeds. There are also four possible machine geometries. The two main classes of grinding are flat surface grinding and cylindrical grinding. Each of these classes can be used to grind with either the periphery (rim) of the wheel or with the wheel face, giving four possible geometries [24]. For work roll texturing, the peripheral cylindrical geometry is used, as the work roll and the grinding wheel are rotated against one another and the grinding wheel periphery is pressed into the surface of the work roll.

A grinding wheel is an abrasive disc made up of grains held together by a bond. The working surface of the wheel is thousands of randomly-shaped and randomly-distributed cutting edges [25]. Four components of a grinding wheel to consider are the abrasive, the bond, the wheel design and any additives [26]. The abrasive is the most important of the components as its characteristics will largely determine the output of the grinding process. The abrasive grains, and their distribution, have significant influence on the wheel-workpiece interaction. This means the wheel wear rate, the surface finish, heat transfer and power consumption are all dependent on the abrasive [25].

Conventional abrasive materials are Al203, SiC or ZrO2. The bond holds the abrasive grains together and is often resin or polymer based. The wheel design determines the thickness and radius of the disc, hub material etc. Finally, the additives can be fillers, grinding aids or lubricants which are included in the bond with the abrasive grains. These can be used to control the structure of the wheel surface by inducing porosity which influences various interactions at the wheel-workpiece interface such as fluid transport and chip formation [26].

There are three mechanisms by which a wheel grain interacts with the workpiece surface. These are rubbing, ploughing and cutting. In rubbing, the grain lightly brushes the material surface without material removal. In ploughing, the grain penetrates the material and deforms it, pushing up ridges but again without necessarily removing the material. In cutting, the wheel grain penetrates the surface and carves out a chip of material. All three processes may be performed by a single grain at different stages of its contact with the workpiece. As the grains wear, they become blunt and their

performance will move from majority cutting contact to majority rubbing contact [24].

The unit event in grinding is a cut, caused by a grit moving in a circular arc [23]. Griffiths describes the mechanism as thermo-mechanical. The mechanism depends on the type of grinding that the surface undergoes. If the grinding is gentle, the dominant mechanism will be mechanical as the grains rub, plough and cut the surface. However, if the forces are very high and the grinding becomes abusive, the dominant mechanism will be thermal as each unit event delivers a high intensity pulse of thermal energy to the surface. The mechanism of conventional grinding will be found somewhere between these two extremes. Grinding is a stochastic process with a marked directionality in the rolling direction. The source of the directionality is the unit event rather than the event distribution. The event distribution is stochastic due to the random shape, size and distribution of grains on the grinding wheel surface.

2.2.5.2 Shot blast texturing (SBT)

Shot blast texturing is a process whereby a workpiece surface is modified by the impingement of hard grains upon the surface. The unit event is a crater, created by the elastic deformation of the surface material. The important parameters are the size, quantity and hardness of the grains and the velocity of impingement. As the texture is created via plastic deformation, this process depends on the relative hardness of the grains and the roll surface. This means that harder, wear resistant material cannot be used leading to a limited lifetime for rolls textured with this process [20]. Sun et al. [**?**] investigated the differences between SBT, EDT and TOPOCROM processes. They cite the advantages of SBT as simplicity and low cost. However, these advantages are negated by the poor uniformity of surface texture, low reproducibility and low wear resistance. They state that the shot blast process is being replaced by EDT. This may be the reason that the literature for the EDT process is much more developed than that of SBT. The author could find no analysis of SBT using the unit event concept in the literature.

2.2.5.3 Electro-discharge texturing (EDT)

During the EDT process material is removed from a workpiece surface by the action of electrical energy. A controlled electrical discharge occurs between electrodes and the work roll surface, vaporising a small volume of surface material. Dielectric fluid

controls the discharge arc and aids with removal of debris from the spark gap. The electrodes are scanned across the surface until the entire workpiece is textured. The size of the individual crater produced is controlled by the type of dielectric used, voltage pulse duration and the peak current of each pulse [27, 28]

Kim et al performed a comparison between EDT and SBT textures. The found that EDT textures show a more uniform peak height distribution and higher peak counts than textures made with SBT. This is related to another finding, that lateral coverage of the texture is more uniform for EDT than SBT. They also establish that it is possible to control Ra and Pc with the EDT process. They characterise the EDT surface texture as having greater homogeneity than the SBT surface texture [29].

Terpak et al. investigated the texturing of work rolls by EDT to determine which process parameters influence work roll texture [28]. They determined that the pulse energy had the largest effect on surface texture, controlled by the pulse current and the pulse time. A higher Ra was obtained with higher pulse energy. However, higher pulse current also gave to lower Pc. This is due to the size of the crater produced by the process. A higher current gives larger craters therefore more space between peaks and a lower peak count. Therefore, for EDT, Ra and Pc are coupled parameters, with an inverse relationship existing between them.

Petropoulos et al. investigated other surface texture parameters to determine if parameters other than Ra and Pc could characterise the EDT surface texture more fully. The discovered that Rsk and Rku had no correlation with pulse energy. They also found that parameters derived from the bearing area curve such as Rtp% were correlated with the pulse energy [30].

The unit event in EDT is a crater. The mechanism is purely thermal as there is no mechanical contact between the tool electrode and the work piece [23]. The electrical discharge melts the surface in the locality of the discharge. Some molten material is removed entirely forming a crater at the spark location. The rest of the material resolidifies forming a ring around the crater rim. EDT is a stochastic, anisotropic process as there is no way to accurately define the exact location of each event. However, there is greater control over the resultant surface topography with EDT than with SBT [31]. Wentink et al. developed an analytical expression to define the EDT unit event [32]. This was used to simulate EDT surface texture.

2.2.5.4 Other texturing processes

Other processes available to texture work rolls are laser texturing (LT), electron beam texturing (EBT) and electrodeposited chromium texturing (TOPOCROM/ECD).

TOPOCROM/ECD stands out as unique among texturing processes. Instead of material being removed from the work roll surface, material is added to the surface by electroplating a chromium layer onto the work roll surface. It is also distinguishable from other processes by the textures it creates on the strip. The additive nature of the process results in convex hemi-spherical structures on the roll texture which in turn results in concave structures on the strip. This contrasts with conventional texturing processes which remove material from the roll, resulting in convex structures on the strip [31]. TOPOCROM/ECD is a stochastic, anisotropic process. The ECD unit event is unique as it is the only process which adds material to the surface. The mechanism is chemical. The geometry of the unit event can be described as a spherical dome. The location of each dome of chromium is determined by the initiation site of the chemical reaction. It is possible to create open or closed surface structures. Open structures are characterised by a sparse distribution of large hemispheres whereas closed structures are characterised by smaller, densely packed hemispheres.

Electron beam texturing (EBT) melts the surface of the work piece using an electron beam gun. This results in the formation of craters on the work piece surface. EBT has been used to etch images and custom patterns onto work rolls so that the image or pattern ends up on the strip [33]. The unit event of EBT is a crater with dimensions determined by the intensity of the electron beam [33]. The mechanism is purely thermal as there is no mechanical contact between the tool and the workpiece. The distribution of events in EBT is unrestricted [33].

Laser texturing uses high powered lasers to ablate the surface of the work piece. There are two main methods used. Laser texturing using CO2 lasers was developed first, followed by Nd:YAG systems. These two different types of lasers have different properties, leading to different texturing mechanisms and different surface textures. With the CO2 laser process, a chopper disc is used to split the beam into pulses which gives discrete texturing events. With NdYAG lasers, high speed pulses are possible without the use of a chopper disc. In both processes, a crater is formed at the location of contact between the laser and the work piece as the material is ablated by the high energy laser. The work roll is rotated, and the laser head scanned laterally in order to

texture the whole surface of the roll [34]. For laser texturing processes, event and distributions depend on the system used. Again, the mechanism is purely thermal as there is no mechanical contact between the tool and the workpiece. The CO2 system has less control over both distribution and unit event than Nd:YAG systems. The distribution of events is dependent on the beam chopper, restricting the process to deterministic distributions. The beam chopper determines the pulse duration and frequency which in turn determine the dimensions of the unit event. High frequency lasers have a greater amount of control over both duration and frequency leading to greater control over the geometry of the unit event. Pomini digital texturing (PDT) is a process that uses high speed laser texturing enabling tight control over the distribution and shape of the texturing unit event.

2.2.5.5 Texture transfer

The next point of interest is the transfer of the texture of the roll onto the surface of the strip. There are two mechanisms by which roll texture is transferred to the strip, namely penetration and reverse extrusion [35]. These mechanisms occur for two reasons. Firstly, the hardness of the roll is much higher than that of the strip. Secondly, to achieve the reduction of the strip, a force is applied by the roll onto the strip. Penetration causes plastic deformation of the strip as the harder asperities of the roll are pushed into the softer material of the strip. In reverse extrusion, the strip material is pulled by the action of closed voids on the roll surface. Buñten et al. developed a finite element model which showed the penetration mechanism dominating at low reductions (low force) and the reverse extrusion mechanism dominating at high reductions (high force). They performed their analysis for structures created by the EBT process. The EBT process leads to surfaces characterised by closed voids, therefore the reverse extrusion mechanism is dominant. Wentink et al. suggest that for stochastic topographies, such as those created by EDT, significantly less closed voids will be created. Therefore, for stochastic topographies, the penetration mechanism will dominate the plastic deformation of the strip [32].

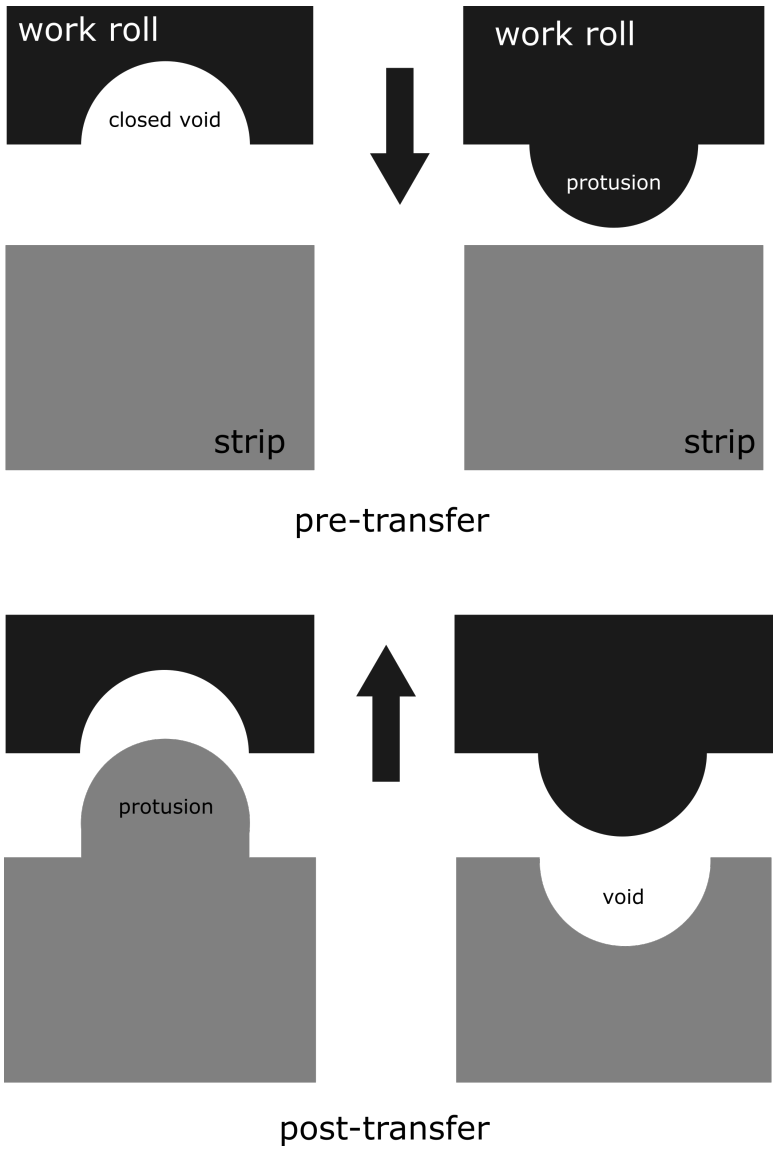

Figure 2.2: Two texture transfer mechanisms. On the left is the reverse extrusion process. On the right is the penetration mechanism.

Rolling experiments and FEM analyses show that the level of texture transfer depends largely on the level of reduction. Higher reductions cause a higher proportion of the roll texture to be imparted onto the strip surface [20, 36, 37]. Strip topography can be altered by increasing rolling speed, increasing the reduction ratio, or altering the topography of the roll [38]. Other experiments show that the transfer of roll texture is a multi-scale phenomenon, with transfer occurring at scales of between 50 nm to 100 $\mu\mathrm{m}$ [39]. Kijima and his colleagues have performed a series of FEM analyses to show that texture transfer can be modelled as vertical indentation (i.e. penetration) of the texture of the roll surface [36, 40–42].

Wentink et al. have implemented a vertical indentation texture transfer model [32]. First, they simulated EDT work roll surfaces by defining the EDT unit event and dis-

tributing multiple instances of the event randomly across a plane. In the texture transfer model, the roll texture is pressed into the strip until the contact area between the roll and the strip is equal to a predefined bearing area. This contact bearing area correlates with rolling force. A higher rolling force will result in a higher contact bearing area and a higher proportion of the roll surface penetrating the strip.

2.2.5.6 Summary

A further consideration is the durability of the surfaces created by the texturing processes described above. According to Hilgenberg, the lifetime of deterministic structures is poor in comparison to stochastic structures. This is due to the physical processes used to create deterministic structures. For processes such as EBT, EDT and LT, the unit event is created via localised melting of the work piece followed by relocation and solidification of the molten material. This leads to a softening of the surface structures for two reasons. First, rapid solidification of molten surface material does not allow for precipitation of new hard phases. Second, there may be insufficient bonding between the newly solidified material and the non-molten substrate [43].

Overall, the historical development of texturing processes has been in the direction of greater control over the dimensions and distributions of the unit event, leading to greater control over the texture of the work roll and strip. This means topographies can be designed that optimise surface functionality. Therefore, considering function to the exclusion of other considerations, EBT and LT texturing systems are desirable. More control over the unit event dimension and distributions opens up a larger function space, enabling the development of differentiated products.

2.2.6 Coating

After rolling, the strip is coated with tin. Tin coating is used to provide several functionalities to the product. Tin provides a barrier coating to protect the substrate from corrosion. It also gives a desirable high gloss finish to the product. The coating is generally very thin ($\sim$1 μm) therefore highly formable and easy to weld or solder.

Electrolytic coating is favoured as a coating method over hot dip methods. This is due to a higher control over coating weight and the possibility of having different coating weights on either side of the strip. The most widely used process is the Ferrostan process which uses a Phenylsulphonic acid electrolyte. Two other processes are

available, differing only in bath type; Halogen, which is fast but toxic, and alkaline which has a bright finish but a high current requirement. The deposited tin for acidic baths is "non-bright" i.e. it has a porous structure and a matt surface appearance. To remedy this, the tinplate is treated by flow melting, also known as reflow.

During reflow, the coated strip is heated to just above the melting point of tin (> 232 °C). The temperature is raised and controlled by resistance and/or induction heating. Reflowing the tin layer causes two processes to occur in the tin-substrate system. The first is a large increase in surface reflectivity. This partly due to the material properties of tin, as the reflectivity of tin is much higher than that of steel. It is also partly due to the modification of the surface texture. The tin coating fills in the valleys of the texture. At high coating weights the coating completely planarises the surface. At low coating weights the substrate texture can still dominate the appearance of the strip [44]. The second process caused by reflow is the formation of an alloy layer between the steel substrate and the free tin layer. The thickness and structure of this intermetallic layer depends largely on the temperature reached and the duration of the heating [17].

Aarnts et al. offer insight into the mechanism of the tin layer formation on the black-plate substrate [44]. Due to its high surface tension and good wetting properties the tin fills the valleys of the blackplate texture, covering the peaks with a thin layer. They show that after reflow, tin fills the valleys of the substrate roughness and is then present above the peaks of the surface texture. The tin above the peaks of the substrate texture is wipeable and scratch sensitive, whereas the tin filling the valleys is non wipeable and not scratch sensitive. A hard alloy layer close to the outer surface gives support to the metallic tin layer, making it less susceptible to wiping. The amount of tin removed during wiping depends strongly on the surface texture. For smooth surfaces a large amount of tin is removed and for rough surfaces only a very small amount is removed. This means that for a reduction in susceptibility to wiping and scratching, the alloy surface must be as close to the tin surface as possible. Aarnts et al. developed a model to predict the amount of tin required to fill the valleys to the optimum level without the excess free tin that leads to damage sensitivity. This was done by calculating the volume of the black-plate surface available to be filled by tin and was used to predict the amount of alloy layer at the surface. A similar approach could be used to determine the level to which the tin fills the valleys for certain finishes and tin weights.

Landskroon investigated the effect of tinplate substrate surface texture on the vi-

sual appearance of the coated product. He measured surface texture parameters of the underlying substrate prior to coating and visual appearance parameters of the tinned surface after coating. He found a clear relationship between the uncoated substrate texture and the coated tinplate visual appearance for an anisotropic surface texture at a low tin weight [45]. Not only is there a difference in the magnitude of gloss before and after tin coating, but also the difference in gloss post-coating is greater than the difference in gloss pre-coating. This means that the coated surface brings out the difference in underlying surface texture. Subtle differences in visual appearance prior to tin coating become large differences after coating.

Luo developed a high-order non-linear mathematical model to describe paint layer formation on rough surfaces for automotive steels [46]. He discovered that long-scale surface waviness has a greater influence on paint layer formation than short-scale surface roughness. This effect is increased for thicker paint layers. When the layer thickness is comparable to the substrate roughness, the surface texture has a considerable influence on the final distribution of coating. During reflow, the tin coating is in its liquid state for a brief time, meaning these results are also valid for tinplate. For the tinplate system, the layer thickness is comparable to the surface roughness amplitude. This means that for tinplate, the substrate texture will have a large influence on the final distribution of reflown tin. The results from the model and the empirical results of Landskroon support one another. For tinplate, the relative thickness of the tin to the roughness amplitude is variable, depending on the chosen surface finish and tin weight. The relative influences of different scales of surface texture on the formation of the tin layer needs to be fully determined.

To summarise, the substrate surface texture has considerable influence on the visual appearance of the final coated product for low tin coating weights. Products for which visual appearance is a critical function (such as baby food) have low coating weights. This means that control over visual appearance of the product will be gained by control over the substrate surface texture. However, any changes made to the substrate texture to positively affect visual appearance must not also have a detrimental effect on the damage resistance of the coating.

2.3 Surface metrology

2.3.1 Overview

Surface metrology is the measurement, characterisation and analysis of surfaces. Surface metrology is used to gain information about surface creation (process) and surface behaviour (function) [6]. For industrial applications of surface metrology, Whitehouse describes the surface as the meeting point of the manufacture and function domains. This leads to applications in fundamental research enabling the development of relationships between surface characteristics and surface function in product design, process design, process control and quality assurance. In this section of the thesis the methods of surface metrology are described in detail and the application of those methods to the work of this thesis is also described. The section begins with an outline which first puts forward some theoretical considerations of surface metrology, followed by an analysis of how those theoretical considerations are applied in practice in industrial settings.

It is generally assumed that the surface of a material is a fundamental property by which it interacts with its environment which can be measured to provide insight into the geometry and functionality of the material surface. However, Leach et al. explain how this is not the case and it is important to think differently about the nature of a "surface" [47]. The set of data obtained through any measurement of a surface is dependent entirely on the physical nature of the measuring system and its spatial frequency bandwidth (i.e. scale). Information obtained from a surface is never a measure of some inherent property of the material but is always a measure of the interaction between the material and the measuring system. From this observation Leach et al. provide a better definition of a surface. The measured surface of material is the position at which the interaction forces between the measuring system and the material become a specific magnitude. This means that there is not one, fundamental property of a material known as its surface available to investigation, but there are an array of possible surfaces each available to the investigator, from which the investigator can make a selection with appropriate choice of measuring system and scale of investigation. Different choices of system and scale will yield different measured surfaces. This means for any metrological investigation of surface, due consideration must be given to the system used and the scale at which it makes its measurements.

Whitehouse provides some advice on the selection of measuring system. When assessing the functionality of a surface, the measuring system should mimic the function that is being assessed [6]. For example, a wear machine should be used to test surface wear or a friction machine to test friction. However, for many surface functions this is not possible. Therefore, the surface is characterised using surface parameters and the function is predicted from the parameters. This requires the development of the relationships between surface parameters and the surface function. Whitehouse states that these relationships are rarely developed and some parameters are used to characterise surface function for which they were never intended [6]. In other words, a surface should be described from the perspective of its function using a measurement which is close to the physical functional behaviour of the surface [47]. If this is not available then a model of the function should be developed to define function-oriented parameters.

This discussion of the fundamentals of surface metrology provides two principles to be taken into account in this thesis:

1. Due consideration must be given to the scale of measurement of surfaces.

2. A model of the function should be developed to define function-oriented parameters.

As described previously, the methods of surface metrology can in general be used for two purposes, firstly to gain information about the manufacturing process of the surface and secondly to make predictions about the functional behaviour of the surface. However, Muralikrishnan investigated the industrial applications of surface metrology and found that this full potential of surface metrology is rarely exploited in industrial manufacturing [48]. After carrying out metrological investigations on several industrial problems, he found that measurements of surface texture were used mainly for specification compliance, and very rarely for the two purposes outline above.

He also found that the standardised roughness/waviness/form filtering cutoffs were not appropriate for many applications, as they are unable to capture the relevant functional bandwidth. This means that parameters derived from the filtered surface texture data, used for compliance to specification, are not representative of the function or the process. The functional bandwidth varies depending on the application, meaning the identification of appropriate cutoffs should be performed for each application.

Muralikrishan summarised his findings as follows:

- Surface texture information is rarely stored for later retrieval and analysis. This prevents the analysis of data sets from parts already manufactured.
- Surface profiles are often not viewed or compared with profiles from other components with superior performance.
- Functional tests, if conducted, are rarely done in the same facility as the production units, making it challenging to obtain both performance and metrology information simultaneously.
- Process information such as tool wear, tool change, grinding wheel dressing etc. is not stored along with metrology data.
- Surface texture instruments used in shop floors have limited analysis capabilities. They report simple parameters such as Ra without display of profiles.
- Instruments used in metrology labs in companies have analysis features that enable parameter computation after filtering at certain pre-defined cutoffs.
- They do not offer any cause-effect modelling tools or process monitoring capabilities.
- Surface finish measurements are often used only for tolerance compliance and rarely for any diagnostics or correlation work.

From these findings he concluded that the application of surface texture measurements as practiced in the industry today is a limitation of its scope [48]. Although these findings date from 2003, the use of surface metrology in the tinplate industry is comparable to his descriptions of the use of surface metrology in industry in general. Although a number of investigations have been performed, as outlined in this literature review, there is little to no awareness of the scale-sensitive nature of surface texture and no attempt to discover the relevant functional bandwidths. Also, any findings from these investigations haven't resulted in any change to the use of surface metrology on the production line. Surface texture is measured with one parameter, at standard cutoffs, to ensure compliance to specification.

The primary message of the above findings is that it is critical to respect the multi-scale nature of surface texture and to perform surface analyses which are scale-sensitive. This means using the methods of surface metrology to discover the bandwidths of surface texture that correlate with function. It is not enough to use standardised filter

cutoffs when calculating surface texture parameters. A more in-depth study on the multi-scale analysis of surface texture data is given in a later section.

2.3.2 Measurement of surface texture

The measurement, processing and characterisation of areal surface texture has been standardised in ISO 25178. For measurements of surface profiles, there 9 ISO standards. In this section, the methods by which surface topography is measured is described, as well as the subsequent processing and analysis of the recorded data.

2.3.2.1 Contact methods

Historically, the most utilised method for measuring and characterising a surface has been the use of a stylus. In this method, a stylus is dragged across the surface and a transducer converts the vibrations into an electrical signal which is then amplified, processed and analysed.

Stylus methods, although widespread and with rigorous standards, have a few major drawbacks. The stylus tip can physically change the surface it is investigating as the instrument must be in contact with the sample. As it is a line trace method, the stylus method can only provide areal measurements by a slow process of successive parallel tracing.

2.3.2.2 Non-contact methods

All optical methods function by projecting light onto the surface under investigation and then examining or recording the reflected light. Optical methods are by nature non-contact processes, therefore avoid the pitfalls of the stylus methods and have the added benefit of being capable of areal measurements and much higher speed of measurements.

Optical methods of surface metrology have a history running back to 1927 and there are a large variety of systems and techniques available. The most widely used of these methods are outlined below. For the work described in this thesis, only white light interferometry and focus variation methods were available. Both were trialled and white light interferometry was selected to be used as there were less missing data points in the measured surfaces.

White light interferometry These systems utilise the phase difference in light rays from the same source reflected off two different surfaces, the reference surface and the surface under examination. This produces interference fringes, the spacing of which can be related to roughness height. White light interferometers now come packaged with software which can extract the full range of surface characterisation parameters.

Focus variation Focus variation is an optical method used to measure surface topography. An optical system with a narrow depth of field is focused on a surface, and then scanned through the vertical axis. A number of in-focus slices of surface topography are captured, which together build up a height field of the surface under investigation. An advantage of focus variation methods is that colour information can also be captured.

Scanning confocal microscopy Another method of capturing topographical information is scanning confocal microscopy. This method also uses an optical system with a very narrow depth of focus, however instead of capturing an entire image of a surface, only information a single point is captured. This is achieved by using a lens to focus light on only a small area of the sample surface. Two-dimensional images are developed by scanning the focused beam of light (often a laser beam) across the horizontal plane, and this process is then repeated across the vertical axis to build up a height field.

2.3.3 Processing

After surface data has been collected using any of the above methods, the data is then processed to be developed into a form which enables characterisation of relevant surface features.

2.3.3.1 Outlier removal

Measured surface data often has outlying data points which appear to be inconsistent with the rest of the sample set. There are two main causes of outliers in surface measurements. The first is related to the method of measurement, for example sensor noise, the second is related to the presence of foreign bodies on the surface, for example dust [49]. The standard approach to the identification of outliers in surface data is the use

of Grubb's test. However, Grubb's test assumes that the data under investigation is normally distributed, which is not always the case for measured surface data[49].

2.3.3.2 Tilt removal

Often measurements of surface texture have tilt running through the data. The source of this tilt is misalignment between the sample and the measuring device. The tilt needs to be removed before calculations of surface texture parameters are made.

2.3.3.3 Filtering

First, to extract the relevant information from the detected signal, filtering must be applied, eg. a low pass filter to remove the waviness/profile signal so as to isolate the roughness signal. It is important to note that the choice of filter can effect the measurement of parameters i.e. a reading of the same parameter will be different if a different filter is used therefore it is vital to quote the filter choice along with the actual reading.

Roughness, Waviness and Form The standardised surface decomposition divides surface data into three bands of spatial frequencies, known as roughness, waviness and form. This decomposition is described in standard ISO 16610 for areal measurements and ISO 11562 for profile measurements.

Gaussian filters The Gaussian filter is the filter most widely used for analysis of surface texture. It is defined for surface metrological applications in ISO 16610 [50].

An implementation of a Gaussian filter is described in more detail in Chapter 3.

The use of Gaussian filters is open to criticism for their relatively poor transmission characteristics [48, 51]. However Gaussian filters have been used for multi-scale analysis of surface texture to good effect [52, 53].

2.3.4 Characterisation

After data collection and processing, the data can then be analysed to draw out the characteristic features of the surface. These characterisations can then be linked with process and/or functional parameters.

Surfaces can be represented in several different ways. The most intuitive is as a heightmap $z(x, y)$ where z is the location of a surface point at x and y. From this basic

heightmap other representations can be derived. The representations outlined here are the distribution of surface heights, the distribution of surface normals (or normal distribution function NDF), the material ratio curve, and several representations of the surface in frequency space (auto-correlation function (ACF), power spectral density (PSD) and Fourier transform). From each of these representations, parameters can be derived to characterise certain surface features, which can then be linked to surface function.

2.3.4.1 Distribution of surface heights

A measured surface can be represented by the distribution of the surface heights contained in the measurement. This is also known as the amplitude distribution. This gives the sum of the surface points at a given height [5]. From the distribution of heights several parameters can be derived. The first is the root mean square amplitude of the surface Sq. This is the standard deviation of the surface heights.

$$S_q = \sqrt{\frac{1}{A} \int \int_A z^2(x, y) dx dy} \tag{2.1}$$

where A is the surface area. For a discretised measurement this becomes:

$$S_q = \sqrt{\frac{1}{NM} \sum_N \sum_M z_{ij}^2} \tag{2.2}$$

Another parameter derived from the distribution of heights is the skewness Ssk. This is the third moment of the distribution and describes the shape of the distribution. The skewness captures the symmetry of the distribution about the mean line and therefore shows if the material contained in the surface is distributed above or below the mean line. A Gaussian height distribution has a skewness of zero. If the surface content lies largely above the mean line the skewness will be negative. If the surface content lies largely below the mean line, the skewness will be positive.

The kurtosis Sku of a surface is a measure of the sharpness of the distribution of the surface heights. A Gaussian height distribution has a kurtosis of 3. A value lower than 3 can indicated a surface characterised by bumps, with a high proportion of surface material in the peaks. A value higher than 3 indicates a surface characterised by spikes, with a higher proportion of material clustering around the mean. Note this normal value of 3 can be shifted such that a Gaussian distribution has $Sku = 0$.

The skewness and kurtosis can be seen in Figure 2.3.

$$Ssk = \frac{1}{S_q^3}\frac{1}{A}\int\int_A z^3(x,y)dxdy \tag{2.3}$$

$$Sku = \frac{1}{S_q^4}\frac{1}{A}\int\int_A z^4(x,y)dxdy \tag{2.4}$$

Another parameter is the mean amplitude of surface heights, Sa, which is the arithmetic mean of the absolute values of the measured surface heights.

$$S_a = \frac{1}{A}\int\int_A |z(x,y)|\,dxdy \tag{2.5}$$

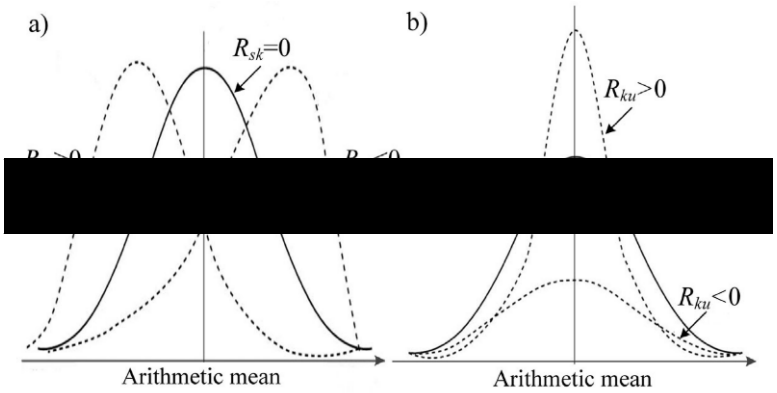

Figure 2.3: The distribution of surface heights, showing a normal distribution in bold, the skewness of the distribution in a), and the kurtosis of the distribution in b). [54].

Sq and Sa are strongly correlated, in that they both capture similar information about the surface. Sq often has more physical meaning than Sa, and has been related to several surface functions [5].

Each of these areal parameters has an equivalent parameter for surface profile measurements, denoted by the symbol Rx where x is the same subscript as the areal parameter. For tinplate, the surface texture of the underlying steel substrate is defined in BS EN 10202 by the nominal average roughness Ra of the surface profile, measured across the rolling direction. This parameter is used for quality control and is insufficient to characterise the total visual appearance of tinplate as it is possible for surfaces to have the same nominal Ra yet different visual appearance. Due to the functional advantages of Sq and the industrial usage of Sa, both Sa and Sq (or their profile equivalents) will be used throughout this thesis.

2.3.4.2 Normal distribution function

The normal distribution function describes the orientations of the normals to the surface at every point of the surface. There are several methods available to calculate the normals to the surface. The method given here involves the numerical differentiation of the surface at each point to determine the surface slopes, which are then inverted to determine the normals.

The numerical differentiation of a function across a seven point neighbourhood is [4]

$$\frac{dz}{dx}|_{z=z_0} = \frac{1}{60h}\left|z_3 - 9z_2 + 45z_1 - 45z_1 + 9z_{-2} - z_{-3}\right| \tag{2.6}$$

where h is horizontal interval between points.

From the slopes of the surface it is then trivial to calculate the normals by inversion.

For an areal surface texture measurement, this numerical differentiation is carried out across both x and y to obtain the slope of the surface at each point. It is possible to derive several parameters from the distribution of surface slopes. The root mean square is taken to give the root mean square slope of the surface.

$$S_{dq} = \sqrt{\frac{1}{A}\int\int \frac{\partial z(x,y)}{\partial x}^2 + \frac{\partial z(x,y)}{\partial y}^2 dxdy} \tag{2.7}$$

discretised:

$$S_{dq} = \sqrt{\frac{1}{A}\sum_i\sum_j \frac{\partial z_{ij}}{\partial x_{ij}}^2 + \frac{\partial z_{ij}}{\partial y_{ij}}^2} \tag{2.8}$$

where A is the area of surface $z(x, y)$.

The Sdq is a unit-less parameter, or can alternatively be expressed as $[\frac{\mu m}{\mu m}]$ or $[\frac{\mu m}{mm}]$ [5]. Leach states that the Sdq parameter can be useful in controlling the cosmetic appearance of a surface [5].

2.3.4.3 Material Ratio Curve

This parameter has historically had a number of names attached to it, including bearing area curve and Abbot-Firestone curve. BS EN ISO 4287 defines the material ratio of the profile as the ratio of the material length of the profile elements at a given level to the evaluation length and defines the material ratio curve of the profile as a curve representing the material ratio of the profile as a function of level.

This parameter shows the distribution of material in the peaks, valleys and troughs

of the surface under investigation, which can potentially be linked to function. A number of parameters are derived from the material ratio curve, which quantify some aspect of the curve. These include (from ISO 13565-2:1996):

- Reduced peak height R_{pk} - measure of peak height above core roughness
- Core roughness depth R_k - measure of core roughness with dominant peaks/roughness removed
- Reduced valley depth R_{vk} - measure of valley depth below core roughness
- Peak material portion M_{r1} - percentage of material that comprises peak regions measured by R_{pk}
- Valley material portion M_{r2} - the percentage of the measurement area that comprises the deeper valley structures given by $100\% - M_{r2}$.

The material ratio and associated parameters can be used to investigate the wear and imprinting of one surface on another. Nagase et al. used the material ratio curve to investigate the imprinting of a work roll on steel sheet [55]. They used the parameter to see how the peaks of the work roll created the valleys of the sheet being passed through the rolls.

The limitations of using the material ratio come in the assumptions one has to make when using it. The parameter relates only to the unloaded surface whereas in reality the surface will be loaded and will undergo elastic deformation. Also, two surfaces are involved and the features of both should be taken into consideration.

2.3.4.4 Signal Analysis

The three techniques outlined below are all fundamentally similar, in that they all function by comparing the signal under investigation to known signals and examining the differences between them. Auto-correlation compares the signal to itself, Fourier analysis compares the signal to sinusoidal functions and the wavelet transform compares the signal to discrete wavelets. The information contained in a Fourier analysis is identical to the information presented by the autocorrelation function, but in a different form [56].

Parameters built from these analyses are functions of the surface rather than plain numbers (such as average roughness Ra) and can reveal much more of the underlying statistics of the surface [6].

Autocorrelation The auto–correlation function is essentially a process of determining the relationship of any point on the profile to all other points [16]. A section of the signal (i.e. surface profile) is compared across the rest of the signal to identify self-similarity or repetitions within the signal. For example, a perfectly isotropic signal would have a low auto-correlation function whereas a perfectly periodic signal such a sinusoidal function would have a high auto-correlation function.

Fourier Transform Fourier analysis of a signal works on the basis that all signals can be approximated by a signal which is a superposition of multiple purely sinusoidal signals. The technique is useful as it can be used to determine the frequency content of a signal. This means the signal is split into harmonics, and the Fourier transform gives the frequency and amplitude of each harmonic.

This is useful in surface metrology as the surface profile can be decomposed into its constituent harmonics which reveals information about the structure of the surface, in particular the frequency or 'vibrational signature' of machine tools used to generate the surface. Fourier analysis works by multiplying each point of the signal with an exponential function and summing over the whole signal. This extracts the amplitude at each frequency.

Power Spectral Density An alternative representation of a measured surface is its power spectral density (PSD). The PSD represents the surface as the strength of variation in the surface across the range of spatial frequencies captured by the measurement. The 2D PSD of surface texture is defined as the squared amplitude per unit area of the spectrum of a surface height map [57]. The PSD is obtained by utilising the Fourier transform to transform the measured surface data from (x,y) space to frequency space [58]. The PSD is the Fourier transform of the autocorrelation function of the signal, which contains just the power (and not the phase) across a range of wavevectors. This allows identification of the spatial frequencies that can be found in the signal [59]. The PSD of surface texture has been used for some time in optics mainly for specifying high spatial frequency characteristics of optical surfaces to quantify their scattering properties.

Jacobs et al. provide a thorough review of the application of PSD to analysis of surface topography [59]. Jacobs et al. main aim with their paper is to develop a strategy for computing, analysing and reporting quantitative PSDs that are accurate and

reliable. Although their work focuses on PSD, their results are more generally applicable to other methods of scale-sensitive surface analyses therefore are worth taking into consideration. Jacobs et al. consider the fact that the spectral content of measured surfaces is only a limited section of the full spectrum of surface spatial frequencies. The spectrum of a measured surface is limited on the one side by the sampling interval of the measurement and on the other by the length of the measurement. This means a PSD derived from a measured surface will be incomplete. This can be overcome by making several measurements of the surface at multiple scales, calculating the PSD of the surface at each of these scales, then reconstructing these PSDs to give one "master PSD" to develop the (more) complete spectral content of a surface.

Jacobs et al. derive a process for measuring surfaces and calculating parameters which gives accurate, reliable, quantitative measures of the spectral content of measured surface data, across a large range of spatial frequencies. The process is as follows:

- Measure multiple surfaces
- Measure at multiple locations
- Measure at multiple scales
- Remove tilt
- Calculate PSDs of each scale
- Reconstruct all PSDs across all measured scales to get "master PSD"

This process can be replicated for any scale-sensitive surface analysis in order to obtain accurate, reliable, quantitative results.

The first two steps in this process are taken in order to get good sampling of surface statistics. Measuring at multiple scales is done to ensure the widest possible range of spatial frequencies are taken into account. An accurate reconstruction of the complete PSD requires tilt correction of the surface data. This is because any tilt in the surface data will be represented by the PSD as long wavelength surface content. When stitching together multiple PSDs, this results in a lack of overlap between the long wavelength content of one surface and the short wavelength content of another. Finally, the PSDs are calculated for each scale, then stitched to create a master-PSD with information across multiple scales of measurement.

2.4 Visual appearance

This thesis focuses on the visual appearance as the key surface function of tinplate. In this section the importance of the visual appearance of materials is discussed, as well as the way in which the visual appearance is created by the properties of the material. Humans are incredibly successful at making subtle visual judgements to determine the properties of a material by its appearance [1]. The appearance of an object is influenced by a large number of variables. These include the nature of the light source, the physical nature of the surface and the interaction of the two, as well as the spatial relationships between light source, object and viewer and the subjective response of the viewer. The human mind parses all the information available in the appearance of the object to make inferences and arrive at a judgement of the properties of the object.

The perceived appearance of materials plays a disproportionate role in the assignment of value to objects [1]. Therefore, it is imperative to have a rigorous understanding of how appearance is created and then perceived if the visual appearance of objects is to be manipulated in an industrial process.

2.4.1 Scattering of light from a surface

Church defines three mechanisms by which light is scattered from a surface [60];

Topographic Scattering due to the surface texture.

Material Scattering due to fluctuations in composition and/or density of the material that forms the surface.

Defect Scattering due to localised perturbations in the surface. This could be topographical in nature i.e. pits or bumps in the surface or material i.e. localised fluctuations and/or densities in the material the composes the surface.

The scattering of light from a surface can be roughly described as falling into two components, specular and diffuse reflectance. The specular reflectance is seen at an angle equal and opposite to the angle of incident radiation. The diffuse reflection is light which is scattered away from the specular angle. This can be seen in Figure 2.5.

The way in which a surface scatters light can be encoded in a function known as the bidirectional reflectance distribution function (BRDF). The bi-directional reflectance

distribution function describes the scatter of light from a surface across the entire wavelength domain and the entire angular domain. The BRDF is the ratio of the radiance reflected from a surface in the direction (θ_r,ϕ_r) to the irradiance onto the surface from the direction (θ_i,ϕ_i) [12].

$$f_r(\theta_i, \phi_i; \theta_r, \phi_r) = \frac{dL_r(\theta_i, \phi_i; \theta_r, \phi_r)}{dE(\theta_i, \phi_i)} \tag{2.9}$$

where $\theta_{i,r}$ are the zenith angles and $\phi_{i,r}$ are the azimuthal angles of irradiance and reflected radiance. dL_r is the reflected radiance and dE_i is the incident irradiance. The coordinate system used can be seen in Figure 2.4.

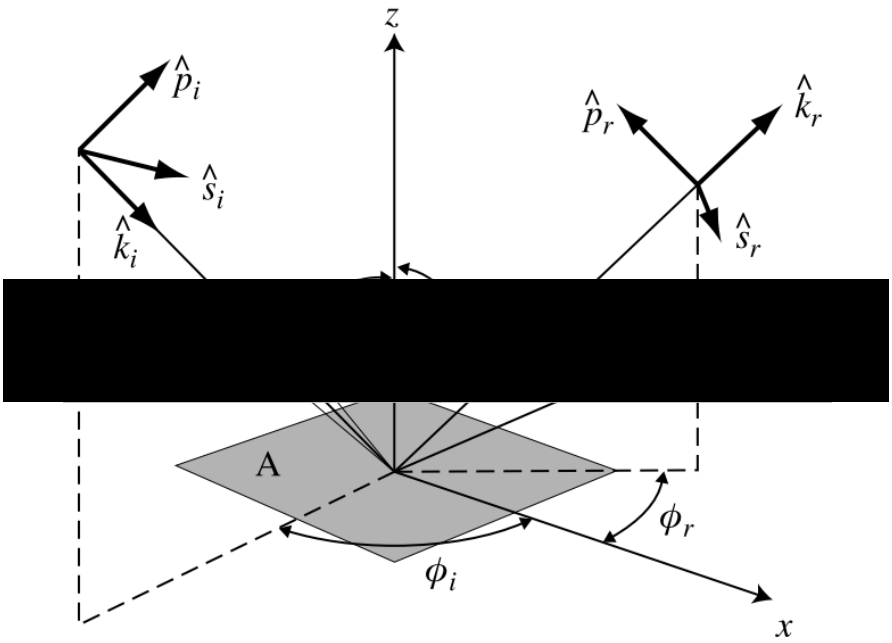

Figure 2.4: The coordinate system used in calculating the BRDF [61].

This function encodes the entirety of the information surface response to irradiance. To get useful results approximations must be made. One approximation is the Kirchoff approximation in which the incident and reflected waves at any point on a surface are approximated by the incident and reflected waves that would be present on a infinite tangent plane at that same point [62].

In the 1960s Bennett and Porteus established the relationship between the reflectance and roughness of a surface, developing work done by Davies [8, 9].

They state this relationship as

$$\frac{S_r}{T_r} = \exp[-(4\pi cos\theta_i \frac{R_q}{\lambda})^2] \tag{2.10}$$

where S_r is the specular reflectance, T_r is the total reflectance, θ_i is the incident angle, R_q is the root mean square (rms) surface roughness, and λ is the wavelength of the incident radiation.

2.4.2 Measurement of visual appearance

2.4.2.1 Goniophotometry

Goniophotometry is the measurement of the BRDF. This is done using a goniophotometer. A goniophotometer measures the intensity of reflected light across the entire wavelength domain and the entire angular domain.

2.4.2.2 Glossmeters

Current industrial methods of measuring visual appearance consider the surface appearance as the aggregate of constituent scattering phenomena such as specular reflectance, off-specular reflectance and diffuse reflectance. Hunter's influential paper categorised these parts of surface reflectance and his taxonomy is still the foundation of contemporary industrial measurement of visual appearance. He described six types of perceptual gloss [63].

- **Specular gloss** - the brilliance of highlights.
- **Sheen** - the gloss at grazing angles reflected off matt surfaces.
- **Contrast gloss** - the contrast between specular highlights and diffusely reflecting areas of the surface.
- **Haze** - the appearance of a dim halo of reflected light surrounding a surface highlight.
- **Distinctness of reflected image gloss** - perceived sharpness of an image reflected by the surface.
- **Absence of surface texture gloss** - perceived smoothness of a surface, due to the uniformity of the surface texture.

Glossmeters attempt to capture and quantify some of these constituent parts of percieved gloss, for example, the specular gloss, the haze and the distinctness of reflected

image gloss. Each of these parts is defined and characterised with a simple, single parameter which can be measured. The task of the researcher is establishing relationships between these measured parameters and the properties of the material.

The efficacy of this method has been questioned by Marlow et al. who suggest that the brain does not operate in any way analogous to this [64]. They review a large number of publications that show perceived surface gloss can vary as a function of an object's 3D shape and its illumination field. They claim that the perception of gloss is dependent on how each illumination field modulates the size, contrast, sharpness, and depth of specular reflections. Differences in lighting and shape of the object have large effects on the apparent reflectance of surfaces [65]. This means the context in which an object is viewed, and its state at a certain stage of manufacture, can have a large impact on how it is perceived. In other words, the perception of gloss is not related to the measurement of gloss. The reduction of the multidimensional nature of perceived surface reflectivity to parameters of a single dimension means the link between perception and measurement is lost.

This weakness in the metrology of gloss is reiterated by several other publications. There are structural issues in the standards which define gloss measurement. Ambiguities across different standards (ASTM and ISO) and assumptions made about the reference surface means there is variation between gloss measurement systems even when those systems are within standard [66]. The method was originally developed for process control to discriminate between different samples of the same product and extensions of the method for other purposes need to be made with caution [67]. It has been shown that specular gloss measurements do not correlate well to visual assessments made by human observers. Roughness measurements do not correlate well with measured gloss and perceived quality [13]. Surfaces can have identical gloss values yet different visual appearance [68].

However, glossmeters are widely used in industry due to their low cost and ease of use. The main reason gloss meters are used is due to the lack of an alternative. Other methods of measuring visual appearance, such as systems for the measurement of the entire BRDF tend to be bespoke laboratory setups, unsuitable for industrial applications. The family of gloss parameters provide a useful method of obtaining quantitative measurements of visual appearance which although cannot withstand strong scrutiny, can provide a good indication of the visual appearance of materials.

A glossmeter measures the intensity of the specular reflection from a surface com-

pared to a reference surface. A specular reflection has angle of reflection equal and opposite to the angle of incidence. The features of the specular highlight are extracted and described by parameters such as gloss, haze and distinctness of image (DOI).

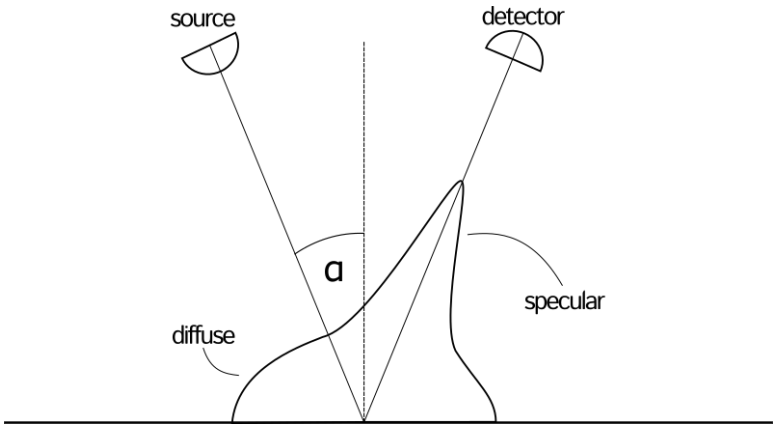

Figure 2.5: Gloss meter geometry ($= 20°, 60°, 85°$) and the specular and diffuse components of surface reflection.

2.4.3 Modelling visual appearance

The BRDF has been used for many years in the computer graphics industry to model the reflectance of simulated surfaces. As part of the process in refining and validating the many BRDF models created by this industry, several experimental studies have been published investigating the correlation between surface texture and visual appearance.

Obein et al. also developed a model to predict BRDF [69]. Their model was based on two assumptions:

1. Reflection can be divided into surface and volume components.

2. Surface is composed of microfacets, distribution of which is described by an isotropic probability distribution.

Surface reflection is modelled as the specular reflection of the facets. It is assumed that the specular reflection of the facets is responsible for the specular peak of the BRDF. The BRDFs were predicted assuming a Lorentzian distribution of microfacets. For the samples used, these assumptions lead to a good correlation between model and measurements, meaning the facet hypothesis is reliable.

Leloup et al. examined the relationship between measured BRDFs and values of measured [70]. Integration of the BRDF over the angles of the gloss detector correlates

with standard gloss measurement results, but only at certain geometries. The lack of detailed information on the optical design of the industrial gloss meter (illuminated area, apertures, . . .) was suggested as the source of this uncertainty. A full description and understanding of the optical system of a gloss meter seems to be necessary to improve the prediction of gloss values from measured BRDFs.

Shipulski and Brown used a similar approach to model surface reflectivity by representing the interaction of light with a surface as a set of discrete interactions with perfectly reflecting triangular mirrors. They triangulated measured surface data at several different scales, by using triangles of different areas. The triangle patch sizes ranged from 0.5 nm to 3 $\mu\mathrm{m}$, which are scales not relevant to the work in this thesis, however they found the assumptions they made lead to predictions that matched measurements of surface reflectivity [11].

Dong et al. developed a method of predicting the BRDF of a material from measurements of surface texture [71]. Using white light interferometry and a microfacet approach, they derived the NDFs and subsequently predicted the BRDFs of those surfaces.

Landskroon applied similar principles to predict the gloss of tinplate surfaces using the proportion of surface points that reflect light specularly into the gloss detector angle [45]. A visual representation of his approach can be seen in Figure 2.6.

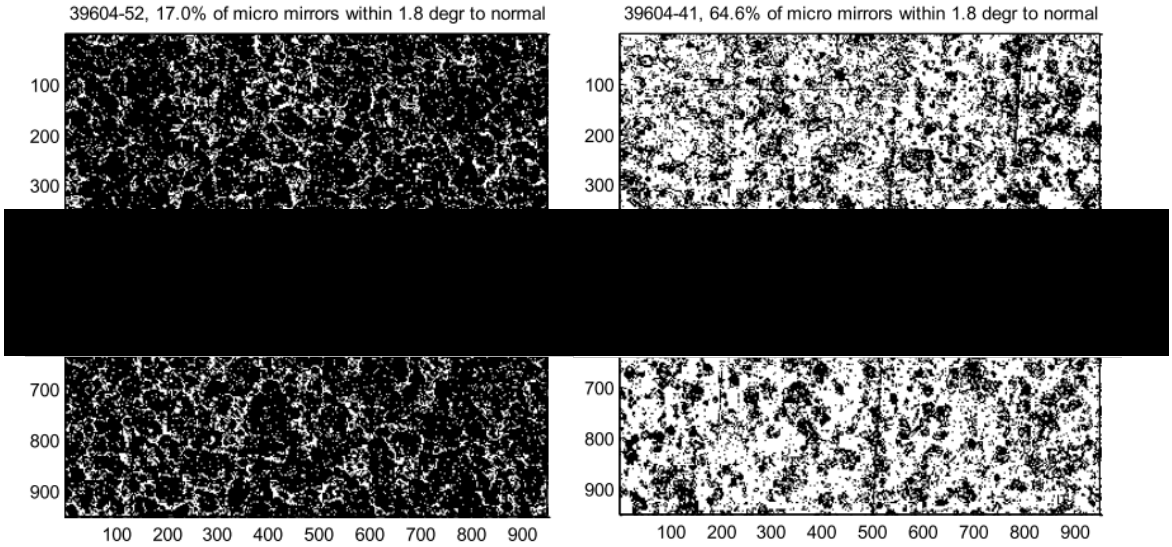

Figure 2.6: Landskroon slope analysis for a two surfaces. The figure on the left shows a low gloss surface, with relatively few microfacets reflecting into the gloss receptor angle. On the right, the surface is high gloss and a larger proportion of the surface reflects into the gloss receptor angle [45].

Whitehouse describes measured gloss of a surface as the ratio of light scattered from the surface that enters a detector to the total light scattered from the surface [10]. This ratio can be controlled by varying the amount of light that enters the detector pick up angle, which can be controlled by positioning the slopes of the surface that scatter light into that angle. By controlling the distribution of slopes, it is possible to control the distribution of intensity of reflected light. Whitehouse uses the concept of the unit event of manufacture, as outlined earlier in this literature review, to analyse the scatter of light from a surface. The unit event is a fundamental link between process and function because it is the aggregate properties of the individual unit events that determine the topographical properties of the surface. In the specific case of light scatter, it is the slopes of the unit event that will control the distribution of intensity of reflected light. According to Whitehouse, the ideal surface for control of scatter is a surface composed of mirror-like facets at random orientations, with a given distribution of slopes. The distribution of slopes then defines the optical properties of the surface [6].

These findings are relevant for the work carried out in this thesis for a number of reasons:

- The unit event concept is key in controlling the surface texture of manufactured surfaces.
- Specular reflectance of manufactured surfaces could be controlled by controlling the angular distribution of surface slopes.

2.5 Multi-scale surface analysis

2.5.1 Background

This chapter describes the multi-scale analysis of surface topography. First, an overview of the subject is given and the reasons for and benefits of using these techniques are described. Then several previous investigations using the techniques are reviewed. Finally, a proposal is made as to how and why multi-scale analysis should be applied to the surface topography of packaging steel.

In the discipline of surface metrology, the term “scale” refers to some subset of the entire spectrum of spatial frequencies of the surface. In other words, it is a narrow band

of surface wavelengths, taken from all the potentially observable surface wavelengths. The term "scale" is often synonymous with "size of surface features" as at a certain scale of observation, certain size features will be observable. The size of observable surfaces features corresponds to the scale of observation [7]. The functional behaviour of a surface often takes place at a certain scale. If the surface has multiple functions then surface features of different sizes, observable at different scales, may be responsible for the governing mechanisms of different functions. Brown et al. give the example of a road surface. A road surface should have low amplitude long wavelength surface components to provide smooth travel. However, the amplitude of the short wavelength surface components should be high to provide high friction for vehicle control. Understanding the correlations between scale and function of a surface can provide useful insights when it comes to designing surfaces for a specific purpose. The same approach can also be used to determine correlations between the scale of a surface and the manufacturing processes that created those features. Throughout this thesis, the term scale is used as shorthand for a band of spatial wavelengths contained within a surface texture measurement. Bigerelle et al. state that surface texture parameters may be insufficient to describe the relationship between surface texture and light reflection because these parameters are often associated with a single cut-off filter, which may not correspond to the relevant functional bandwidths[72].

The determination of these correlations depends on how those features are measured and analysed at different scales [7]. Brown et al. show that multi-scale analyses of surface topographies have a wide application. Their review shows multi-scale behaviour of surfaces across many fields, including but not limited to:

- Conventional manufacturing technologies (grinding, milling, turning, injection molding, micro-EDM)
- Adhesion
- Tribology
- Scattering
- Wetting
- Transfer phenomena
- Electrochemistry

From the above list, this thesis covers both conventional manufacturing technologies (grinding, EDT, SBT) and scattering. As these processes and function have been shown to exhibit scale-dependent behaviour, the multi-scale nature of the surfaces in this thesis should be considered. The surface of packaging steel specifically has not yet been investigated using multi-scale techniques.

2.5.2 Multi-scale analysis methods

A general outline of the method of multi-scale analysis of surface topographies is as follows; First, the surfaces are measured. Then, the measurements of the surface are decomposed into multiple bands of spatial frequencies. There are a number of methods available for this decomposition. The simplest method to obtain surface information at multiple levels of scale is to make the measurements at multiple levels of scale. For example, by using different cut-off lengths of a profilometer or different magnification lenses on a white light interferometer. However, if the measurements are made at a single scale of measurements, then the surface information at different scales needs to be extracted from the superposition of all surface scales present in the single measurement. There are several methods available to achieve this. The measured surfaces can be filtered using a variety of filtering methods. Linear, area, slope and curvature analysis are also available. In these analyses, different measures of the surface are extracted at different scales by down-sampling the measured surface data and calculating the measures (length, area, slope, curvature) for each down-sampled surface. These two techniques are described in greater detail in a later section.

Once the measured surface information has been decomposed into the scales of interest, each scale is characterised with appropriate surface parameters. These parameters can then be regressed against either process parameters or functional parameters to obtain the correlation strength for each scale. The variation of the correlation strength with scale can then be shown for each pair of surface and process/function parameters. This information can be used to provide insight about the scales at which the most important mechanisms occur, whether that is the formation of surface features in the manufacturing process or the causation of certain surface behaviours. The scale of surface topography most responsible for the relevant surface behaviour is known as the functional bandwidth. Discovery of functional bandwidths is the main purpose of multi-scale surface analysis.

2.5.3 Decomposition of surface information into multiple subsets of spatial frequencies

In this section the decomposition of measured surfaces into their component spatial frequencies is described. Broadly speaking, there are two main approaches available to achieve these decompositions. The first is filtering of the surfaces, the second is the calculation of certain geometric measures of the surface at different scales.

Goïc et al. provide an overview of the filtering methods available and the relative strengths and weaknesses of each method [53]. The filtering methods they investigate are Gaussian filtering, wavelet transform and discrete modal decomposition (DMD). Goïc et al. applied each of these decomposition methods to a range of surface topographies, then calculated standard surface texture parameters for each method, at each scale, and for three types of filter (high pass, low pass and band pass). They found clear differences between the three methods. It was found that wavelet decomposition gave better results than other methods when surfaces being characterised had localised topographical features, such as pits and other localised surface inhomogeneities. Gaussian filtering was found to give better results than other methods when surfaces with highly periodic morphological structures were being characterised. DMD was shown to fall somewhere between these two methods. DMD gave better results than Gaussian filtering for localised surface features and better results for periodic surfaces than the wavelet decomposition method.

A description of the down-sampling method is given in [7, 73]. This method relies on the fact that geometric properties of surfaces are scale dependent. For example, the length of a profile, or the area of a surface, is scale dependent. For example, the apparent length of a profile is calculated by tiling the profile with a certain length line segment. This tiling routine is repeated for different length line segments, from the horizontal interval between measurement points up to the nominal length of the profile. The apparent length of the profile is calculated for each of length line segment by multiplying the line segment length with the number of line segments required to completely tile the profile. This apparent length can then be plotted against scale (which is the length of the line segment) and can reveal certain information about the multi-scale nature of the surface under investigation. This analysis can be extended to areal measurements of surfaces by using different size areas to tile the surface instead of a line segment. In this way, how the apparent area of the surface varies with scale can

be determined. This gives much useful information, as many surface interactions are influenced by the area available to the interaction, such as surface transfer phenomena and adhesion [7]. These analyses can be further extended to other geometric measures of surfaces, such as the surface slopes and surface curvature.

2.5.4 Correlation of surface texture parameters and functional and/or process parameters

After the surface has been decomposed into its component bands of spatial wavelengths, the features of interest of each band are characterised. For this purpose, it is common to use the standard set of surface texture parameters from ISO . As shown above, it is also possible to use geometric measures of the surface features to gain information about the scale dependent properties of the surface. The general aim of surface metrology is to develop the relationships between surface features and either (or both) manufacturing process mechanisms or surface function. Therefore, the characterisation of the surface features needs to be combined with a characterisation of the process and/or function. Then a regression analysis can be carried out between the surface parameters and the process/functional parameters to determine the correlation between the two and the scale at which those correlations are strongest.

Ho et al. used multi-scale and statistical analyses to model the relationship between a process condition (sand-blasting, working pressure) and surface texture [74]. Their investigation is interesting due to the method they use to determine an optimal set of filtering and regression settings. They attempt a regression fit for every combination of surface roughness parameters, cut-off lengths, filter types (high pass, low pass) and regression fit models (linear, logarithmic, power law and exponential functions). The method used was as follows. A set of sample surfaces were created by sandblasting steel substrate, keeping all variable process setting constant, except for the working pressure which was set at $1 - 7$ bar. The surfaces were measured using white light interferometry with x20 lens, providing areal measurements with a lateral resolution of 0.71 μm. The surfaces were decomposed using Gaussian filters. High pass and low pass filters were used at 23 cut-off lengths varying between $5 \breve{} 1000$ μm. Surface roughness parameters were computed from these decomposed surfaces and regressed against the process parameter using 4 different regression models to obtain the R^2 coefficient of correlation. These R^2 correlation coefficients were then classified in

descending order such that the most relevant combination of all analysis settings could be determined. Overall, they were able to assess the relevance of 10^4 combinations of 55 roughness parameters, 2 filter types, 23 cut-off lengths, and 4 regression models and determine the optimum combination that provides the strongest correlation between process setting and surface texture. The discovered that the influence on the surface texture of the working pressure of the sand blast process is best characterised by the root mean square slope surface roughness parameter (Sdq), computed at a scale of 120 μm with a low pass filter. This correlation was best modelled with a power law function and was this combination of analysis settings gave a correlation strength R^2 =0.995. This method provides a strong and comprehensive way of discovering the functional correlations of surfaces and is used in this thesis to determine the correlations between surface texture and visual appearance of packaging steel.

Li et al. investigated the BRDF of several rough metallic surfaces. Various surface textures were created by using substrates of either steel or glass which were textured with grinding, bead-blasting or etching, then coated with a thin film ($\sim$ 50 nm) of Aluminium [12]. The surfaces were measured with a stylus profilometer which had 1 Å vertical and 0.1 μm horizontal resolution. Each profile was 400 μm long and 9 measurements were made in random locations and random directions. The raw data was then filtered with a high-pass filter to decompose the surface data into two frequency bands; one containing the high frequency components and the other containing the lower frequencies. The reasoning behind this decomposition was that as it has been shown that surface components with highest slopes have greatest influence on light scatter [75], and for this range of surface the highest slopes were at highest frequencies, then those are the frequencies that should be isolated for investigation. The filter cut-offs varied from $25 - 40$ μm, depending on the surface. From this filtered data, the RMS height τ and the auto-correlation length σ were calculated, then the slopes of the filtered surface data were determined using σ/τ. The BRDFs of the surfaces were measured using a gonioreflectometer. The BRDF was modelled using the He-Torrance model. Measurements of σ/τ (from high frequency components) were used as inputs into the model to predict the BRDFs of the sample set. Measured BRDFs were then compared to predicted BRDFs and good agreement was found between the two. This shows that the highest frequencies of surface texture have greatest influence on the scatter of light from surfaces. This is a type of multi-scale surface analysis, however the surface has been decomposed only into two bands, rather than decomposed across

multiple bands to enable the functional correlation to be elucidated across the spectrum.

Berglund et al. investigated the relationship between surface topography and surface friction using multi-scale techniques [52]. They used Gaussian bandpass filters to determine the scales at which the correlation between surface topography parameters and the coefficient of friction was strongest. The process investigated was stamping of metal sheets. Six sample workpiece surfaces were created using 3 different workpiece materials processed to give 2 different types of surface roughness. The function, friction, was characterised using the coefficient of friction and was measured using the bending under tension method. The workpiece surfaces were measured using WYKO RST+ white light interferometer at x10 magnification, giving a measurement size of 577×428 µm, with sampling interval dx = 0.785 µm. Measured surfaces were characterised using standard surface topography parameters. Surface topography parameters were regressed against the coefficients of friction to obtain the coefficients of correlation. The two parameters most strongly correlated with friction were Sdr (R^2 = 0.72) and Sdq (R^2 = 0.7). Measured surfaces were then filtered using bandpass filters. The bandpass filters were created by using Gaussian high pass and low pass filters to remove unwanted high and low spatial frequencies to obtain a band of spatial frequency to be investigated. Three different bandwidths were used (20, 50, 100 µm) with centre wavelengths ranging from $10 \breve{} 180$ µmin increments of 10 µm. After filtering, surface parameters were computed for filtered surface data and regressed against the coefficients of friction for those surfaces. The strongest correlation found was for the parameter Sa (R^2 = 0.94) at centre wavelengths of 10 µm and 20 µm with bandwidths of 100 µm and 50 µm respectively. The strength of the correlation of Sdq increased to $R^2 > 0.75$. With no filter, there were 2 surface topography parameters with $R^2 > 0.7$. With band pass filtering, 10 parameters were found to have $R^2 > 0.75$ with 6 of those parameters showing $R^2 > 0.9$. This investigation shows that by considering only the relevant surface scales it is possible to develop strong relationships between surface topography and surface function.

Vessot et al. investigated the correlation between gloss reflectance and surface texture of photographic paper [76]. They measured a set of 72 different photographic papers with laser scanning confocal microscopy. They used four different lenses to measure the surfaces (x5, x10, x20, x50). It was found that using x5 and x10 magnification gave measurements with artefacts, displaying large spikes in the measurement

which were not present on the real surfaces. The reflectance was measured using a micro-TRI-gloss GB-4430 gloss meter. The parameter measured was gloss, at angles of 20°, 60° and 85°. A set of 28 surface texture parameters were computed from the measured surface data. The gloss was linearly regressed against the surface texture parameters to determine the R^2 correlation coefficient. An area-scale analysis was also carried out. Strong correlations of $R^2 > 0.8$ for surface texture and surface reflectance were found. These strongest correlations were found for measurements made at the 5x and 10x magnification, using the area-scale fractal complexity. Measurements made with 20x and 50x magnification showed considerably weaker correlations. The sampling interval of the 5x lens is 2.5×2.5 μm^2, and the x10 is 1.25×1.25 μm^2. The sampling interval of the x20 lens is 0.63×0.63 μm^2 and the x50 is 0.25×0.25 μm^2.

Bigerelle et al. performed a multi-scale analyses on brass surface textured with various texturing processes [72]. They used Gaussian filtering to decompose the surface data, using high pass, low pass and band pass filters at 21 different cut off lengths. They calculated a range of surface texture parameters and correlated them against measurements of surface gloss. They found a strong correlation between gloss and the root mean square surface slope Sdq, computed using a cut-off length approximately equal to 8 μm with a low-pass filter. They state that the Sdq parameter can be used to differentiate between surfaces having similar average roughness amplitude. They also relate the Sdq parameter to the texturing process via the process parameter polishing angle of attack. This could be linked further to the texturing unit event, displaying the link between unit event, Sdq, and surface reflection.

To summarise, these papers show that multi-scale analysis can deliver insights not obtainable with non-multiscale analysis of surface texture. They also show that using Gaussian filters to decompose the surface data yields good results.

2.5.5 Multiscale analysis of surface coatings

In the automotive industry, the appearance of surface texture after coating with a layer of paint is of critical importance. Mezghani et al. introduced the multiscale attenuation function (MAF) as a method of quantifying the changes to surface texture caused by the addition of a coating to the substrate [77]. The MAF is a measure of the difference in roughness amplitude before and after coating, decomposed across the spatial frequencies of the surface. The MAF shows how the coating of a substrates affects the

texture across different scales.

The MAF is defined as

$$MAF(\lambda) = \left| \frac{MS_a^{post}(\lambda) - MS_a^{pre}(\lambda)}{MS_a^{pre}(\lambda)} \right| \tag{2.11}$$

Where $MS_a^{pre}(\lambda)$ and $MS_a^{post}(\lambda)$ are the multiscale roughness spectrum of the surface pre- and post-coating and λ is the spatial wavelength [77]. Mezghani et al. derived the multiscale roughness spectrum using wavelet decomposition of the surface data, then calculated the average amplitude of roughness of each scale. The resulting function is called 'MSa' (multiscale average roughness). MSa(λ) is the average roughness at different spatial wavelengths. This labelling convention (the prefix 'M' denoting 'multiscale') will be adopted throughout this thesis to differentiate between parameters calculated from the bulk surface data and parameters calculated from surface data decomposed across scale.

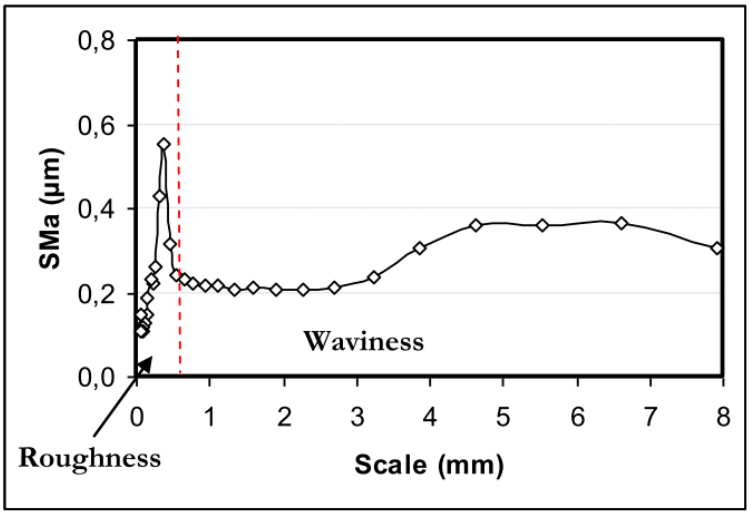

Figure 2.7: The multi-scale roughness spectrum for an uncoated substrate

Mezghani et al. made surface texture measurements on initial uncoated substrate, then further measurements on first paint layer, the sealer layer and the lacquer top coat. The measurements contained surface data in the wavelength bandwidth of 0.2 mm to 6 mm. They derived the multi-scale roughness spectra for each successive layer of paint, then calculated the MAF for each layer. Using the MAF they found that the first coat has a major influence on the texture in the shorter wavelength surface components, and the sealer and the lacquer modify the longer wavelength structures of the surface. The coating attenuates surface features most heavily in the 0.2 mm to 2.5 mm range.

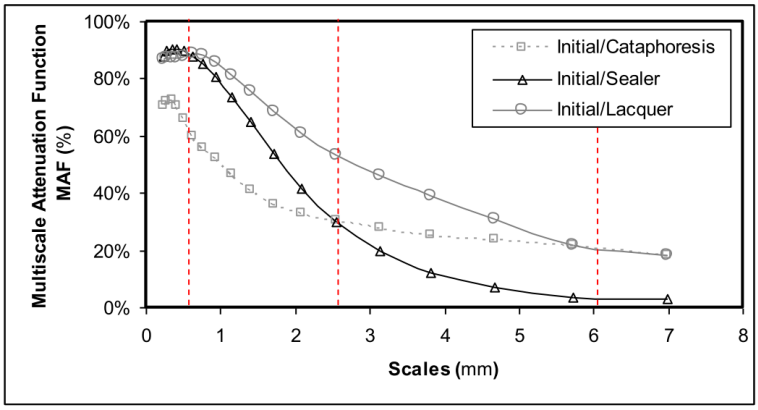

Figure 2.8: The multi-scale attenuation function for the successive application of coatings to a surface.

For tinplate, the layer thicknesses of the tin coating are much less than in the autobody paint coating systems. The tin coating is on the order of 1 µm thick whereas the multiple autobody paint layers sum to 80 µm. This means that the roughness attenuated by the tin coating will be at wavelengths even shorter than for the autobody system. The layer thickness and therefore MAF will be dependent on tin coating weight.

In this thesis, the MAF has been used to analyse the multi-scale modification of surface texture of steel strip that is electrolytically coated with tin and reflowed. It is also possible to extend the application of the MAF to analysis of processes other than coating. Essentially, the MAF quantifies the change in surface texture parameters across scale, throughout a process. In this thesis, this method has been applied to characterise the change in multi-scale surface texture parameters throughout a wear process.

2.6 Summary

In Chapter 1, Figure 1.4 showed three domains relevant to the surface texture and visual appearance of packaging steel, and the relationships between the three domains were discussed. This literature review has described work carried out by others who have developed the relationships between process, surface and function. Some of the main findings are reiterated below and used to guide the work of this thesis.

Leach et al. have shown that there no such thing as a surface as naively conceived of in every day language. The only surface available to investigation is the *measured* surface, which is the measurement of the magnitude of the interaction between probe and

material. Using different measurement probes for the same material will result in different surfaces being measured. Therefore, surfaces should be measured using methods with underlying physical principles comparable to those that generate the surface function of interest. As this is not always possible, the function should be modelled with the aim of discovering function-oriented parameters which can be measured using alternate methods. They also show that any surface analysis should be scale-sensitive. The functional parameter(s) should be matched to its functional bandwidth(s).

Muralikrishnan showed that these fundamental principles of surface metrology are rarely considered in industrial settings. Although his research is dated, it is still relevant for the packaging steel industry.

Landskroon showed that for low tin weights, substrate texture is critical for visual appearance. Li et al. show that the highest frequencies of the surface texture of metallic surfaces have greatest influence on visual appearance. Several other studies show that the functional behaviour of surfaces is scale-dependent and that a full characterisation of the correlation between surface texture and surface behaviour needs to be scale sensitive [74, 78]. Obein et al. show that it is possible to predict the BRDF of surface by considering distribution of normals of a surface. Leloup et al. show that it is possible to predict gloss of surfaces from measurements of their BRDF. Dong et al. show that it is possible to predict the BRDF of surfaces from calculations of the NDF of measured surfaces.

The above insights together with the outline given of the manufacturing process of tinplate provide a logic underlying the approach taken in this thesis. It is the texture of the work rolls that creates the texture of the strip which in turn is responsible for the visual appearance of the final product. Therefore it is at this stage of the process that visual appearance of the final product can be influenced. This thesis utilises the methods of surface metrology to gain insights into the behaviour of the substrate-coating system of tinplate, with due consideration given to the scale-sensitive nature of surface function. Those insights are then used to generate substrate textures that enhance surface function and/or control over substrate function. This is done by modelling the function of tinplate following the chain outlined in the above list of publications. The NDF of the measured surface is found, from which the BRDF is calculated, from which visual appearance parameters can be calculated (gloss, haze etc.). This model of the function can be used to provide information about simulated surface textures to develop advanced, manufacturable surface texture designs, providing a pathway to

differentiated tinplate products for markets in which visual appearance is a key product function. The work in this thesis has been undertaken bearing in mind Whitehouse's recommendations at the end of his paper [79]:

"What is needed next is a much more exhaustive check on the validity of the theory by means of computer simulations and preferably some practical results obtained from real manufactured surfaces. The areal properties of the surface... and directionality have also to be considered. These are tasks for the future."[10]

In this thesis, the concepts and theory outlined above have found practical application in the tinplate industry, using computer simulations and measurements on real manufactured surfaces.

Chapter 3

Materials and Methods

3.1 Overview

In this chapter, the materials on which measurements of surface texture and visual appearance were made are described. The methods by which those measurements were made are also described. The production, procurement and handling of the physical samples is described, along with the details of the machines used to make the measurements, the post-processing of the data and the details of the characterisation of the processed surface data. Justification is given for the sample sets used and the approach taken in the measurement of those samples.

3.2 Materials

In this thesis, most analysis was carried out on two sample sets. In the tinplate manufacturing process the surface texture of the final strip is called the "finish". Several finishes are produced in the manufacturing process, depending on the end-product, and a several coating thicknesses can be applied to those textures. This gives a wide range of possible permutations of surface texture and coating properties. However, not all permutations are realised in the manufacturing process. Also, not all of the actual permutations used are relevant for the end-products that this thesis focuses on. The products for which visual appearance is particularly pertinent as a surface function are products such as baby food packaging and similar.

For this reason, two samples sets were used to gather information about the surface texture and visual appearance of packaging steel. The first sample set covers the majority of surface finishes and all coating weights. The second set contains samples from only one finish, at one tin weight. In this way, using these two sample sets, variation across finishes is captured, along with variation within a specific finish. The specific finish chosen is one that is sold into markets for which visual appearance is highly relevant, namely 'fine stone finish'.

The two sample sets have been labelled 'Sample Set 1' and 'Sample Set 2' and will be referred to by these labels throughout the thesis. The detailed description of these sample sets is given in this chapter.

3.2.1 Sample set 1

Sample set 1 is the same sample set used in reference [44]. The samples were created at Tata Steel's Ijmuiden plant in the Netherlands for the purpose of investigating the effect of substrate texture on tin layer performance. Six coils were produced with different finishes and these were then coated with four different tin weights. The coils were all reflowed with the same settings to give the same alloy layer properties for each coil. The six roughness variants were stone, heavy stone, light stone, bright, MATT1 and MATT3. The four tin weights used were 2.8, 5.6, 8.4 and 11.2 gsm. All 'stone' finish variants are anisotropic finishes, created by the combination of ground work rolls and SBT work rolls. These three finishes vary in nominal Ra. Light stone has lowest nominal Ra and heavy stone has highest Ra. Bright, MATT1 and MATT3 finishes are isotropic finishes created using SBT work rolls. These three finishes also vary in nominal Ra. Bright has lowest nominal Ra and MATT3 has the highest. Altogether these six finishes represent the total breadth of finishes available in the tinplate industry. The sample set was initially created in order to determine the effect of the substrate roughness on the performance of the tin layer. Properties such as scratch resistance, surface chemistry, visual appearance and wipeability of the coating were investigated. The tin weight was varied in order to determine the variation in the aforementioned properties as a function of the tin weight.

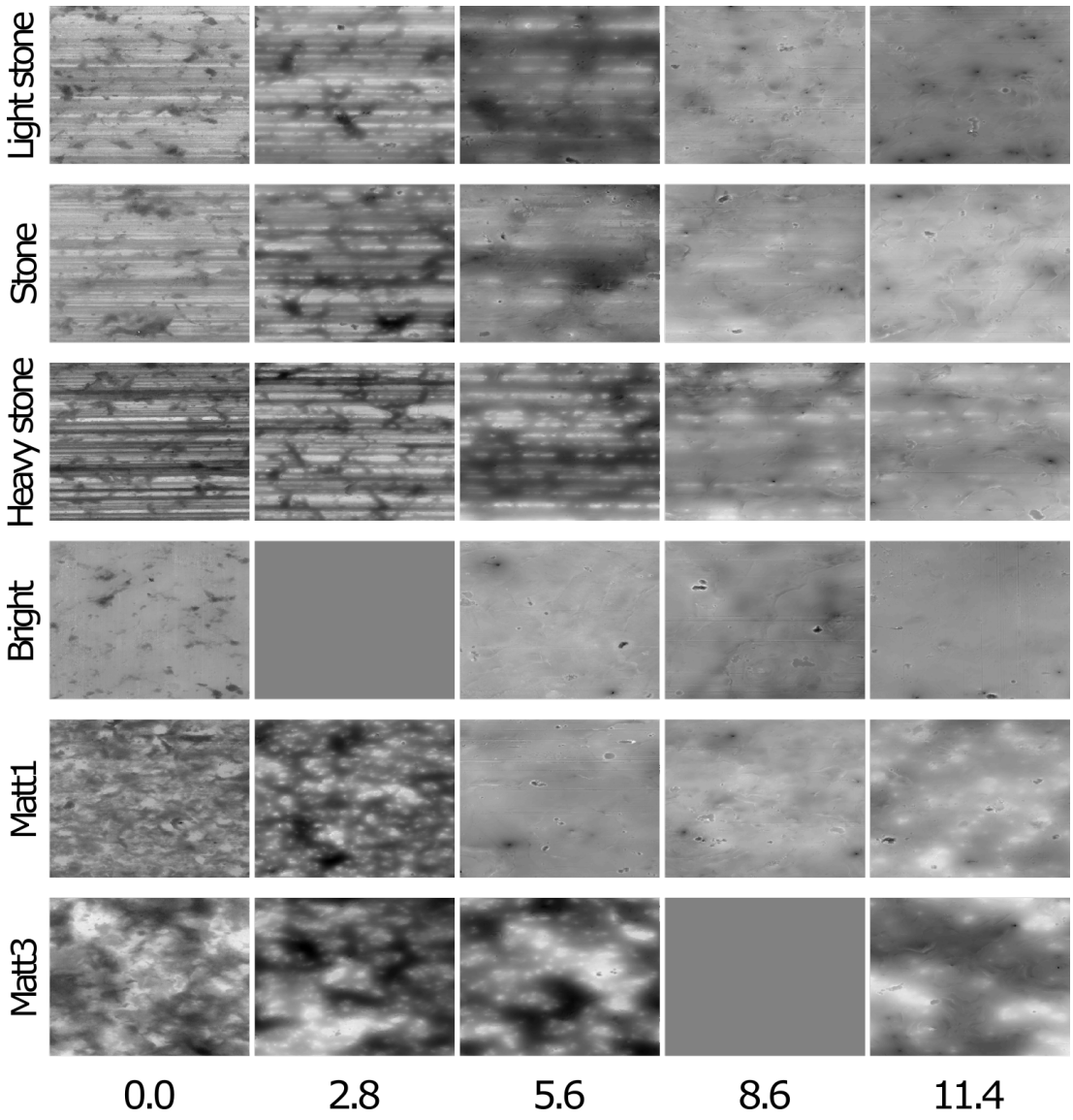

Figure 3.1: Images of surface textures of samples from Sample Set 1. Note there were no samples available for Bright 2.8 and Matt3 8.6.

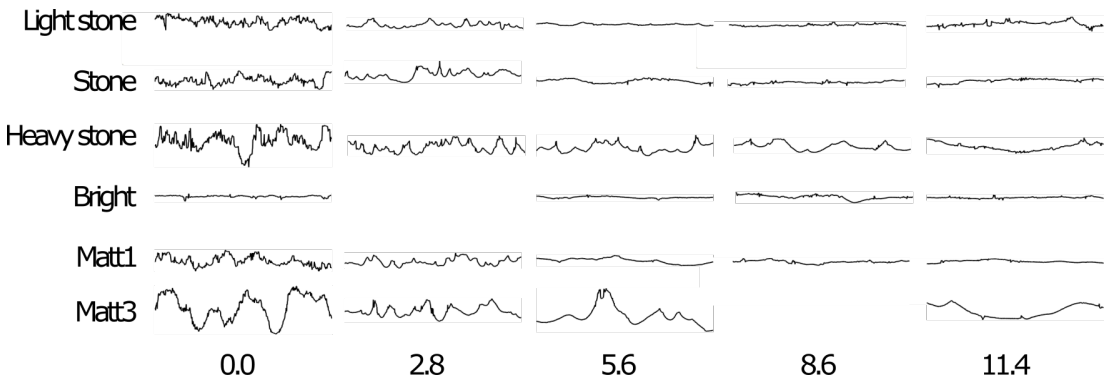

Figure 3.2: Profiles of samples from Sample Set 1.

3.2.1.1 Tin coating removal

For Sample Set 1, no uncoated substrate samples were available. To enable measurements of the underlying substrate to be measured, the tin layer was removed from the surface of the coated samples. There are a number of processes available to remove tin from a tinplate surface, such as Clarke's method, coulometric methods, and the Bendix method [18]. The method used in this thesis to remove the tin coating from samples is a coulometric method. This method is well-established as it is a standard method used to determine the mass of the tin coating, standarised in ASTM A630. A small section of the sample surface is sealed off and hydrochloric acid is pumped into the sealed region. A current is passed through the sample and a reverse electrolytic process results in the dissolution of tin into solution. This results in a small section (5cm radius) of the samples which is stripped of tin.

3.2.2 Sample set 2

Sample set 2 was created at Tata Steel's Trostre plant in Wales. This sample set contains surface textures within one finish and at one tin weight. The samples were collected in November 2018. As each coil was rolled, a section of the strip was cut off the end of the coil after it had passed through the mill. The section of strip cut off was the entire width of the coil. From this large section of strip, three A4 size samples were cut, one from either side of the strip and one from the centre of the strip. This process was repeated for 22 successive coils rolled by the temper mill, resulting in a total of 66 samples. As these samples were taken directly from the manufacturing line, they accurately represent surfaces that are in actual production. The roughness variant used for this was fine stone, which is an isotropic texture, created by ground textured work rolls in both stands of a 2-stand temper mill.

The reasoning behind the use of this sample set is as follows. To find correlations between surface texture parameters and surface function, it is necessary to have a consistent variation of surface texture across a specific range, to ascertain the influence of texture on the dependent surface function. For the packaging steel manufacturing process, it is impossible to get this consistent variation across a specific range due to inherent constraints of the manufacturing process. This is for two main reasons. First, there is no independent control of surface texture parameters in the manufacturing process. Second, products created in discrete finishes, only within bounded specifications

of surface texture parameter Sa. In other words, work rolls surface textures are set at beginning of production run, defined by one parameter within a specific range. However, the work roll surface texture varies across production run due to surface wear phenomena. Although this variation in surface texture is uncontrolled, it can be exploited to learn about the relationship between surface texture and the visual appearance it produces.

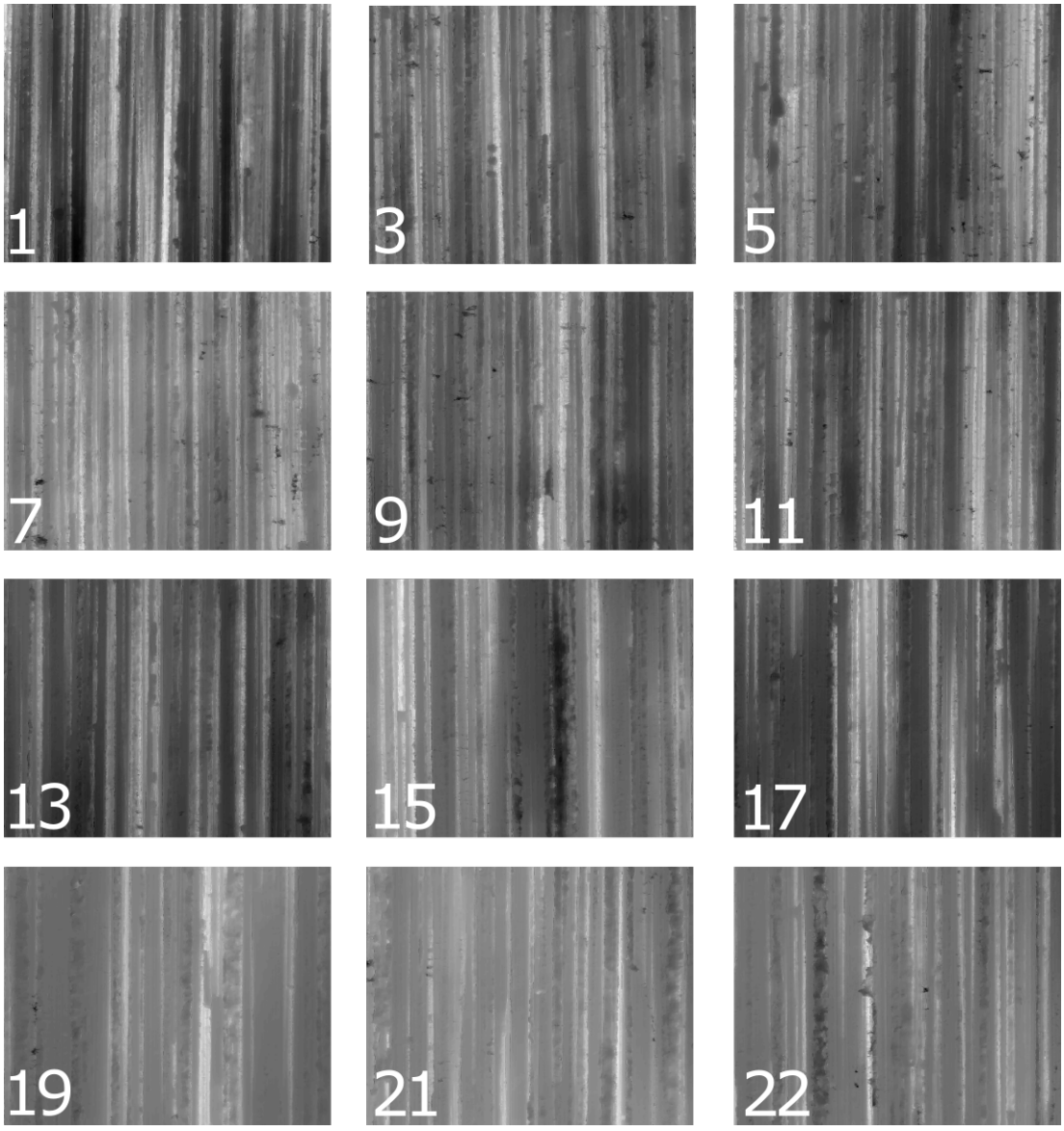

Figure 3.3: Images of samples from Sample Set 2.

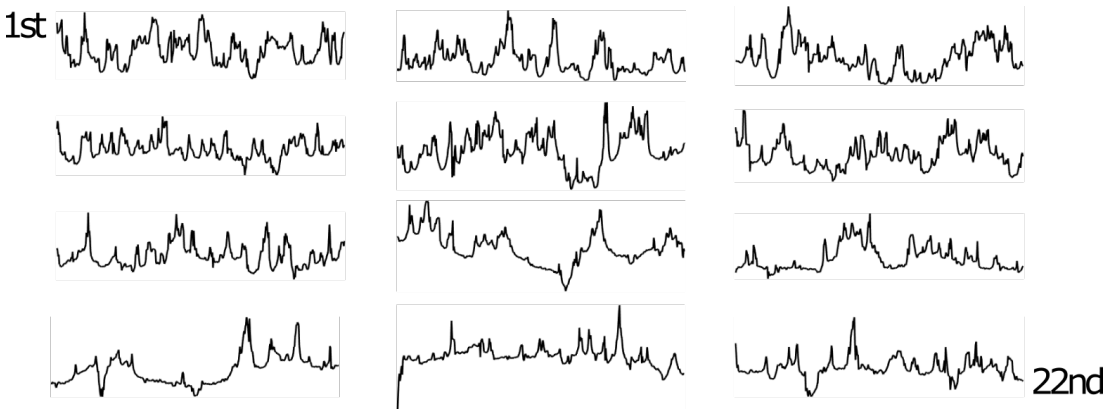

Figure 3.4: Profiles of samples from Sample Set 2. The profile labelled "1st" is the first coil rolled in the campaign, with each profile representing a successive coil until the 22nd coil rolled in the campaign.

3.3 Measurement of surface texture

3.3.1 Data collection

All surface texture measurements made in this thesis were made on a Wyko NT9300 white light interferometer. Surface texture measurements have been made at various scales. Each sample was measured in 3 locations and at 3 different magnifications. The magnifications chosen were x11, x20 and x41. These were chosen such that the widest possible width of spatial frequencies could be measured, while considering the constraints of time and over-production of data. It may be possible that spatial frequencies of interest were excluded from this range. However, as the correlations are to be made against measurements made with a glossmeter, and the internal optics of a glossmeter do not allow for discrimination at high resolution, it is expected that the range of spatial frequencies captured are sufficient to allow these correlations to be made. Ideally, measurements would be made all the way down to the highest lateral resolution available on the instrument. However, the associated small measurement size would then exclude larger features of interest. This could be overcome using stitching, however that functionality was not available on this instrument.

Table 3.1: Table shown the spatial characteristics of surface texture measurements made with Wyko NT9300 white light interferometer.

Magnification	x11	x20	x41
Measurement area [mm x mm]	0.578×0.433	0.310×0.233	0.154×0.116
Sampling length [μm]	0.903	0.485	0.241

3.3.2 Data processing

All processing of surface texture data in this thesis was done using the MatLab numerical computing environment. A mixture of custom built scripts and MatLab standard scripts were used. The process of data analysis was generally as follows:

- Process data from Wyko format (`.opd`) to MatLab readable format (`.asc`).
- Remove any tilt in measured surface texture data.
- Perform any filtering/measured surface texture data decomposition.
- Perform operations to calculate surface texture parameters or other characterisations.

Each of these processing steps is described in detail in this section.

3.3.2.1 Outlier removal

Outlier removal requires surfaces data to be normally distributed. This condition is not met by the surfaces considered in this thesis. To avoid the presence of unwanted artefacts created by impurities such as dust on the surfaces, the surface were cleaned thoroughly prior to measurement.

3.3.2.2 Tilt removal

Major tilt in surfaces is removed in their measurement, as the sample stage of the Wyko NT9300 can be adjusted in the x-y plane to compensate for tilt. Any residual tilt in measured surface data is removed by fitting a plane to the data, then subtracting that plane from the data. This script was written in MatLab by the author of this thesis. The fitting is done using MatLab's inbuilt fitting function `fit`, using a first degree polynomial.

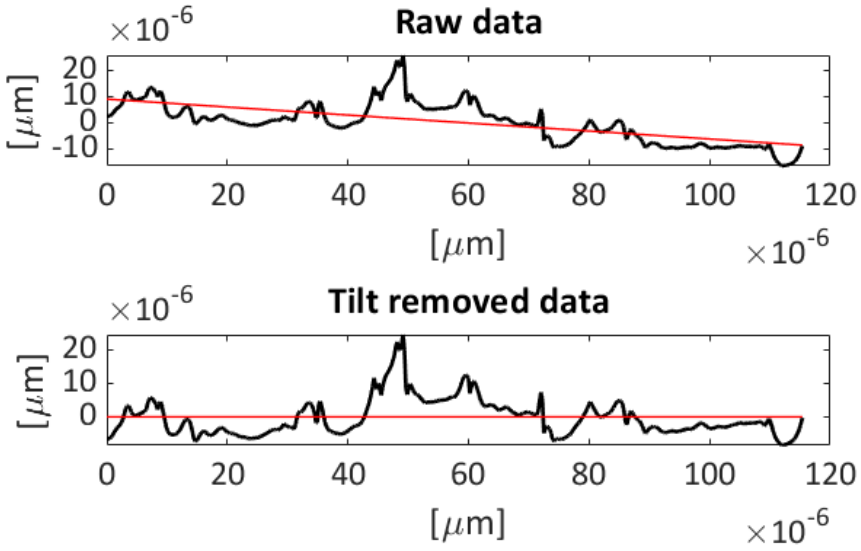

Figure 3.5: The effect of the tilt removal routine. The red line is the plane fitted to the original data in the upper figure, which is then removed from the data, resulting in the profile shown in the lower figure.

3.3.2.3 Gaussian filtering

Gaussian filters were implemented in MatLab using methods described by Muralikrishnan and Raja [51]. A high pass and low pass filter were created. The inputs for these functions are the height map to be filtered, the horizontal interval between each point of the heightmap and the cut-off wavelength. A band-pass filter was created using a high-pass filter and a low-pass filter together in succession to remove the upper and lower frequency bands, leaving the desired band of spatial frequencies. The inputs for the band-pass filter are the height map to be filtered, the horizontal interval between each point of the heightmap, the centre wavelength of the band-pass filter, and the bandwidth.

The filter script operates as follows. First a Gaussian weighting function is created according to the cut-off wavelength. This weighting function takes the shape

$$f(x,y) = \frac{1}{\alpha^2 \lambda_{xc} \lambda_{yc}} exp\left[-\pi\left(\frac{x}{\alpha\lambda_{xc}}\right)^2 - \pi\left(\frac{y}{\alpha\lambda_{yc}}\right)^2 \right] \tag{3.1}$$

where $\alpha = \sqrt{\ln 2/\pi}$ and λ_{xc} and λ_{yc} are the x and y cut-offs respectively [51]. For all purposes in this thesis $\lambda_{xc} = \lambda_{yc}$.

Then, for a heightmap $z(x,y)$, the filtered surface $z_f(x,y)$ is obtained by subtracting from the original heightmap data the convolution of the original heightmap and the weighting function as follows:

$$z_f(x,y) = z(x,y) - z(x,y) * f(x,y) \tag{3.2}$$

The convolution is performed using the MatLab function `conv2`.

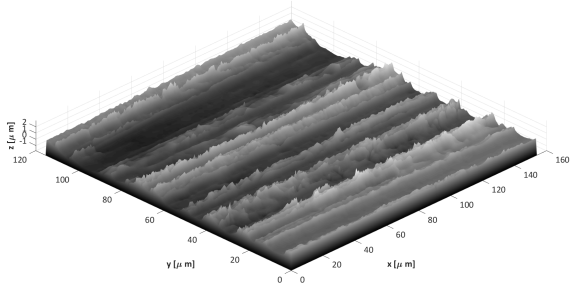

Figure 3.6: Unfiltered surface texture measurement.

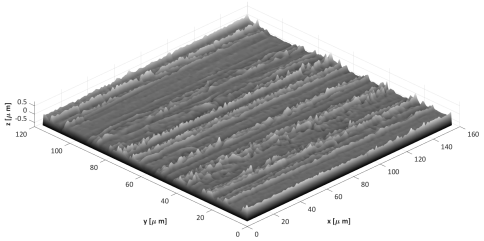

(a) Filtered surface texture measurement, band between 2 and 4 micron.

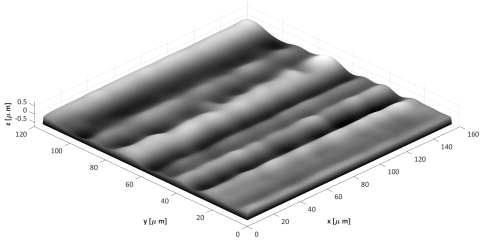

(b) Filtered surface texture measurement, band between 19 and 30 micron.

Table 3.2: Table showing the parameters of the band-pass filters used in the multi-scale analysis.

Lower bound [μm]	**Upper bound [μm]**	**Centre wavelength [μm]**	**Bandwidth [μm]**
0.5	1.5	1.0	1.0
2.0	4.0	3.0	2.0
5.0	10.0	7.5	5.0
11.0	18.0	14.5	7.0
19.0	30.0	24.5	11.0
31.0	45.0	38.0	14.0
46.0	62.0	54.0	16.0
63.0	80.0	71.5	17.0
81.0	101.0	91.0	20.0
103.0	126.0	114.5	23.0
128.0	155.0	141.5	27.0
159.0	190.0	174.5	31.0
195.0	230.0	212.5	35.0
235.0	290.0	262.5	55.0

3.3.3 Data characterisation

Surface data was characterised using a number of different surface texture parameters. For calculation of surface parameters from heightmaps, the discretised versions of the formulas were used. These parameters are described in Section 2.3.4. Matlab scripts were written for parameters Sa, Sq, Ssk, Sku, and Sdq parameters, as well as their profile equivalents. These parameters were chosen because of their functional capabilities as described in Chapter 1.

3.4 Measurement of visual appearance

As described in the literature review section of this thesis, the scattering of light from a surface can be described by the BRDF. The BRDF of a surface can be measured by a goniophotometer which measures the intensity of reflected light across the full angular domain of the upper hemisphere. A glossmeter measures a subset of this domain. A glossmeter was used for all measurements of visual appearance in this thesis. For

visual appearance measurements carried out in this thesis, a Rhopoint IQ glossmeter was used.

The Rhopoint IQ uses an array of 512 diodes to capture the reflected light from the surface, meaning the machine does not only report values for gloss, haze etc, but also records the angular distribution of light from $\pm 7.5^\circ$ from the specular angle. These curves will be referred to as reflection distribution functions (RDF). Examples of these curves can be seen in Figure 3.9. Figure 3.8 shows the diode array setup for the 20° geometry.

For all measurements made in this thesis, the glossmeter was calibrated against a high gloss "mirror" calibration tile. This tile is defined in standard ASTM E430–05. It is made of aluminium evaporated onto glass substrate, coated with a protective layer. The specular gloss at 20° of this tile is defined to have the value of 1656 gloss units. All other measurements of specular gloss are then made relative to this value.

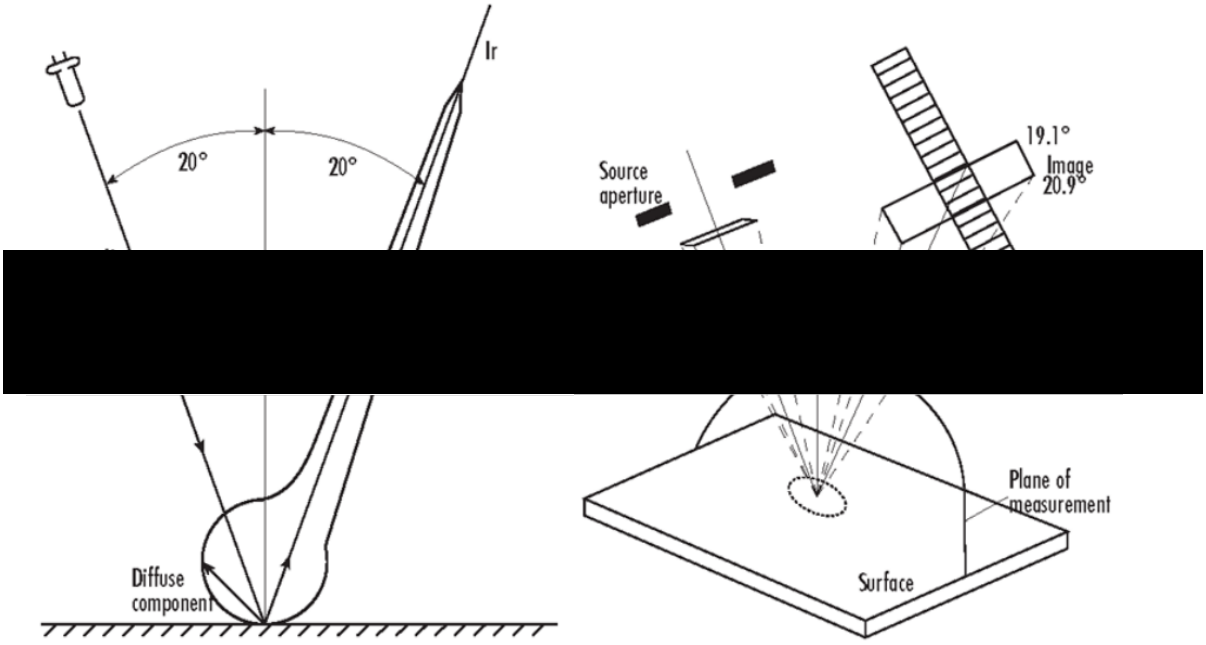

Figure 3.8: The 20° geometry of the Rhopoint IQ glossmeter. The LDA (Linear Diode Array) lies in the plane of measurement. The distribution of light falling across the LDA creates the Reflection Distribution Function (RDF) [80].

Visual appearance parameters are then derived from the RDF. Gloss is defined as the sum of the recorded reflectivity in the range $\pm 0.9^\circ$ around the specular angle. Haze is similar, but the summation is across the angles $-1.0^\circ \rightarrow -2.0^\circ$ and $1.0^\circ \rightarrow 2.0^\circ$. These definitions are taken from the Rhopoint user manual, which adheres to ISO . It is also possible to derive other parameters to characterise other aspects of the RDF,

which my be more or less relevant depending on the application. For example, the RSpec parameter which characterises the very peak of the distribution, across an even narrower range than the gloss parameter, and the distinctness of image (DOI) parameter which characterises the ratio between peak and shoulders of the distribution.

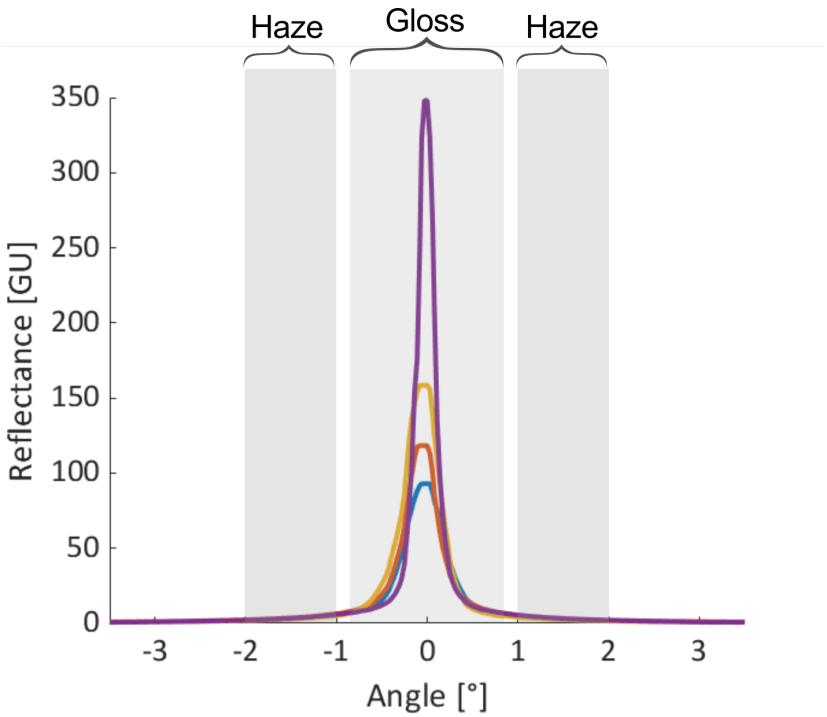

Figure 3.9: An example of various reflection distribution functions from different surfaces measured with the Rhopoint IQ glossmeter. The purple line has much higher reflectance at the specular angle, which results in a higher value of gloss. The shaded areas show which regions of the RDF contribute toward the gloss and haze parameters.

Unless otherwise stated, all measurements of visual appearance were performed in two directions, in the rolling direction of the strip and across the rolling direction. For each direction, 5 measurements were made and the mean was taken. Then the mean of the measurement in the rolling direction and the measurement across the rolling direction was taken.

3.5 Summary

In this chapter, the materials used in this thesis have been described. The methods used to capture, process and analyse data have also been described.

The two sets of surfaces described in this chapter are used to gain insights into the surface texture of packaging steel. One sample set is used to gain information about different surface finishes and surface coating and the other set is used to investigate the

underlying substrate of one finish in higher detail.

Two types of data are presented in this thesis, surface texture data and visual appearance data. The surface texture is measured with a WYKO white light interferometer and the visual appearance data is measured with a Rhopoint IQ glossmeter.

The overarching aim of the work described in this thesis, presented in the next chapters, is to find correlations between these two data types.

Chapter 4

Substrate

4.1 Overview

In this chapter, the substrate of tinplate packaging steel is investigated. Measurements were made of surface texture and visual appearance of packaging steels and correlations between the two sets of measurements were made. The surface texture of Sample Sets 1 and 2 were measured using white light interferometry and characterised using various techniques. First, standard non-multiscale characterisations are shown, followed by multi-scale characterisations of the substrate texture. The visual appearance of the samples was measured with a glossmeter, and the relationship between the substrate texture and the visual appearance was investigated, using both standard and and multi-scale methods. The intention behind this work was to characterise the types of surface textures used in the packaging industry, as well as the visual appearance produced by those textures, and to ascertain the influence of different spatial wavelengths on the visual appearance of the substrate. The multi-scale analyses carried out in this chapter were used due to the success of similar methods in discovering the functional bandwidths of surface texture as outlined in the literature review.

This chapter is structured in three sections. In the first, the characterisation of substrate texture is described, in the second the visual appearance, and in the third the correlations between the two sets of measurements.

4.2 Characterisation of surface texture

In this section the surface texture of the uncoated substrates of Sample Set 1 & 2 are described. All surface texture measurements were made on the Wyko NT9300 white light interferometer as described in Chapter 3.

4.2.1 Standard characterisation

In this section, all parameters were calculated after first performing a tilt removal operation the data, then filtering to obtain the roughness data. This was done by first filtering the data with a low pass Gaussian filter at a cut-off of $0.8\mathrm{mm}$, then subtracting the resulting waviness data from the original raw data. This operation is a standardised method for calculating surface texture parameters according to ISO 16610 [50]. A number of surface texture parameters were then calculated for each surface from this

roughness data.

4.2.1.1 Sample set 1

The samples of Sample Set 1 were taken once the coating process had already been carried out, and no uncoated material was available. Therefore, these measurements were made on surfaces that were first coated, before having the tin coating removed. The tin removal process may have an effect on the surface texture, such that the texture post-removal is different to the texture pre-coating. The extent of this difference is not known. The cause of this effect on surface texture is the corrosive nature of the tin removal and the subsequent rapid oxidation of the unprotected steel substrate.

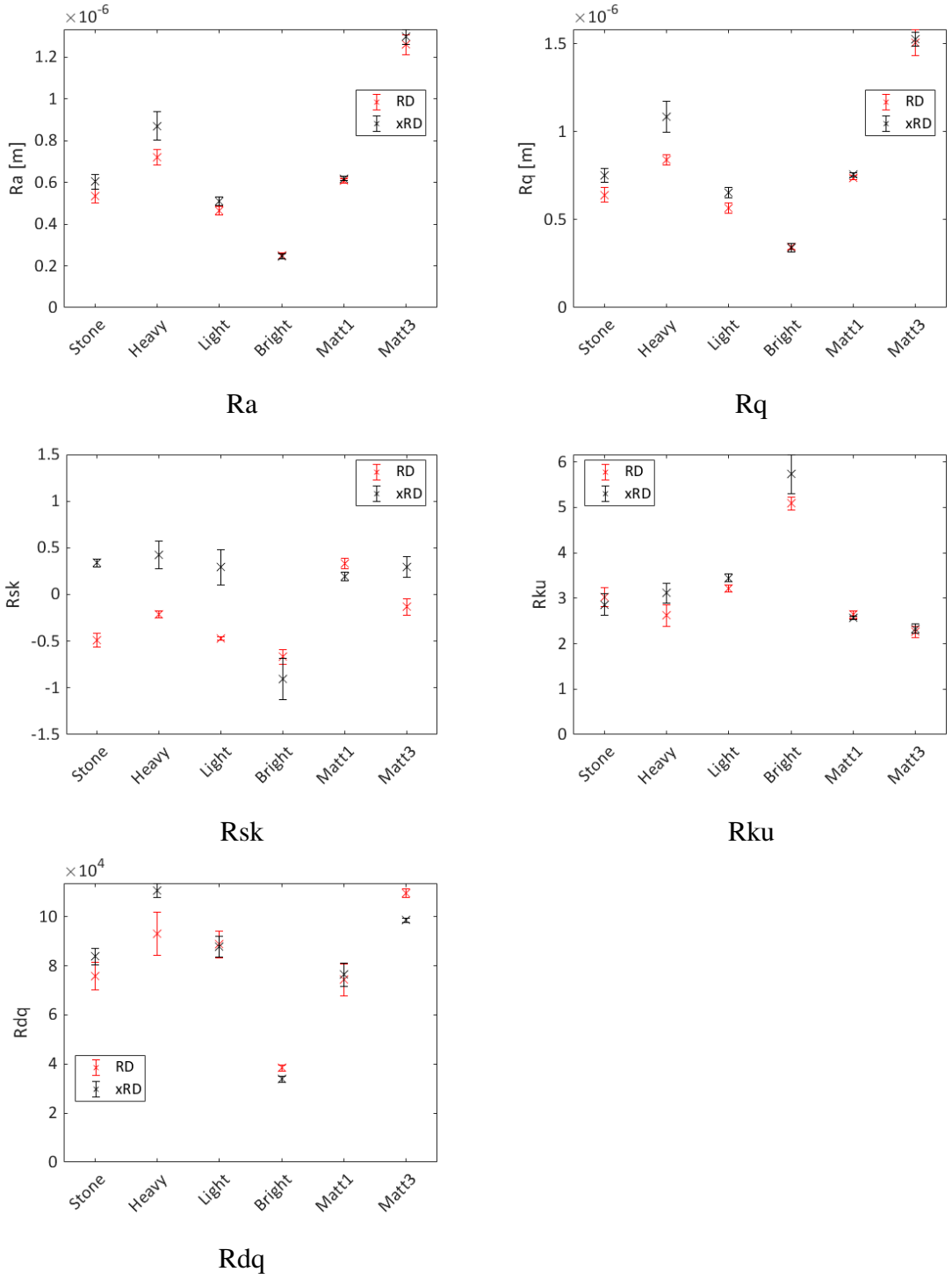

Figure 4.1: Surface texture parameters for Sample Set 1, calculated for surface profiles, both across and along the rolling direction. Parameters calculated along the rolling direction are denoted with 'RD' and parameters calculated across the rolling direction are denoted with 'xRD'.

Figure 4.1 shows the surface texture parameters of the surfaces in Sample Set 1. These plots show the values of surface texture parameters for a number of different surface finishes, calculated both across and along the rolling direction. From this, the differences and similarities between the finishes can be observed.

The anisotropic (ground) surfaces exhibit directionality in the surface texture which can be observed in the differences between the values of parameters along and across the rolling direction. Isotropic (shotblast) surfaces do not display the same behaviour, with parameter values near equal for measurements taken across and along the rolling direction. An immediate observation is the relative similarity between several of the parameters. The Ra, Rq, and Rdq parameters all follow the same pattern. When one is high, so are the others, when one is low, so are the others. This shows a coupling between the surface parameters. The coupling between Ra and Rq is already well known and is a feature of the method of calculating the parameters [5]. They are both measures of the distributions of surface heights (with Ra being the mean and Rq the standard deviation).

The coupling between Ra and Rdq implies that

a) these parameters are characterising similar aspects of surface texture or

b) the manufacturing process is unable to independently control any of these parameters.

4.2.1.2 Sample set 2

In this section, all parameters were calculated in the same way as for Sample Set 1 in the previous section. Figure 4.2 shows the surface texture parameters for Sample Set 2.

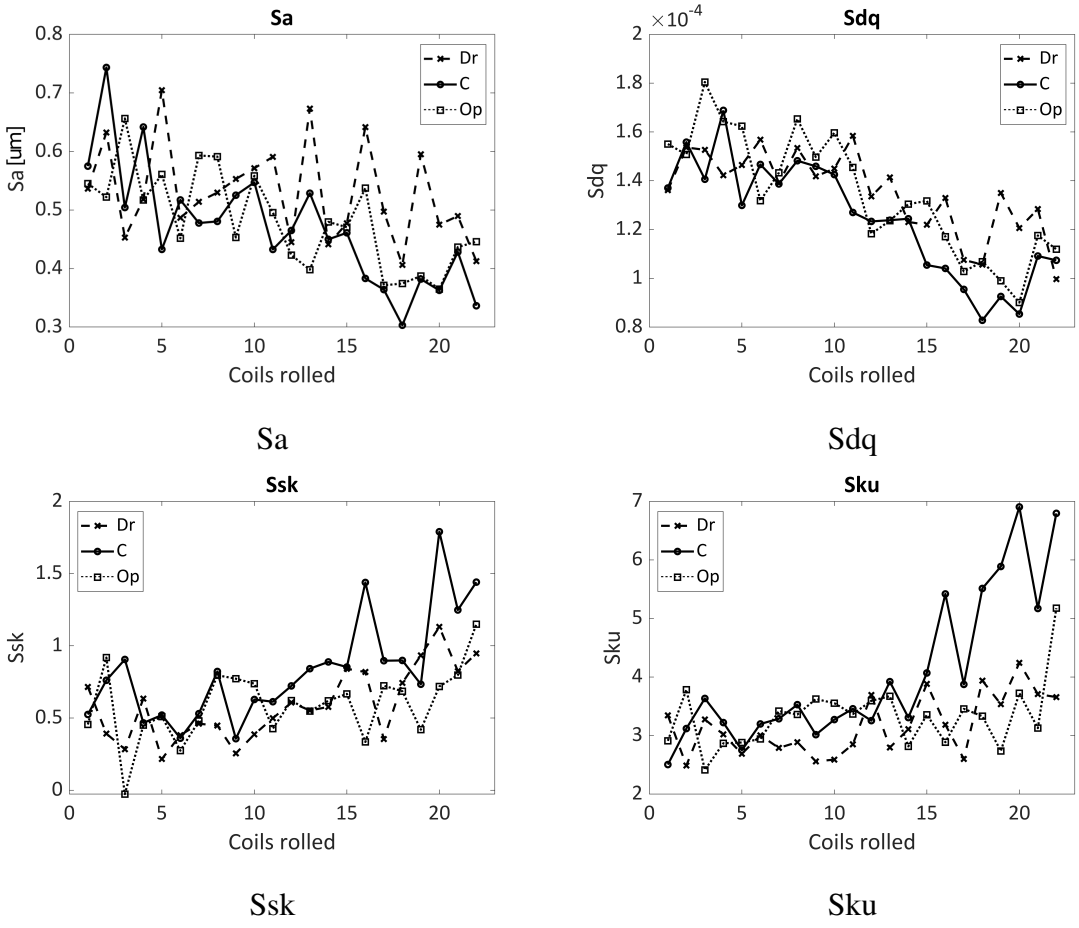

Figure 4.2: The surface texture parameters for Sample Set 2. The legend indicates Dr/C/Op, which denotes drive side, centre and operator side respectively. These show the locations on the strip from which the samples were taken, whether from the edges (Dr/Op), or from the centre (C).

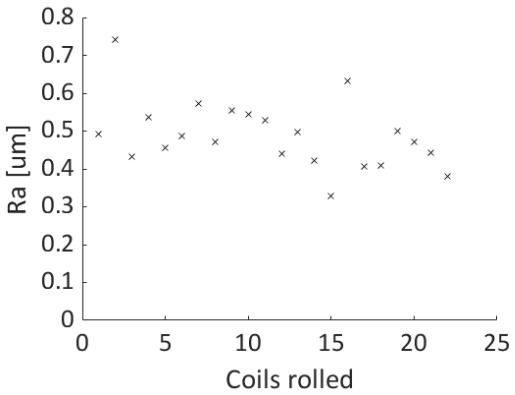

Figure 4.3: The Ra with a 0.8 mm high-pass cut-off at magnification of X11 to replicate as closely as possible the measurements made by profilometers on the production line.

Figure 4.3 shows the Ra of the 22 coils of Sample Set 2. The parameters were calculated for samples taken from the centre of the strip, across the rolling direction, with a Gaussian high-pass filter at 0.8 mm, taking a mean of 3 measurements. The majority of the coils fall within the 0.25 - 0.5 $\mu\mathrm{m}$ Ra specification for the Fine Stone finish.

There a several possible reasons for the outliers, the main reason being that a different measurement system was used from that normally used on-line. A profilometer operates with a different mechanism than the interferometer used for these measurements, meaning a different measured surface would be produced. However the measurements presented in Figure 4.3 suffice for illustrative purposes and show that there is no large and obvious difference in measurements across the length of roll campaign, with only a slight overall decrease visible. This shows that the measurement of Ra used in the production process cannot pick out the same changes in topography that are possible using finer scale measurements, areal measurements and other parameters, such as those presented in 4.2.

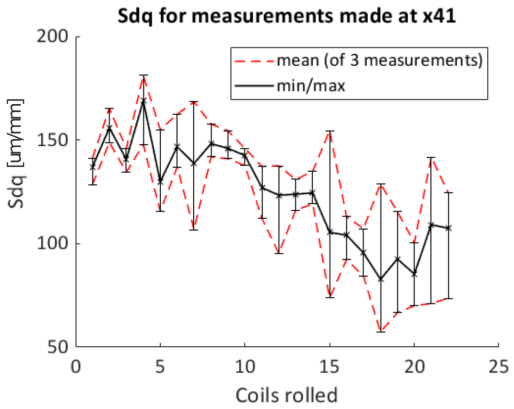

Figure 4.4: Sdq - root mean square slope, showing mean and the spread of 3 measurements.

In Figure 4.2 it can clearly be seen that the surface texture changes with coils rolled. The root mean slope parameter Sdq decreases with coils rolled. This can be explained by the wear mechanisms of rolling. As the strip is rolled, material on the roll surface experiences forces causing deformation of the surface features. This results in a smoothening of the surface features and therefore a drop in the value of Sdq.

In addition to this, Figure 4.4 shows that as the roll campaign progresses not only does the Sdq decrease but the spread within each coil also increases. This shows that as the rolls wear, the level of control over surface texture decreases. This increase in the spread of the values of Sdq indicates a 3 stage process of roll wear. In the first stage, the roll surface maintains its integrity and there is not a large variation in the parameter across coils rolled, and no large spread in parameter value within a single coil. The roll surface is resistant to large changes to its topography. In the second stage, the roll surface loses its integrity. Large variation in surface texture parameters can be observed across a relatively small number of coils. In the third and final stage,

it appears that the roll surface reaches another equilibrium state, in which there are not large variations in average parameter values. However, there is large variation of parameter values within each coil, showing that surface has degraded and control over surface texture has been lost.

Comparisons between the sample sets indicate that the tin removal process does have an effect on the surface texture. The finish from Sample Set 1 most suitable for comparisons with Sample Set 2 is the 'Stone' finish. These two finishes have similar values of Sa (at least at the start of the roll campaign for Sample Set 2), however the values of Sdq are very different. Whether this is due to the nature of the texture or due to the tin layer removal process is impossible to say with certainty. However, when considering the nature of the Sdq parameter, the discrepancy between levels of Sdq points to an increase in the variation of the surface slopes at the shortest bands of spatial wavelength.

Due to the way in which the Sdq parameter is calculated, it is sensitive only to the smallest scales of surface texture. For example, the Sdq would be calculated in the same region as only the first point in Figure 4.6. When the parameter is calculated from measured surface data, it will return a measure of only the highest spatial frequencies contained in the measurement. This is because the parameter is calculated from the surface slopes at each point determined by a 7 point central difference [5]. The scale at which the slope is calculated is on the order of $6h$ where h is the horizontal sampling interval. For example, for the X41 magnification surface data used in this thesis, $h = 0.2409$ µm and the total lengths of the measurement are 116×154 µm. For these measurements, the Sdq is calculated at a scale of 1.45 µm along a profile and 2.15 µm^2 across an area (for a total measurement area of 1780 µm^2. In fact, the central 3 points are more heavily weighted therefore more significant in the calculation, so the true scale is somewhere closer to $2h$). In other words, the Sdq parameter measures only some of the the highest frequency components of the surface data. Note also that this is the surface content most heavily affected by measurement noise and uncertainty. The fact that the Sdq is so much higher for the 'Stone' finish of Sample Set 1 compared to the first coil of Sample Set 2 implies that these bands of surface data are heavily influenced by the detinning process.

A final comment on these results is with regard to wear. All parameters vary with coils rolled but also across the width of the strip. Values of surface texture parameters for Dr/C/Op are different. This is because the forces of the roll on the strip vary across

the strip, resulting in a different texture being imparted from the roll to different regions of the strip. This reiterates the findings of Landskroon who states that differences in surface texture across the strip result in large and easily discernable differences in visual appearance across the strip [45].

4.2.2 Multi-scale characterisation of surface texture

In this section some of the parameters examined in the previous section are decomposed across scale. This was done by using a Gaussian band pass filter to select discrete bands of spatial wavelengths then calculating the parameters for each of those bands. The parameters chosen are the mean amplitude of roughness Sa and root-mean-square slope Sdq. Most models of visual appearance use some measure of the roughness amplitude (either Sa or Sq) as a basis for the prediction of visual appearance, and the Sdq parameter is cited in literature as a good candidate for a parameter which controls visual appearance [10]. The analysis was based on the work of Jacobs et al. and Mezghani et al. as described in Section 2.3 of the literature review.

4.2.2.1 Sample set 1

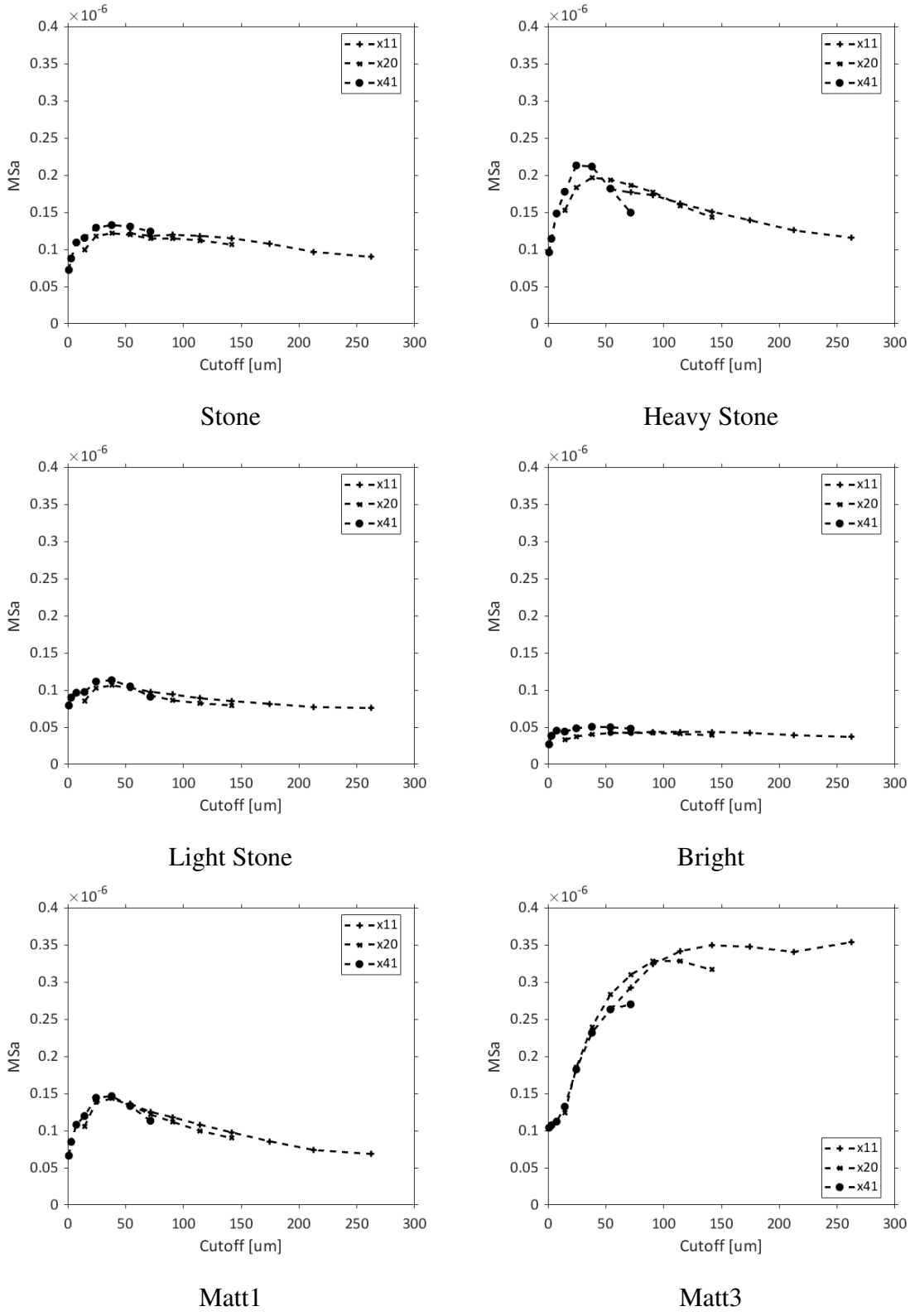

Figure 4.5: The Multiscale average roughness amplitude MSa for surfaces from Sample Set 1. The units of the y-axis are metres.

The plots in Figure 4.5 show the amplitude of roughness expanded across scale for the six different finishes of Sample Set 1, for the detinned substrate surfaces. In the literature review, the method of Jacobs et al. of deriving the 'master-PSD' by stitching together measurements of the PSD across multiple scales to achieve a PSD that spans a larger range of surface wavelengths was described. Also described was the work of Mezghani et al. who calculated the multi-scale attenuation function (MAF) of painted surfaces using the standard surface texture parameters decomposed across scale. In this piece of work, the stitching method of Jacobs et al. has been combined with the multi-scale parameter approach of Mezghani et al. [59, 77]. Results from measurements made at three different magnifications have been collated to form the 'master-MSa' for each finish. This was done in order to get the widest possible multi-scale profile of the surface textures. The general principles of Jacobs et al. outlined in the literature review were followed which resulted in generally good overlap of the plots across magnifications. The decomposition within each magnification was carried out using bandpass Gaussian filtering at different wavelengths and bandwidths. The values of wavelengths and bandwidths are found in Table 3.2.

In general, the MSa is lowest at shortest wavelengths, rises to a peak at what could be termed a characteristic wavelength, before decreasing again at longer wavelengths. The characteristic wavelength is the band of surface texture with highest amplitude, which means that features of those sizes dominate the topography. This characteristic wavelength band is a function of the manufacturing process. For the anisotropic surfaces of Sample Set 1, the characteristic wavelength would be related to the size of grit used in the grinding wheel, and the cutting depth of the wheel, which create a series of peaks and valleys in the surface at a size comparable to the characteristic wavelength. For the isotropic surfaces the characteristic wavelength would be related to the size of the shot used in the shot blasting of the surface, and the force of impact, which creates a cratered surface, which the craters having a size comparable to the characteristic wavelength. For the surfaces in Figure 4.5, for both ground surfaces and SBT surfaces, the characteristic wavelength appears to be on the order of $40\mu\mathrm{m}$.

The two exceptions to this are the 'Bright' and 'Matt3' finishes. These are both isotropic finishes created by SBT, one of very low average amplitude and one of very high average amplitude. Neither of these surfaces have a band of surface wavelengths within which the surface has a degree of prominence over neighbouring bands.

For the anisotropic surfaces (Stone, Heavy Stone, Light Stone), although the char-

acteristic wavelengths are all at a similar wavelength, the relative prominence of the peak to neighbouring bands is different for each of the surfaces. This may be explained in terms of the mechanisms of surface grinding. The characteristic wavelength is determined by the size of the grit in the wheel. This determines the distance between peaks and valleys in the horizontal. The relative prominence is determined by the cutting depth. The determines the distance between the heights of the peak and valleys in the vertical.

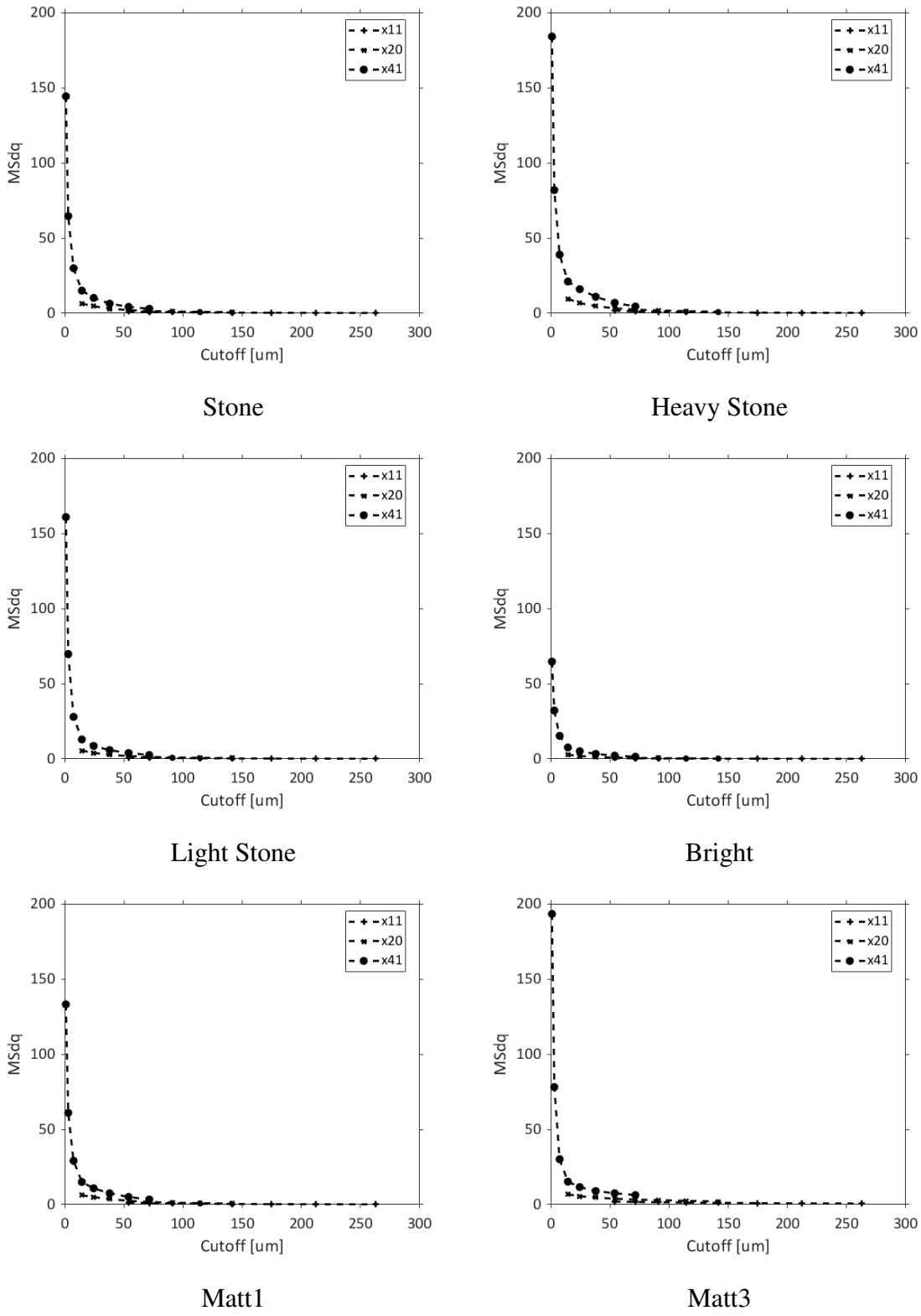

Figure 4.6: The multiscale root-mean-square gradient MSdq for the surfaces of Sample Set 1. The units of the y-axis are $[\frac{\mu m}{mm}]$.

The plots in Figure 4.6 show the root-mean-square slope Sdq of Sample Set 1 decomposed across scale, labelled 'MSdq' to denote multi-scale root-mean-square slope. The same method as that used to calculate the plots of MSa in the previous section was

used to calculate these plots.

Figure 4.6 shows that in general, for all finishes, the mean surface slope is relatively high at short wavelength scales ($\lambda < 30\mu m$) compared to at longer wavelengths. At the longest wavelengths, the Sdq tends to zero. Figure 4.5 shows that these same regions of surface texture have relatively low amplitude. In other words, the same bands of surface data have high MSdq and low MSa. These results show a region of low amplitude but quickly varying "noisy" surface variations, for all finishes.

4.2.2.2 Sample Set 2

Figures in this section were created with the same methods as those in Section 4.2, applied to Sample Set 2. Sample Set 2 is a set of 22 samples of Fine Stone material taken from successive coils rolled on a temper mill. In these figures, the x-axis again represents the scale and the y-axis represents the parameter value, however each line represents the parameter value of a single coil, with colour representing the number of coils rolled in the campaign. Lighter colour represents coils toward the start of the roll campaign, darker colour indicates coils toward the end of campaign. In this way, the surface texture evolution can be seen across both scale and number of coils rolled. Figures 4.7 and 4.8 show the surface texture evolution only for measurements taken from the centre of the strip and for the X41 magnification.

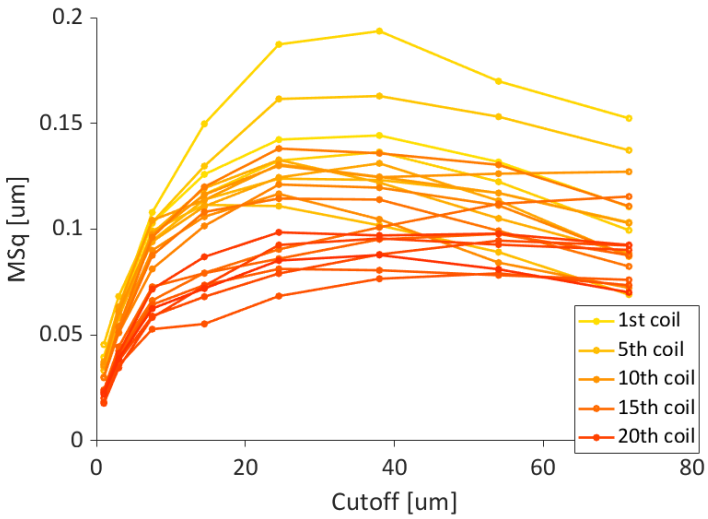

Figure 4.7: Multi-scale decomposition of root mean square amplitude.

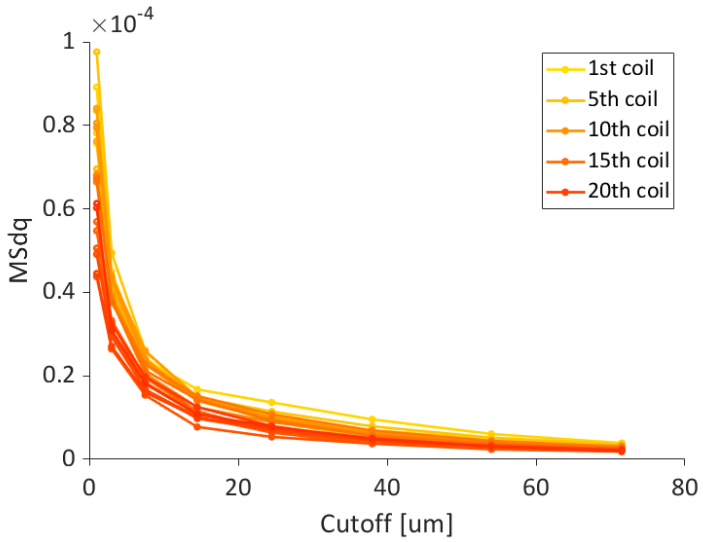

Figure 4.8: Multi-scale decomposition of root mean square slope.

The overall shape of the curves follow the same general pattern as that observed in Sample Set 1, with MSa starting from a minimum, rising to a maximum at about $40\mu m$ and then decreasing. The shape of the MSa curve changes over the course of the roll campaign, with the prominence of the characteristic wavelength peak being reduced. MSdq also follows the same general pattern as that observed in Sample Set 1, with the highest value at the smallest wavelength, tending to zero at longer wavelengths. The evolution of MSdq over the roll campaign can clearly be seen, with the biggest changes in MSdq occurring at the smallest scales. The shows that the mechanisms of wear have largest effect on the surface slopes at smallest scales. It is important to note that the surfaces of Sample Set 2 differ from those of Sample Set 1 in that they were never coated, therefore did not go through the tin removal process. Therefore the uncertainties related to the modification of surface texture by that process do not apply to the results presented in this section.

These results help build the picture that is developing of the scales of interest for packaging steel. There are two bands of interest, that of the local prominence of surface texture and that at the smallest scales of surface texture. The local prominence acts as a finger print of the manufacturing process. The surface data at smallest scales is most unreliable and also most heavily affected by uncontrolled aspects of the manufacturing process, such as wear.

4.3 Characterisation of surface function

One of the main purposes of surface metrology is to use the topographic information to assess the functionality of the material surface. In this case the function is visual appearance. In this section, measurements of the visual appearance of packaging steel substrate are shown. No measurements of visual appearance were made on the detinned surfaces of Sample Set 1, so the results in this section are for Sample Set 2 only.

4.3.0.1 Sample Set 2

All measurements in this section were made on Sample Set 2 with the Rhopoint IQ glossmeter. Measurements were taken along the rolling direction and across the rolling direction. Five measurements were taken for each orientation and the mean was taken.

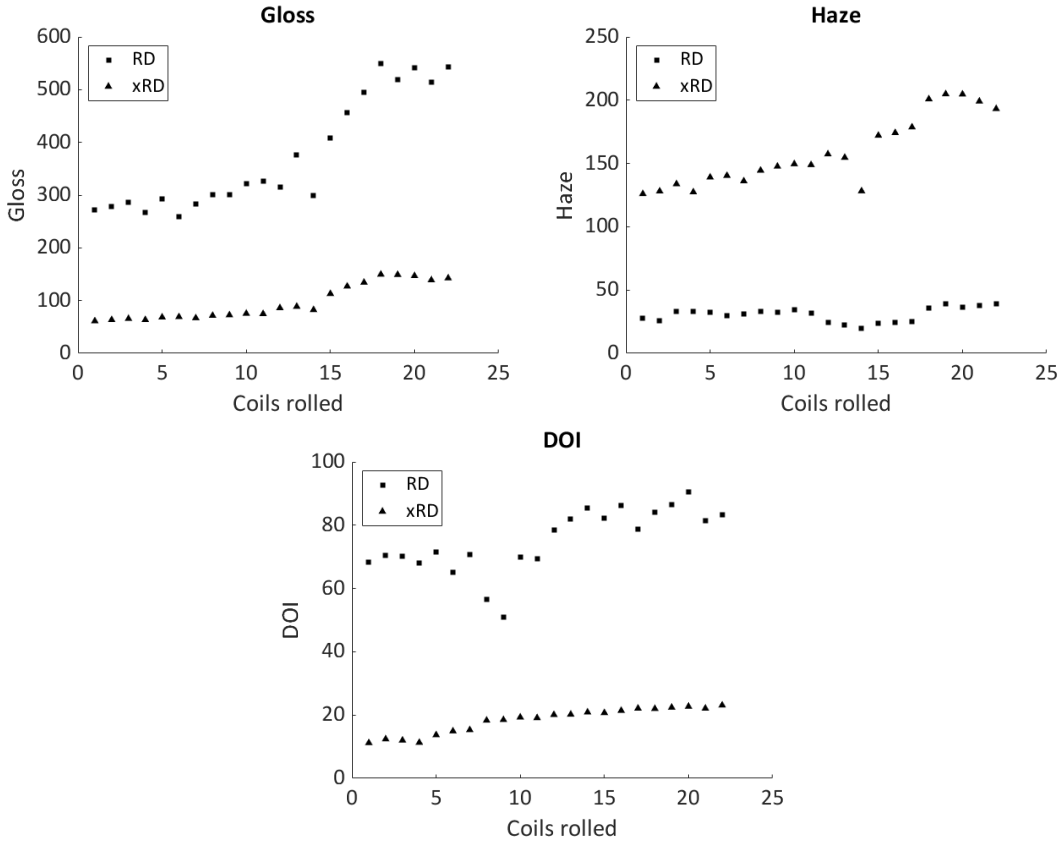

Figure 4.9: These figures show various visual appearance parameters measured both across and along the rolling direction. RD denotes measurement made in rolling direction, xRD denotes measurement made across rolling direction. The surfaces measured here were taken from the centre of the strip.

Figure 4.9 shows the evolution of visual appearance parameters as the roll campaign progresses. The immediate observations are that there are large differences in

visual appearance parallel and perpendicular to the rolling direction and that the visual appearance of the strip (as measured by a glossmeter) changes dramatically as the roll campaign progresses.

The gloss (at 20°) along the rolling direction is much higher than the gloss measured across the rolling direction. The gloss along the rolling direction doubles from a value of 270 GU to a value of 540 GU. The increase in gloss across the rolling direction is much less in absolute terms but similar in relative terms, as it also doubles.

Contrary to the gloss, the haze across the rolling direction is much higher than the haze along the rolling direction. There is a marked increase in the haze across the rolling direction, whereas the haze along the rolling direction remains relatively stable along the entire roll campaign.

For the DOI, increases in the parameter value can be observed for measurements made both along the strip and across the strip. The values of DOI are much higher along the strip than across it.

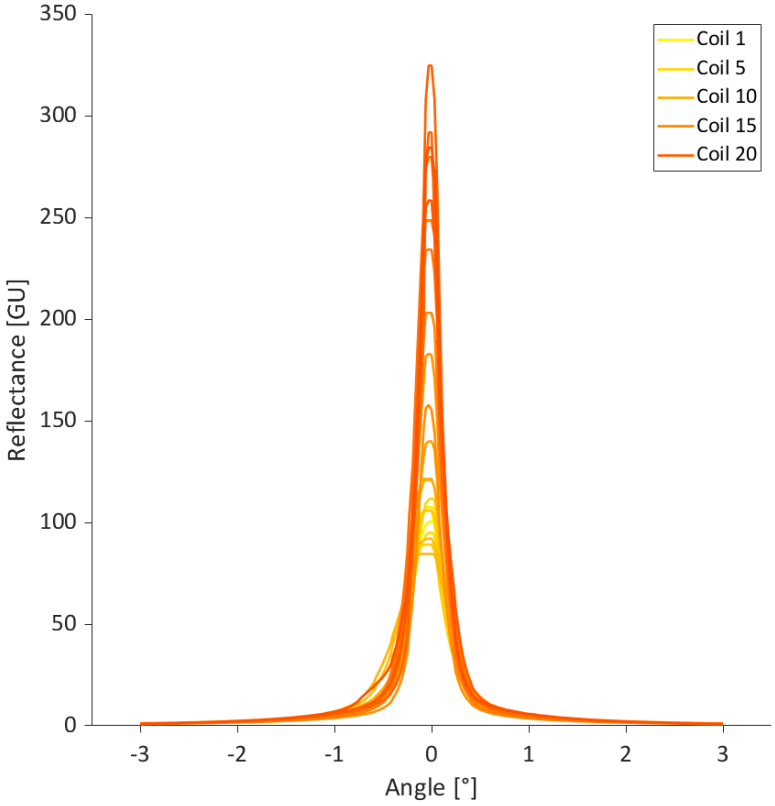

Figure 4.10: The RDFs of surfaces of Sample Set 2, showing the development of reflectivity of the surfaces over the length of the roll campaign. The surfaces were taken from the centre of the strip and measured with a glossmeter along the rolling direction. Each curve is the mean of five measurements.

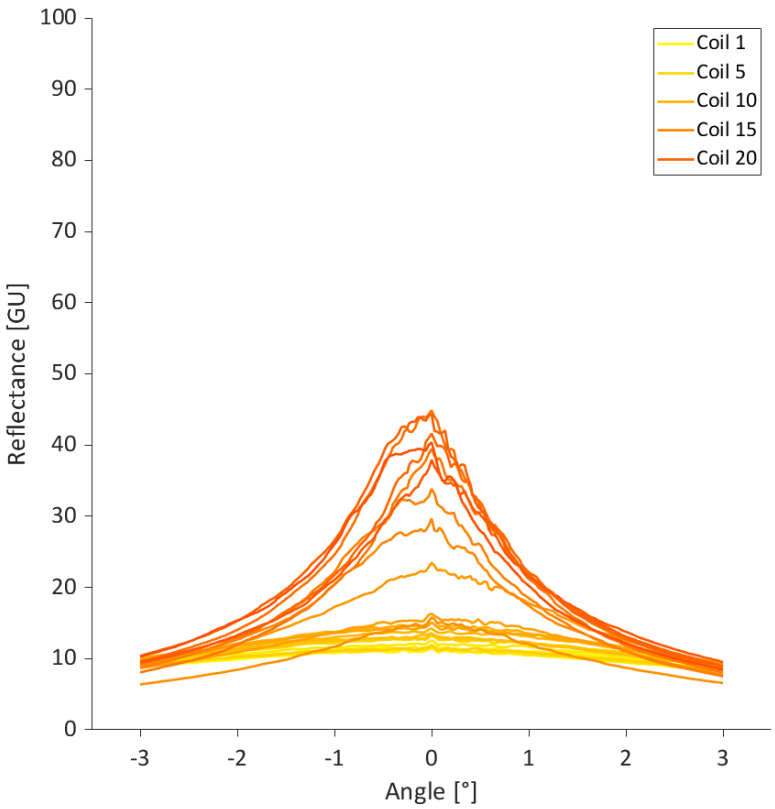

Figure 4.11: The RDFs of surfaces of Sample Set 2, showing the development of reflectivity of the surfaces over the length of the roll campaign. The surfaces were taken from the centre of the strip and measured with a glossmeter across the rolling direction. Each curve is the mean of five measurements.

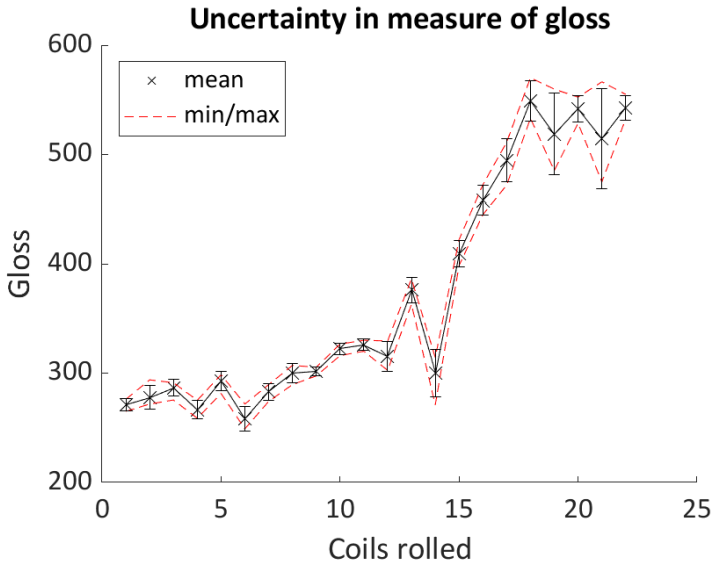

Figure 4.12: The gloss of surfaces of Sample Set 2, measured parallel to the rolling direction. The solid black line shows the mean of 5 measurements, the dashed red lines show the minimum and maximum of the 5 measurements.

The evolution of these parameters can be observed directly from the changes to the

shape of the reflection distribution curves. Figures 4.10 and 4.11 show this. Starting with the measurements made along the rolling direction, which can be seen in Figure 4.10, the increase in gloss can be seen in the increasing amplitude of the curves in the specular direction (i.e. at $0° \pm 0.9°$). The relative stability in the haze as measured along the rolling direction is shown by the small fluctuations in the shoulders of the peaks in the haze regions of $-2° \rightarrow -1°$ and of $1° \rightarrow 2°$. For measurements made across the rolling direction, seen in Figure 4.11, the increase in the amplitude of the RDF in the haze regions is now visible. Note the difference in the range of the y-axis of the two figures.

Figure 4.12 shows the effect of the loss of surface integrity, as described in Section 4.2.1.2, on visual appearance parameters. Not only do surface texture parameters change over the course of the roll campaign, with a correlated effect on visual appearance, but the deviation in visual appearance parameters at the end stages of the run is greater than in earlier stages. In other words, there is more variability in the visual appearance of packaging steel substrate as a roll campaign progresses due to the wear processes that take place during rolling.

4.4 Correlations

The aim of the work in this section was to establish the relationship between the substrate texture and the visual appearance of the surface. The aim was to determine how the surface features are responsible for the creation of surface appearance.

The work contained in this section uses the measurements made of surface texture and visual appearance from Sample Set 2, already presented in earlier sections of this chapter. Two analyses were carried out on this data. The first was a standard exercise to determine correlations between surface texture parameters calculated from the raw height field data and the visual appearance parameters. No filtering of the surface data was done for this analysis. The second analysis was a multi-scale analysis in which the surface data was filtered with several different filters and filter settings. Surface texture parameters calculated from the filtered surface data were then correlated against surface texture parameters to determine the dependency of the strength of correlations on the spatial frequencies of the surface. The first analysis was carried out for two reasons. First, to determine parameters of interest which could be investigated in more detail in the multi-scale analysis. Second, to provide a benchmark against which the

multi-scale analysis can be compared. The aim was to determine if by filtering the data, tuning out non-pertinent spatial frequencies, increases the strength of correlations between surface features and surface functionality, thereby determining the functional bandwidths of surface texture.

4.4.1 Standard correlations of surface texture and surface function

The results in this section were obtained by correlating the surface texture parameters from Sample Set 2 with their corresponding visual appearance parameters. The surface texture parameters were calculated from raw surface data measurements. The parameters used for this analysis were: Sa, Sq, Ssk, Sku, Sdq. Also, the profile versions of these parameters were calculated (Ra, Rq, Rsk, Rku, Rdq). These parameters were calculated along the rolling direction and across the rolling direction. No filtering was applied to the surface data, however a tilt removal operation was performed. The measurements were made with the Wyko NT9300 at 41X magnification.

The visual appearance measurements were made with the Rhopoint IQ. The visual appearance parameters used were: gloss at $20°$, $60°$ and $85°$, haze, DOI and RSpec. These parameters were measured both along and across the rolling direction.

The visual appearance parameters were then plotted against the surface texture parameters and a exponential fit used to determine the R^2 regression coefficient. Note, the MatLab routine used to calculate R^2 returns negative values when the fit type used (in this case an exponential) produces a worse fit than a straight line would. The exponential function is commonly used in the literature to model the relationship between surface texture parameters and visual appearance [9, 81, 82]. This regression analysis was carried out for the directional parameters across and along the rolling direction. These are denoted by the labels 'RD' for along the rolling direction and 'xRD' for across the rolling direction. Areal surface texture parameters were regressed against the mean of the visual appearance parameters along and across the rolling direction.

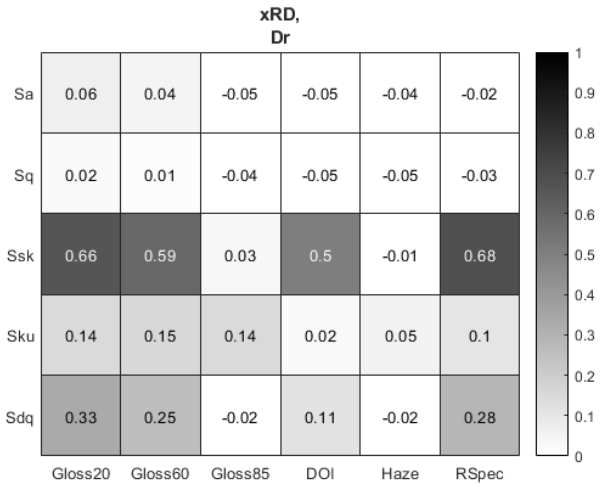

Figure 4.13: Correlations across the rolling direction, for samples taken from the edge of the strip, on the Drive side (Dr).

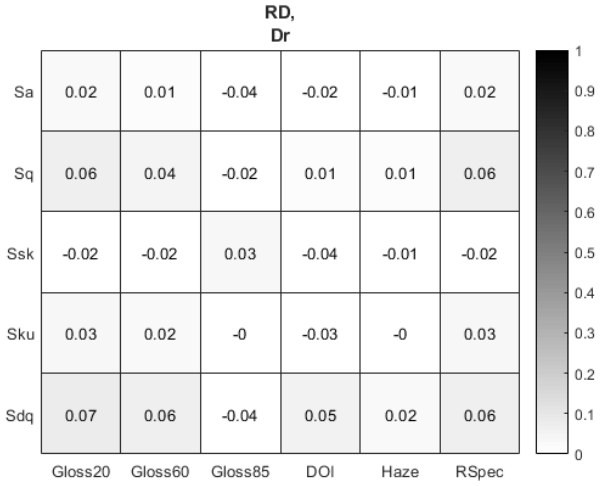

Figure 4.14: Correlations along the rolling direction, for samples taken from the edge of the strip, on the Drive side (Dr).

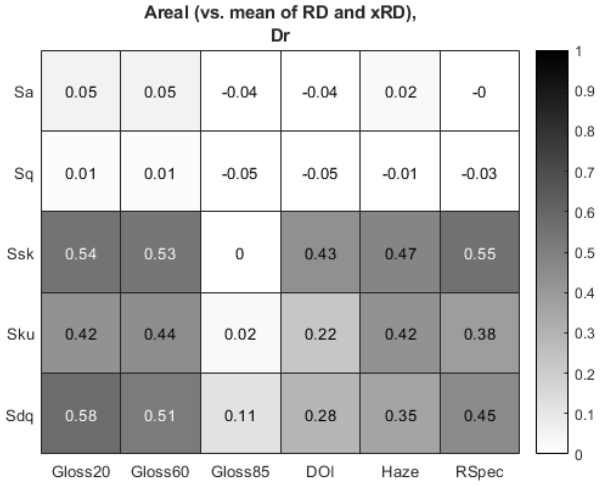

Figure 4.15: Correlations between the means of measurements taken both along and across the rolling direction, for samples taken from the edge of the strip, on the Drive side (Dr).

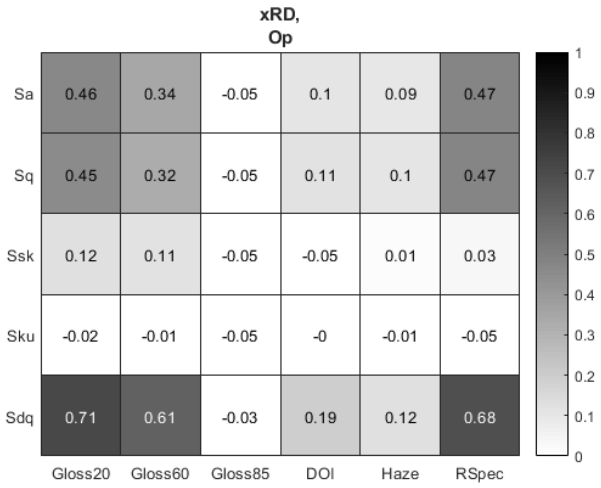

Figure 4.16: Correlations across the rolling direction, for samples taken from the edge of the strip, on the Operator side (Op).

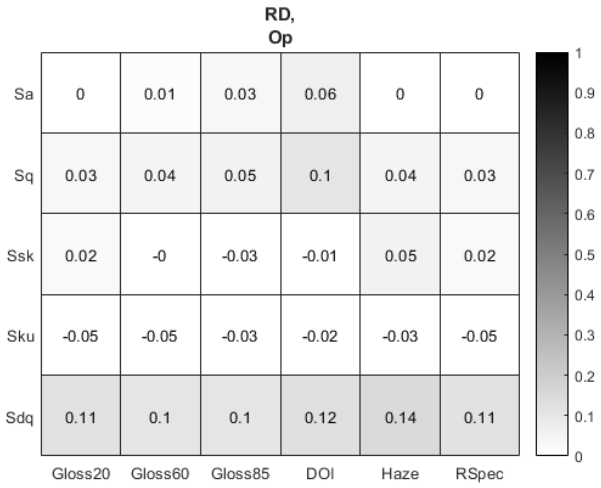

Figure 4.17: Correlations along the rolling direction, for samples taken from the edge of the strip, on the Operator side (Op).

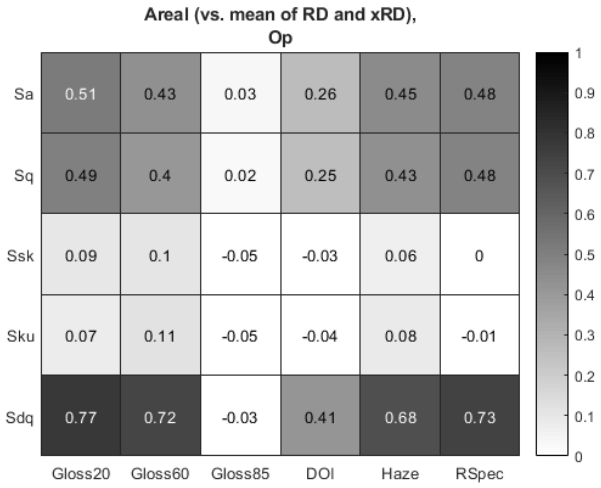

Figure 4.18: Correlations between the means of measurements taken both along and across the rolling direction, for samples taken from the edge of the strip, on the Operator side (Op).

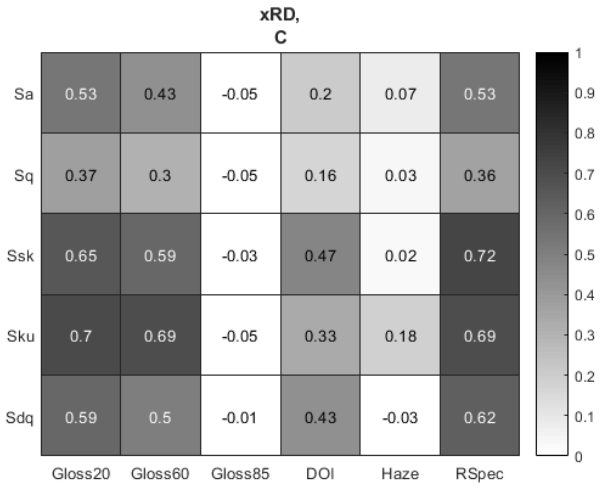

Figure 4.19: Correlations across the rolling direction, for samples taken from the centre of the strip (C).

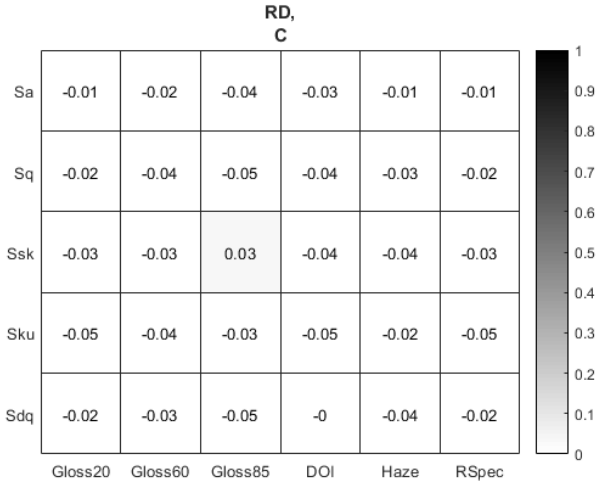

Figure 4.20: Correlations along the rolling direction, for samples taken from the centre of the strip (C).

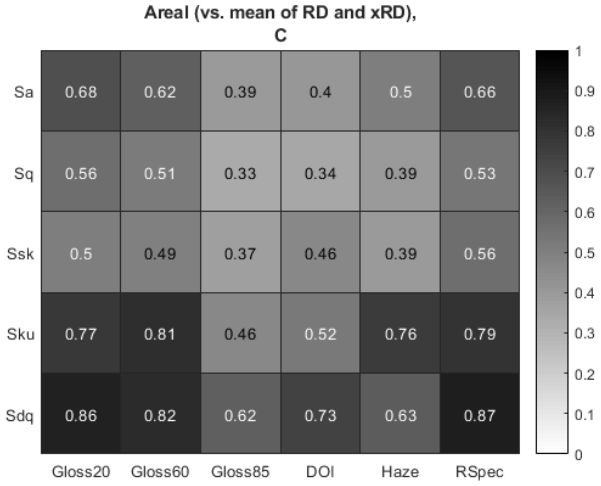

Figure 4.21: Correlations between the means of measurements taken both along and across the rolling direction, for samples taken from the centre of the strip (C).

Figures 4.13 through to 4.21 show the R^2 correlation coefficients for correlations between surface texture parameters and visual appearance parameters. Each cell in a figure represents the correlation strength between the corresponding parameters on the x and y axis. The darker the colour of the cell, the stronger the correlation. An R^2 value of 1 indicates perfect correspondence between the two parameters, an R^2 of 0 implies no relationship between the parameters.

Figures 4.14, 4.17, 4.20 show the R^2 correlation coefficients for correlations between surface texture parameters and visual appearance parameters for measurements made along the rolling direction. There is little to no correlation between surface texture parameters and visual appearance parameters along the rolling direction. This is due to the fact that the Fine Stone finish sampled here is created by two ground rolls in series, meaning the surface texture is anisotropic. There is large variation of surface texture across the rolling direction but little variation along the rolling direction. Therefore the variation in visual appearance is most related to the variation in surface texture across the rolling direction.

There is a large difference across the strip locations between the types of parameters that are correlated and the strength of those correlations. For example, for the drive side, the skewness parameter is strongly correlated with visual appearance, however this behaviour cannot be seen for the samples taken from the centre or operator side of the strip. The locations have different correlations. The changes to topography across the roll campaign are different in different locations which implies that different wear mechanisms occur across the strip. The difference between operator side and drive side in terms of the manufacturing process, is that the forces applied to the rolls are applied from the drive side. Surface texture parameters calculated from the centre of the strip show the strongest correlation overall with visual appearance parameters.

Figure 4.21 shows the strongest correlations. The strongest correlations are for the parameter Sdq and for visual appearance parameters which characterise the specular reflectance, with the gloss at 20° having an Rsq of 0.86 and the Rspec parameter having an Rsq of 0.87. This confirms the suggestions by Whitehouse and others that the slopes of a surface control the visual appearance [10].

4.4.2 Multi-scale correlations of surface texture and surface function

In this section, the analysis of correlations between surface texture and visual appearance is expanded to a multi-scale analysis. As in Section 4.2.2, a Gaussian band-pass filter was implemented in Matlab and used to decompose the surface data. Details are given in Section 3.3. The filter extracts surface information at spatial wavelengths within a certain band from the entire spectrum of spatial wavelengths contain in the measurement. The bandwidth and centre wavelength of the band are variable. The bandwidths used in this analysis were chosen so that each band was narrow enough to represent unique area of the spatial spectrum and broad enough such that meaningful information was retained. The values of the filter parameters can be found in Table 3.2.

Standard surface texture parameters were calculated from the band-passed surface data. The parameters chosen for this were the root mean square roughness amplitude Sq and the root mean square slope Sdq. It has already been shown that these two parameters are strongly correlated with visual appearance parameters for raw, unfiltered data. This multi-scale analysis is performed in order to discover at what specific scale are those correlations strongest.

To do this, the surface texture parameters were calculated for each band. The parameters at each band were then regressed against the visual appearance parameters and the R^2 correlation coefficient was calculated. The visual appearance parameters used in this analysis were the mean of values recorded along and across the rolling direction. This analysis produces a plot of correlation strength at each wavelength band. These plots show the strongest correlations between pairs of parameters and the scale at which the correlation is strongest.

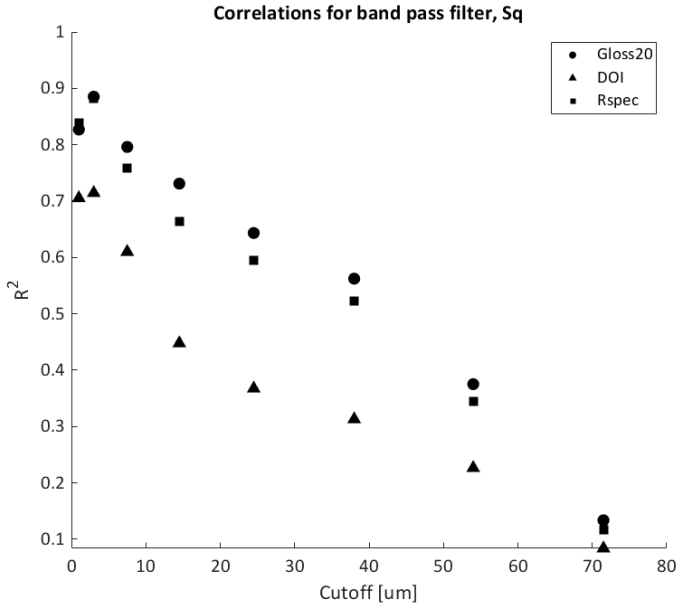

Figure 4.22: The multi-scale correlations between surface texture parameter Sq and a number of visual appearance parameters.

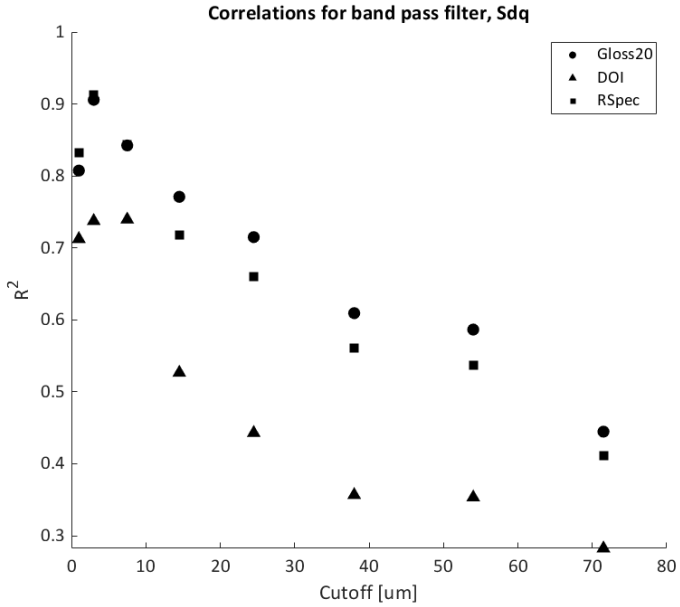

Figure 4.23: The multi-scale correlations between surface texture parameter Sdq and a number of visual appearance parameters.

Both Figures 4.22 and 4.23 show that that the strongest correlation between surface texture and visual appearance is at the smallest scales of measurement.

4.4.2.1 Discussion

In Figures 4.22 and 4.23, it can be seen that the correlations between surface texture parameters and visual appearance parameters are strongest in the 3 ± 1 μm range.

Considering the gloss(20°), for the parameter Sdq, the strength of these correlations increases from $R^2 = 0.86$ for unfiltered data to $R^2 = 0.91$ for filtered data. For the parameter Sq, the increase is from $R^2 = 0.56$ to $R^2 = 0.88$. The increase is not as large for Sdq because the parameter is already scale-sensitive as described previously in Section 4.2.1.2. The increase in correlation strength is most likely due to the removal of unreliable surface data at the highest frequencies of measurement.

This shows that for Fine Stone blackplate, the variation in surface features of sizes below 10 μm, as characterised by slope parameter Sdq, are strongly correlated with the variation in the specular reflectance from the surface, characterised by the gloss parameter at 20°. This implies that these features have a relatively large influence on the visual appearance. For packaging steel, the functional bandwidths of visual appearance occur at spatial wavelengths $< 10\mu$m.

These results can also be related to the results of Section 4.2.1.2, in particular Figure 4.3 and the associated discussion. Figure 4.22 shows that visual appearance is strongly correlated with a measure of the variation in the mean amplitude at only the smallest scales of surface texture. Figure 4.3 shows that a measure of mean amplitude of surface roughness at much larger scales cannot detect these fine-scale variations. This is the reason that two sheets of packaging steel can have the same Ra yet differ in visual appearance. The Ra parameter is blind to the scales which most strongly influence visual appearance.

The mechanism underlying the results shown in Figures 4.22 and 4.23 can be explained with the help of Landskroon analysis. Landskroon analysis is described in the literature review. This analysis determines the percentage of surface slopes which will reflect light into the angle at which gloss is detected, which is $\pm 0.9°$ either side of the specular angle. A surface with a higher percentage of slopes reflecting into the gloss detector angle will have a higher gloss. The proportion of the surface area reflecting into the gloss detector can be thought of as the active surface area. Figure 4.24 was generated by first filtering the 22 surfaces of Sample Set 2 with the filter settings that give the highest correlation between Sdq and gloss as seen in Figure 4.23. The surfaces taken from the centre of the strip were used. Figure 4.24 shows that as the roll campaign progresses, there is an increase in the active surface area from a minimum of $\sim 8\%$ to $\sim 25\%$. This accounts for the close relationship between Sdq and gloss at this scale, and can be seen more clearly in Figure 4.25. Figure 4.25 shows a number of surfaces as the roll campaign progresses. The increase in surface slopes over the roll

campaign can clearly be seen, showing the effect of wear on the roll texture which is then imparted to the strip.

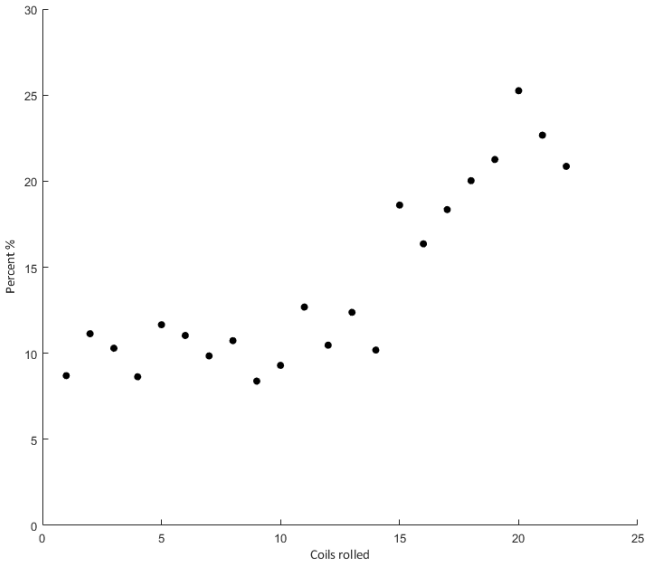

Figure 4.24: The increase in percentage of surface slopes reflecting into the gloss detector angle ($\pm 0.9°$), for surfaces filtered with a bandpass filter at a wavelength of $3\mu m$ with a bandwidth of $1\mu m$. They show only a slight increase until about 15 coils rolled, after which there is a steep increase in the proportion of the surface reflecting into the specular gloss angle.

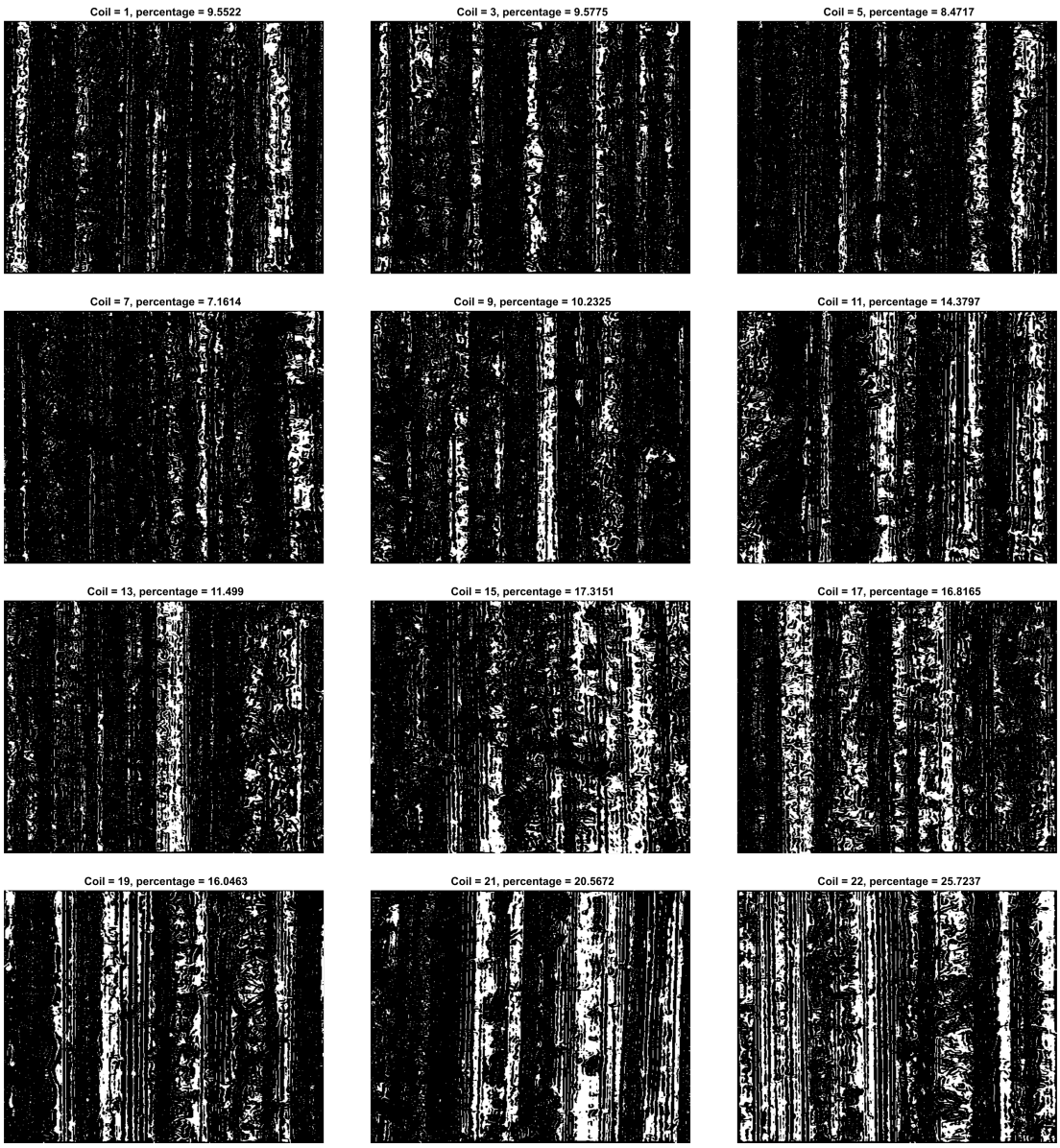

Figure 4.25: The active area of the surfaces of Sample Set 2.

The multi-scale effect of wear on the roll texture can also be seen in Figure 4.23. Figure 4.6 shows that the difference in Sdq between coils rolled at the start and end of the campaign is greater at smaller scales. This means it is exactly those bands of spatial wavelengths that are responsible for the function of interest that are most heavily influenced by wear. In other words, the very scales that need to be controlled are those that are most influenced by a process over which there is no control. Figure 4.25 shows the percentage of surface points that are oriented to reflect light into the gloss detector angle. A white point indicates a point that is oriented to reflect light into the detector. The images show the increase in the active surface area, that is in the proportion of surface that reflects into the gloss detector angle ($\pm 0.9°$), at a scale of $3\mu\text{m} \pm 1\mu\text{m}$. This demonstrates the effect of wear on the functional bandwidths

of packaging steel. These images can be compared to the images of the surfaces in Figure 3.3. The variation in surface slopes is larger at smaller scales. It is this variation that is responsible for the change in surface gloss. However, the wear phenomena that occur during rolling of strip have a relatively large influence on those same scales. This variation needs to be controlled to achieve more consistent visual appearance across the strip and along the wear process. Surface features of sizes below 10 μm, as characterised by slope parameter Sdq, have a relatively large influence on the specular reflectance from the surface, characterised by the gloss parameter at 20°.

This is significant for several reasons. Blackplate texture has a large influence on tinplate visual appearance. This result shows at what scale surface texture should be:

Measured Surface texture should be measured at scales according to function of interest. Current practice of measuring a single amplitude parameter across rolling direction at scales not pertinent to visual appearance are not capable of controlling for visual appearance.

Modelled Surface function should be modelled at the scales at which the mechanisms operate. Light interaction with surfaces occurs at the smallest scales, texture disruption at scales <10 μm causes scattering of incident light. When modelling the surface it it is these scales that must be considered.

Modified These results show that to control visual appearance, the slopes of surface features <10 μm should be controlled. This information is useful when thinking about surface designs which offer enhanced control over surface function.

4.5 Conclusions

A standard analysis of the surface texture of packaging steel substrates showed that:

- There is a coupling between amplitude of surface roughness and the rms slope parameter for all surfaces.
- Across the length of the roll campaign, the deviation of mean roughness amplitude Ra remains within the 0.25 μm window determined by the product specification.
- However, analysis of the same sample set showed a large deviation in the Sdq parameter across the same range.

- The wear processes involved in surface rolling have a significant effect on surface texture, both across the strip and along the length of the roll campaign.

Multi-scale analysis of the surface texture of packaging steel substrates showed that:

- Most surface finishes have a characteristic wavelength around $40\mu\mathrm{m}$, as described in Section 4.2.2.
- For Sample Set 1, all finishes show a region of low amplitude but high variation in the the highest frequency bands.
- Analysis of Sample Set 2 also showed a characteristic wavelength around 40 $\mu\mathrm{m}$, however the prominence of the material at this wavelength reduces over the length of the roll campaign.
- The high frequency band of low amplitude but high variation is the band most heavily affected by the wear process.
- Measurements of the visual appearance of Sample Set 2 revealed that the visual appearance change over the course of a roll campaign, with specular gloss doubling after 20 coils.
- Specular gloss is strongly correlated with Sdq, with $R^2 = 0.86$ for gloss at 20° and $R^2 = 0.87$ for RSpec.
- When this analysis was expanded to a multi-scale analysis, the correlation strength between Sdq and gloss at 20° increased to $R^2 = 0.91$, at a wavelength band of $3 \pm 1\mu\mathrm{m}$.
- At the same spatial wavelength band, the correlation strength between gloss at 20° and Sa increased from 0.56 to 0.88.
- The wear process causes variations in surface slopes at the smallest of scales, which causes the change in visual appearance of the packaging steel substrate.

Chapter 5

Coating

5.1 Overview

In this chapter, the addition of the tin coating to the substrate is considered. The aim of the investigation described in this chapter was to learn how the tin layer modifies the surface topography and contributes toward the visual appearance of the final product. The motivation for this is to learn how any designed surface textures would be affected by the addition of a tin coating. After consideration of other approaches, the multi-scale attenuation function (MAF) as described in Chapter 2 is used to analyse surfaces coated with differing coating weights. Three different approaches were considered and are outlined in this overview. The advantages and disadvantages of each approach are discussed and justification is given for the decision to use the MAF approach.

The three approaches considered were:

1. Computational fluid dynamics
2. Morphological filtering
3. Multi-scale attenuation function

These three approaches are described in more detail in the following sections.

5.1.1 Computational fluid dynamics

As described in the literature review, Luo used computational fluid dynamics to describe paint processes on rough surfaces [46]. He used the Navier-Stokes equations to model the behaviour of a thin film on a rough surface, under the effect of surface tension and gravity. He constructed a set of partial differential equations which are solved using the finite element method in COMSOL. The model was developed for application to automotive steels and an attempt was made to apply it to tinplate under the assumption that there were enough similarities between the two systems for the equations to be valid. In the tinplate manufacturing process, tin is electrolytically coated to a steel substrate then reflowed. The tin is heated to its melting point for a short period of time before re-solidifying. In this reflow stage, the molten tin flows into the valleys of the substrate and the surface is planarized. This is analogous to the levelling of paint on a surface therefore Yuchen's model may be applicable to tinplate.

The model was obtained from its developers directly. The most significant model inputs are the viscosity and surface tension of the coating and a heightmap representing

a surface. The model then calculates the behaviour of the coating, according to its properties, on the surface. The output is the coated surface data. The model was used to simulate ideal surfaces which had some features resembling real surfaces but were simple enough for the model to handle. Several triangle wave surfaces were generated with varying steepness of surface slopes. The surfaces were run through the model using coating settings for liquid tin. These combination of surfaces and coating settings enabled the equations governing the behaviour of the film to converge to a solution.

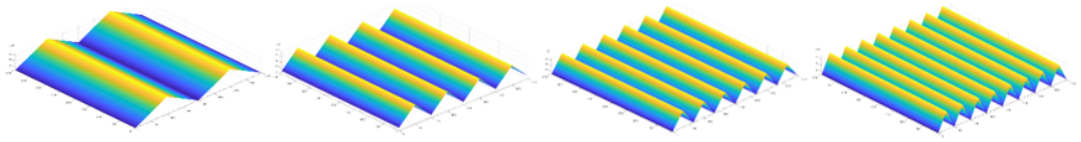

Figure 5.1: Simple surfaces for which the CFD model was able to converge to a solution.

However, for measured steel substrate data it was impossible to find the right combination of settings such that the equations converged to a solution. The viscosity of liquid tin is much lower than that of paint and the surface tension is much higher. For example, Luo used a value of 1 $\mathrm{Pa \cdot s}$ for the viscosity of paint, whereas the viscosity of tin at temperatures just above its melting point is in the region of 1.5 - 2 $\mathrm{mPa \cdot s}$. In addition to this, the amplitude of variation in the short wavelengths of blackplate substrate data is very high. These two considerations, the nature of liquid tin and the nature of the blackplate surface, meant that the model was pushed beyond its capabilities, and without attempts to simplify the surfaces, the model failed in its application to packaging steel.

5.1.2 Morphological filtering

Due to the lack of success using the CFD approach, a simpler approach was sought for. One potential method was the use of morphological filters to represent the modification of the substrate texture by the tin coating. Morphological filters modify a function by operating on it with a structuring element. Operating on a surface profile with a morphological filter results in a filtered profile which is some combination of the original surface and the structuring element. A surface profile can be considered as a discrete function of a single variable with spacing between values determined by the sampling interval of the measurement. The structuring element is then discretised with the same interval. This structuring element is then placed over each point of the

profile and a new profile is created by either taking the maximum or minimum point of the structuring element at that location. If the maximum point is taken, the operation is known as dilation. If the minimum is taken, the operation is known as erosion. By combining these two primary operations, secondary operations can be formed. A closing operation is created by first performing dilation then performing erosion. An opening operation is created by first performing erosion and then dilation. The figure below shows these operations for a circular structuring element [83]. Morphological filtering has been used in analysis of surfaces to partition bandwidths of surface texture, thereby isolating scales of interest [84–86].

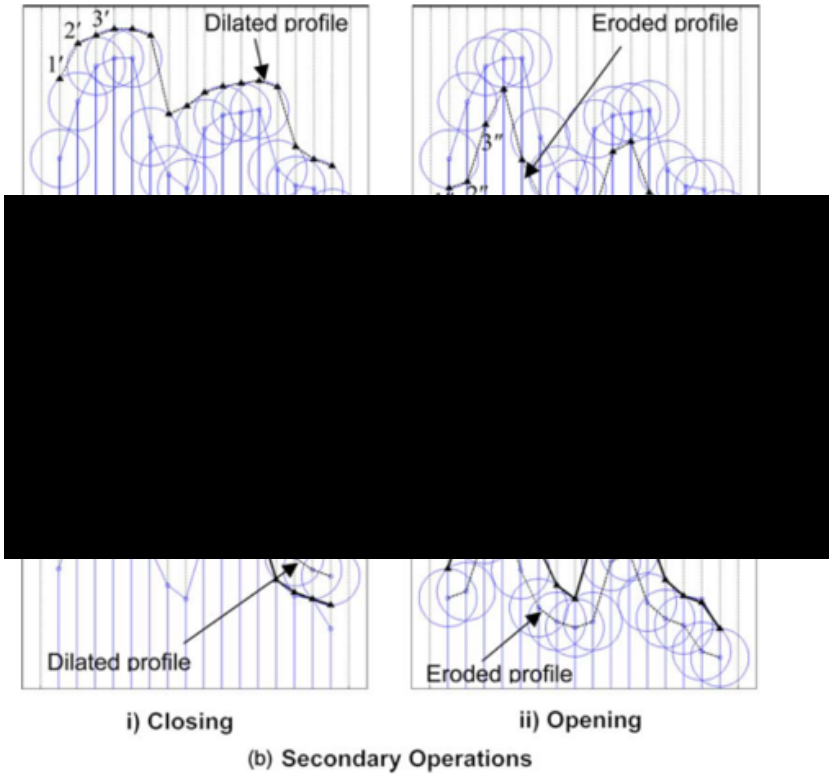

Figure 5.2: Figure showing the operations of morphological filters [83].

Aarnts et al. developed a model to predict the amount of tin required to fill the valleys to the optimum level without the excess free tin that leads to damage sensitivity. This was done by calculating the volume of the black-plate surface available to be filled by tin and was used to predict the amount of alloy layer at the surface [44].

Closing filters can be used to "close" the voids in a surface, or in other words to fill the valleys. This valley-filling behaviour is similar to the action of a tin coating which, when reflowed, flows to fill the valleys of the substrate texture. These considerations suggest the possibility of using morphological filtering as an extension of the volume-filling modelling approach. The possibility of using morphological closing filters to

represent this behaviour of tin coating was investigated, with the size of the structuring element controlling the coating weight.

A morphological filtering system was implemented in MatLab, following the work of Kumar et al. [83]. The algorithm is a simple one; for some profile $p(x)$ of length L and some structuring element $s(x)$, for every point of the profile $i = 1 : L$, the dilated profile $d(i) = max(p(i), s(i))$ and the eroded profile $e(i) = min(p(i), s(i))$. Closed and opened profiles are then obtained by running dilation and erosion operations in series.

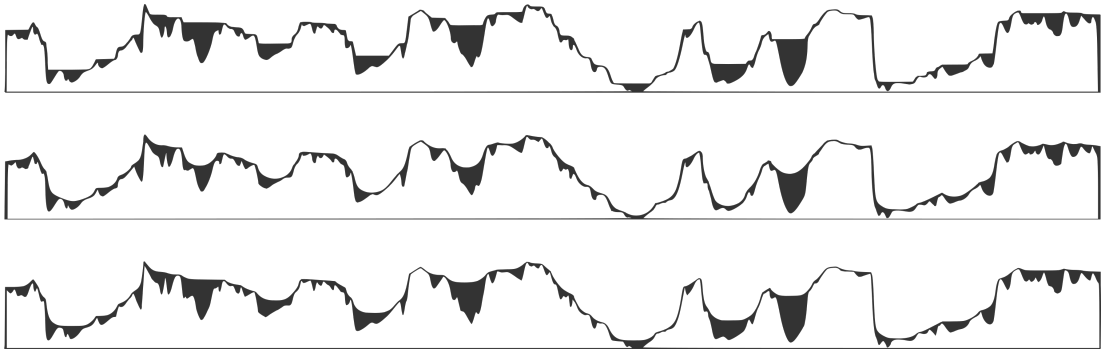

Figure 5.3: The results of a closing operation on measured surface profiles. The original surfaces are white and the filtered profiles are dark grey. The top profile shows the result of using a circular structuring element, the middle shows the result of using a linear structuring element and the third profile shows a combination of linear and circular structuring elements.

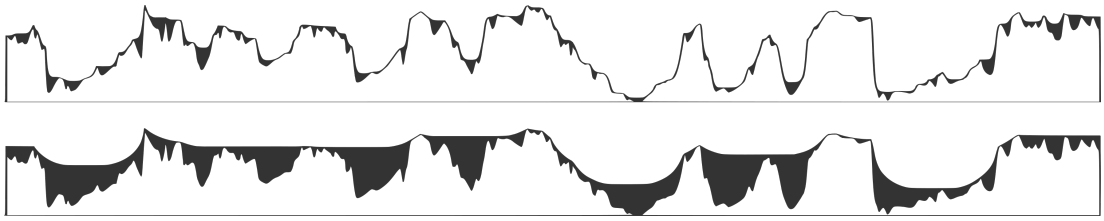

Figure 5.4: Figure showing the results of a closing operation on measured surface profiles, with combined circular and linear structuring elements. The top profile shows the result of using structuring elements of length of 4 sampling intervals and the bottom profile length 25 intervals.

Figure 5.3 shows the results of operating with a closing filter on real measured surfaces. Figure 5.4 shows the result of using different size structuring elements. These figures show a qualitative similarity with the tin layer system. However, issues arise when attempting to establish a quantitative link between the physical tin layer system, measured by tin weight in gm^{-2}, and its representation by the filtered profile. The fundamental difficulty in establishing this link is the lack of correspondence between the action of the closing filter and the physical phenomenon of tin coating. The surface created by a closing filter can be considered as the surface delineated by a sphere

rolling across the original surface (in the case of a circular structuring element) or as a plane sliding across the surface (in the case of the linear structuring element). Neither of these processes closely represent the a fluid re-solidifying on a surface. This fundamental discrepancy means any parameter controlling the thickness of the coating, i.e the size of the structuring element, would need empirical qualification.

5.1.3 Multi-scale attenuation function

In Section 2.5.5, the MAF is defined. The MAF describes the modification of surface wavelengths due to a coating process and was developed by Mezghani et al. [77].

The MAF is defined as

$$MAF_{Sa}(\lambda) = \left| \frac{MS_a^{post}(\lambda) - MS_a^{pre}(\lambda)}{MS_a^{pre}(\lambda)} \right| \tag{5.1}$$

Where $MS_a^{pre}(\lambda)$ and $MS_a^{post}(\lambda)$ are the multi-scale roughness spectrum of the surface pre- and post-coating and λ is the spatial wavelength [77]. In this case, the surface texture is characterised by the parameter Sa.

In an extension of the method of Mezghani et al. the MAF was also derived from MSdq, the multi-scale root mean square slope of the surface texture. This function describes how the slopes of the surface texture are modified by a coating layer at different spatial wavelengths. It is calculated in much the same way:

$$MAF_{Sdq}(\lambda) = \left| \frac{MS_{dq}^{post}(\lambda) - MS_{dq}^{pre}(\lambda)}{MS_{dq}^{pre}(\lambda)} \right| \tag{5.2}$$

The MAF in this case shows the difference in the surface slopes, with respect to surface scale, before and after the tinning process. The parameter Sdq was chosen as both the literature and investigations performed on packaging steel substrate show that it is an important parameter for controlling visual appearance of a surface. The MAFs derived from MSa and MSdq are differentiated by the relevant parameter in the subscript.

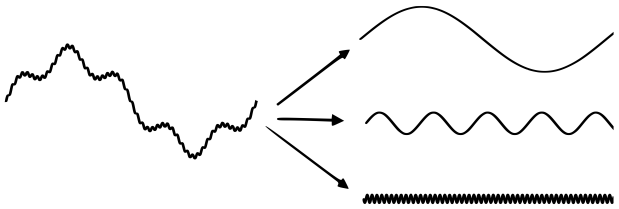

An illustration of the multi-scale nature of surfaces. A surface is a superposition of multiple scales.

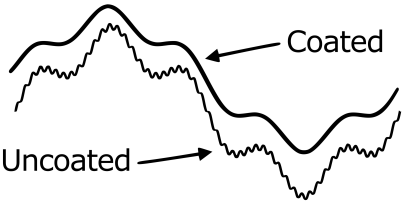

Figure illustrating the attenuation of surface scales by a coating.

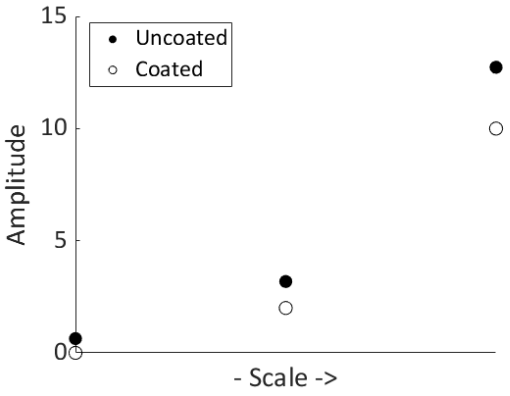

The multi-scale Sa of the above surface.

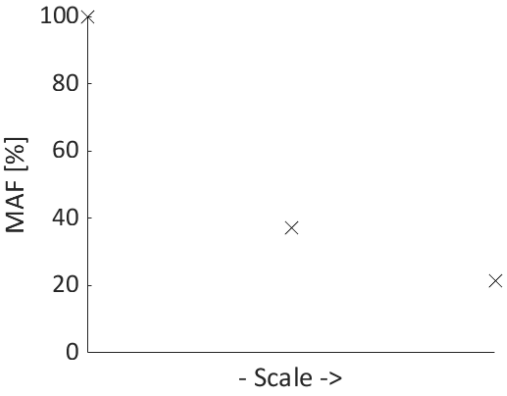

An illustration of the MAF.

Figure 5.6: A set of figures illustrating the information represented by the MAF. The MAF encodes the difference between coated and uncoated surface parameters across scale.

Figure 5.6 gives a visual illustration of the information encoded in the MAF, for an idealised surface.

5.1.4 Conclusions

A number of difficulties were encountered when attempting to model the tin coating. A physically-based CFD approach was unsuccessful because it was, in a sense, "too physical", in other words its realistic representation of fluid on a surface failed when the substrate became too complex for the governing equations to handle. A filtering based approach using morphological filtering was also unsuccessful as it was, in a sense, not physical enough and did not closely represent the phenomena of coating on substrate. A third, empirical approach has been described, which uses data of measured surfaces to build a picture of the multi-scale properties of surface texture after coating with tin.

The decision was made to use the MAF as described by Mezghani et al. to investigate the tin coating for several reasons:

1. The lack of success using fluid dynamics or morphological filters to model the tin layer.

2. The previous success of multi-scale analyses in this thesis in providing insight into the substrate of tinplate.

3. The previous success of Mezghani et al. in using the MAF to investigate similar systems.

5.2 Results

In this section, the MAF is used to analyse the multi-scale modification of surface texture of packaging steel resulting from the application of a layer of tin to the surface. $MS_a^{post}(a)$ was calculated from measurements of the surface texture of tinplated material. $MS_a^{pre}(a)$ was calculated from measurements made on the same material after the tin layer had been removed using electrolytic methods. This tin layer removal method was used as there was no uncoated substrate material available for analysis. The MAF shows the difference in surface texture, with respect to surface scale, before and after some process (in this case, tinning) has been applied to the surface.

These functions were calculated for the surfaces found in Sample Set 2. This sample set consists of 6 different surface finishes, each coated with four different levels of tin coating. Two of the 24 possible permutations are missing from the set, giving a set of 22 permutations of finish and tin weight. The tinned surfaces were measured using the WYKO NT9300 white light interferometer at x41 magnification. This magnification was chosen as prior investigations show that this is the scale regime that has most influence on visual appearance of packaging steel. Three measurements were made on each surface at each magnification. The tin coating was removed from a small circular area of diameter $\sim 4\mathrm{cm}$ on the surface and three measurements were made within this area, at each magnification, for each surface finish.

The MS_a and MS_{dq} for each variant was calculated. The process by which these are calculated is found in Chapter 4.1. The MAFs were then calculated for each parameter by comparing each tin weight variant to the detinned surface. In other words, MS_a^{pre} and MS_{dq}^{pre} were calculated from the detinned surface data. MS_a^{post} and MS_{dq}^{post} were calculated from the 2.8, 5.6, 8.4 and 11.2 gsm tin weight variants. These four MAFs were then plotted on a single graph for each surface finish and surface texture parameter. This shows the evolution of surface texture, across scale, as the tin layer thickness increases.

The bandwidths used in this analysis were chosen so each band was narrow enough to represent unique area of the spatial spectrum and broad enough such that enough meaningful information was retained. This information is found in Table 3.2.

5.2.1 Sample Set 1

5.2.1.1 Multi-scale attenuation functions of Sa

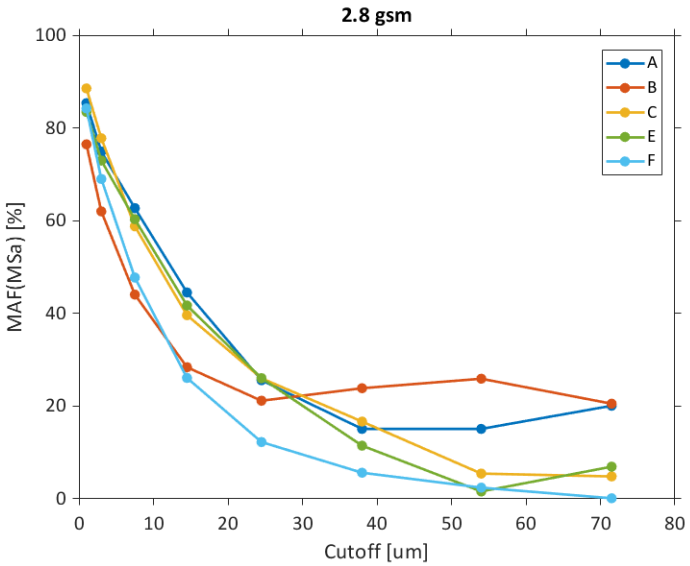

Figure 5.7: The multi-scale attenuation functions (MAF) for the mean surface amplitude Sa, for surfaces with 2.8 gsm coating.

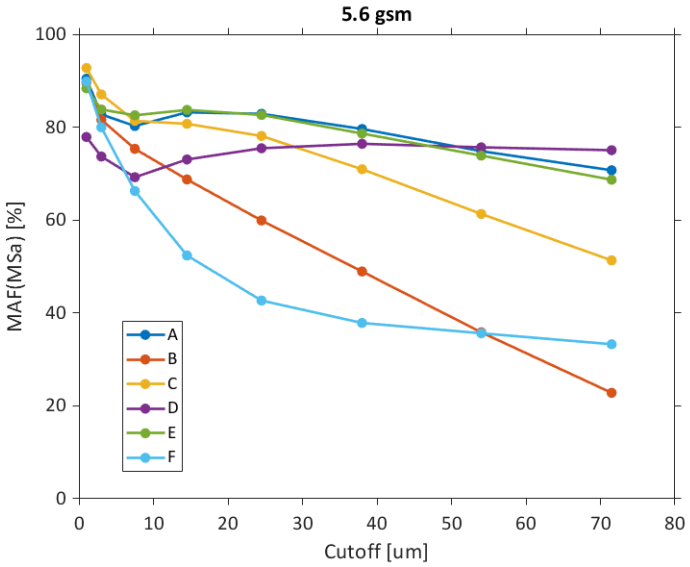

Figure 5.8: The multi-scale attenuation functions (MAF) for the mean surface amplitude Sa, for surfaces with 5.6 gsm coating.

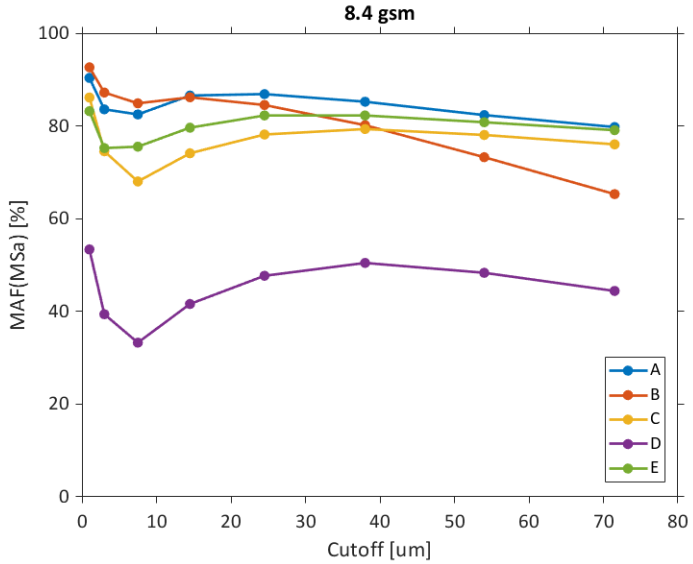

Figure 5.9: The multi-scale attenuation functions (MAF) for the mean surface amplitude Sa, for surfaces with 8.4 gsm coating.

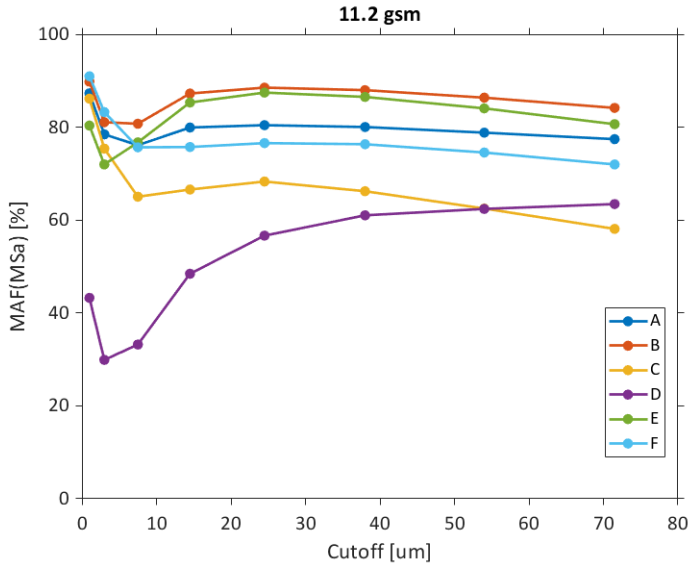

Figure 5.10: The multi-scale attenuation functions (MAF) for the mean surface amplitude Sa, for surfaces with 11.2 gsm coating.

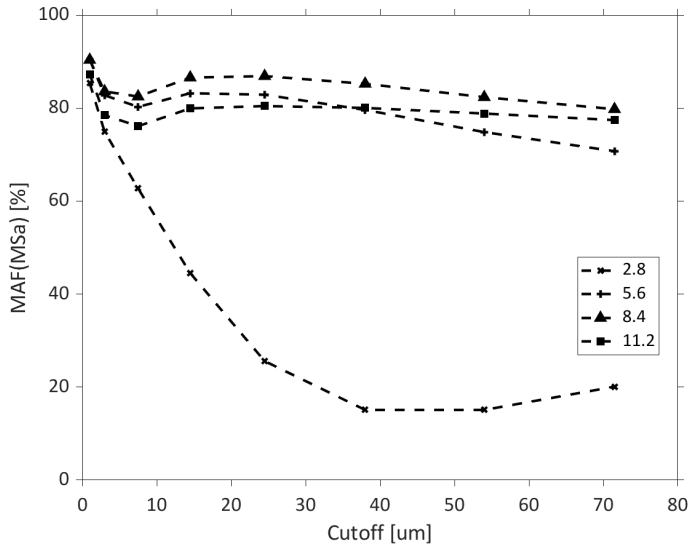

Figure 5.11: The multi-scale attenuation functions (MAF) for the mean surface amplitude Sa, for all tin weights on one finish (Light Stone finish).

Figures 5.7 through to 5.10 show the multi-scale attenuation functions of the surfaces of Sample Set 1, for the surface texture parameter Sa. These figures can be interpreted as showing the amount by which a surface texture parameter is modified by a process, at a certain scale. The surface scale runs across the x-axis. The y-axis runs from $0 \rightarrow 100\%$, showing the value of the MAFs as calculated by Equations 5.1 and 5.2. A value of 0% means that there is no difference in the value of a surface texture parameter at a specific scale before and after some surface process. The value of the MAF on the y-axis tends to 100% with the increase in the difference between the surface parameter at a specific scale before and after the surface process. In this case the parameter characterises the roughness amplitude and the process is tin coating, therefore these figures show the effect of tin coating on the amplitude of roughness across different scales. Figure 5.11 is an exemplar figure showing the MAF of different levels of tin weight on one type of surface finish. In this figure, the effect of different levels of tin weight on the substrate texture can be seen, decomposed across different wavelength scales.

Table 5.1: Table showing the centre wavelength of the bands of minimum attenuation for the samples of Sample Set 1. These values can be related to the filter settings of Table 3.2.

Sample	Band of minimum attenuation for 2.8 gsm coating [μm]
A	38
B	24.5
C	54
D	no data
E	54
F	71.5

5.2.1.2 Multi-scale attenuation functions of Sdq

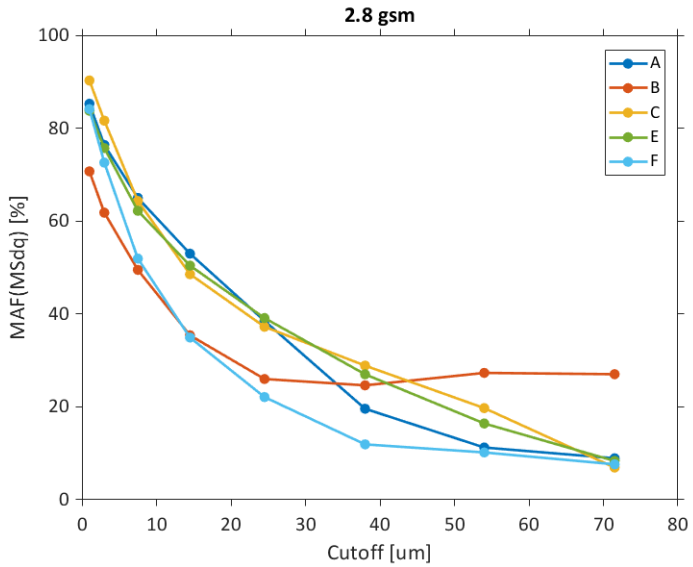

Figure 5.12: The multi-scale attenuation functions (MAF) for the root-mean-square surface slope Sdq, for surfaces with 2.8 gsm coating.

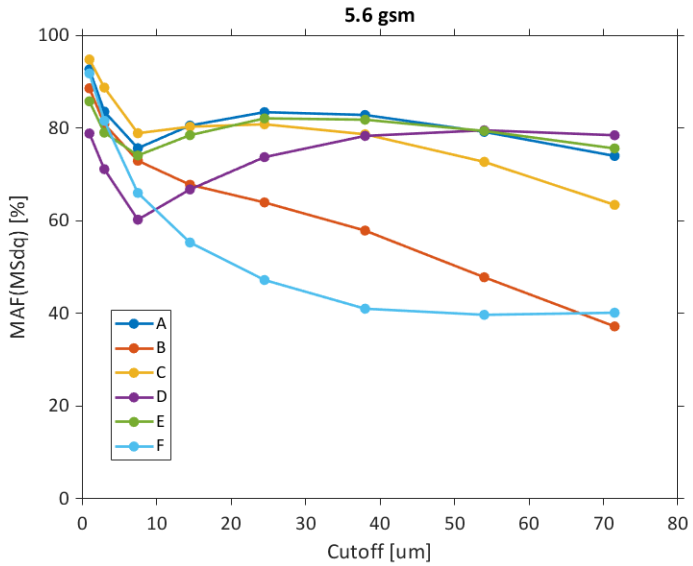

Figure 5.13: The multi-scale attenuation functions (MAF) for the root-mean-square surface slope Sdq, for surfaces with 5.6 gsm coating.

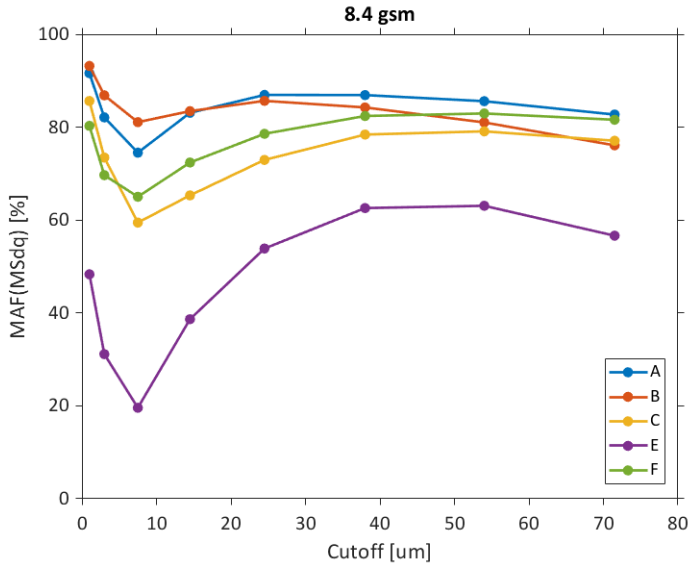

Figure 5.14: The multi-scale attenuation functions (MAF) for the root-mean-square surface slope Sdq, for surfaces with 8.4 gsm coating.

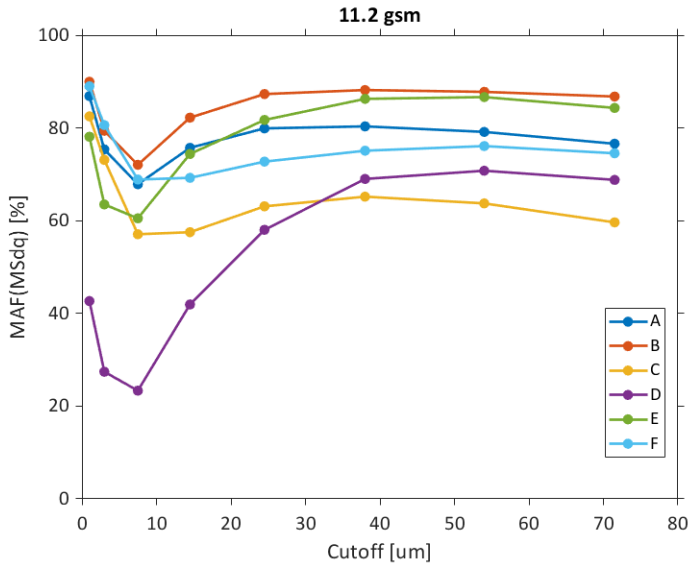

Figure 5.15: The multi-scale attenuation functions (MAF) for the root-mean-square surface slope Sdq, for surfaces with 11.2 gsm coating.

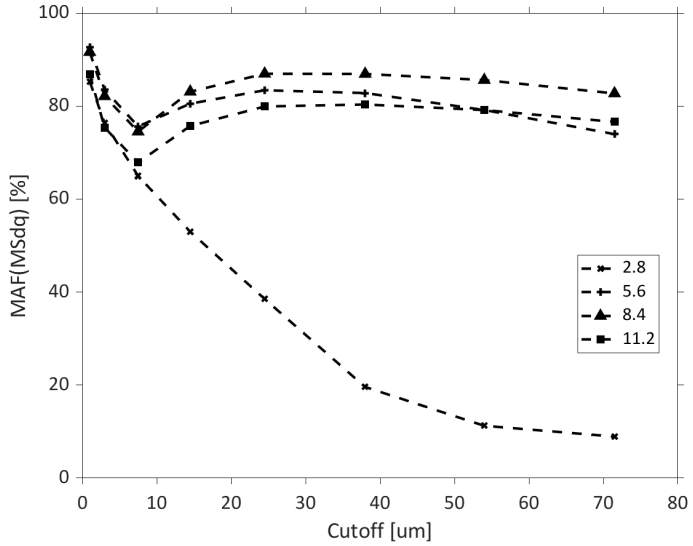

Figure 5.16: The multi-scale attenuation functions (MAF) for the root-mean-square surface slope Sdq, for all tin weights on one finish (Light Stone finish).

Figures 5.12 through to 5.15 show the multi-scale attenuation functions of the surfaces of Sample Set 1, for the surface texture parameter Sdq. These show the effect of the tinning process on the surface slopes, decomposed across scale. Figure 5.16 is an exemplar figure showing the MAF of different levels of tin weight on one type of surface finish.

5.2.2 Sample Set 2

Due to limitations inherent in the manufacturing process, only a small number of coils from the original series of 22 were available. Not every coil from the original series was sent from the temper mill through to the tinning line. Others were instead sent to different coating lines. This meant that only a series of 6 coils from the original 22 were available for analysis. These 6 samples were coated with tin at a nominal coating weight of 2.8 gsm. There are other considerations that need to be taken into account when assessing the results of analyses carried out on this sample set. The tin weight is only a nominal value and the actual tin coating weight can fluctuate. Furthermore, the coated samples were not taken from the same coil location as the uncoated samples. This is because samples are taken a the end of the line; after rolling for uncoated samples, after tinning for coated samples. Samples are always taken from the accessible "tail" of the coil, not from the inaccessible "core". However, coils are unwound and fed through each line starting with the tail and ending with the core, meaning when rewound at the end of the line, what was the core becomes the tail, and what was the tail becomes the core. In other words, there is at least the length of a coil between the coated and uncoated samples, meaning the surface texture of the uncoated samples is not directly comparable to that of the coated samples as the rolls used to create the surfaces have undergone different amounts of wear. The situation is complicated further as sometimes, depending on customer orders, two or more coils are welded together before being run through the tinning line, meaning the region of a coil from which an uncoated sample was taken could even be located in the inaccessible core of a larger coil. In summary, this considerations mean that it was not possible to obtain reliable measures of the MAF using the substrate samples and coated samples of Sample Set 2. In future investigations, the available coated samples should be detinned and the detinned area compared to the coated measurements, as was the case for Sample Set 1.

5.3 Discussion

In Chapter 4.1, the multi-scale parameter decompositions, MSa and MSdq, were calculated. These showed that at short wavelength scales ($< 30\mu\mathrm{m}$), the amplitude of surface texture is low while the variation in surface slopes is high. Figures 5.7 through to 5.15 show that in general, for all surface finishes and at all tin weights, it is these

bands containing shortest spatial wavelengths that are most heavily attenuated. This is true for both MSa and MSdq. The application of tin coating to uncoated packaging steel substrate reduces the amplitude and flattens the slopes of the short wavelength surface content. When considering topographic influences alone, these results show that the reflectivity of coated packaging steel is much higher than that of uncoated steel due to the attenuation of surface texture at these short wavelength scales.

Although this is generally true for all measured surfaces, the variation between different surfaces of this general principle is interesting. The MAF quantifies the difference between surface texture parameters of coated and uncoated surfaces at specific spatial wavelength bands. For example, considering the three finishes with directional texture content (A, B, and C) for the 2.8 gsm coating weight in Figure 5.7, the MAF(MSa) reaches a minimum at a different scale for each of the surfaces. This minimum is at the 24.5 μm band for B, 38 μm band for A and 54 μm band for C. This shows that surface features above this minimum point of the MAF are relatively less attenuated. This is interesting because it quantifies the scale, for a certain tin weight and certain surface finish, at which surface features remain visible beneath the coating. This provides insights into the underlying mechanism of tin coating which become relevant when designing surfaces with enhanced control over visual appearance.

Still considering finishes A, B, and C, but now considering the effect of increasing tin weights, for the finishes with lower bulk (i.e. without decomposition) amplitude of surface variation, tin weights of 5.6 gsm (in Figures 5.8 and 5.13) and above have a dramatically higher attenuation of the longer wavelength surface content, however with less difference between the successive tin weights. In other words, there is a large difference between 2.8 and 5.6, but little difference between 5.6, 8,4 and 11.2 gsm. This shows that after a certain point, the surface is planarised and the underlying substrate texture is not visible through the coating.

For the non-directional surface finishes, D, E and F, there are no data for finish D (Bright) for the 2.8 gsm tin weight, and finishes E and F show similar results to the directional surfaces, however the bands of least attenuation tend to be at longer wavelengths. For MAF(Sa), for E, the minimum attenuation is at the 54 μm band and for F, the minimum attenuation is at the 71.5 μm band. For MAF(Sdq), the minimum has not been reached at the longest wavelength scale present on the plots.

All surface finishes show a phenomena at the wavelength band between 5 and 10 μm, at which point the attenuation is lower than the surrounding values. The reason

for this is not clear.

In comparing these results to the work of Mezghani et al., similar behaviour can be observed between the autobody paint system and the tinplate system. The initial coat influences the shorter wavelengths, and successive coating thicknesses influence the longer wavelength bands of surface texture. However the results differ, as expected, in that the tin layer system operates on much shorter wavelengths of surface texture than the autobody paint system. In autobody applications, often the waviness of a surface is controlled in order to control the visual appearance. However, these results show that this does not carry over to the tinplate industry. Controlling the waviness will have little effect on tinplate visual appearance, as the phenomena responsible for tinplate visual appearance occur at scales far below that measured by waviness parameters.

In Chapter 4.1, it was shown that visual appearance parameters are most strongly correlated with surface texture parameters at scales of <10 μm. To control the visual appearance of packaging steel via the surface texture, features at these scales would need to be controlled. However, the results in this chapter show that the situation has an added layer of complexity. Any control over visual appearance by control of surface texture at the relevant functional bandwidths would be attenuated by the addition of a tin layer. This has implications for the design of surfaces with advanced control over visual appearance. Surface textures need to be created at scales small enough to influence visual appearance, yet large enough not to be totally obscured by the tin coating. The results in this chapter quantify these scales.

5.4 Conclusions

- The modification of the surface texture of packaging steel by a tin coating process has been quantified across multiple scales.
- The functional bands of surface texture, at scales $< 30\mu$m, with low amplitude but high variation in surface slope, are most heavily attenuated by the surface coating.
- The application of tin coating to packaging steel substrate reduces the amplitude and flattens the slopes of short wavelength surface content.
- For 2.8 gsm the minimum attenuation is at different wavelengths for different finishes, varying from 24.5μm to 54μm for anisotropic finishes - this quantifies

the scale at which surface features retain prominence through the coating layer.

- These occur at wavelengths much lower than those quantified by the waviness parameter, therefore controlling the waviness parameter would not aid in controlling the visual appearance of tinplate packaging steel.

It is already known from the work of Landskroon, that for low tin weights (2.8gsm), visual appearance is largely defined by substrate texture. These results show for a range of surface finishes, at what scale the substrate texture will remain visible through a 2.8 gsm coating. This information is useful when texturing surfaces with the purpose of controlling visual appearance. It is not necessary to create surface features to control visual appearance, if those surface features will be heavily attenuated by the addition of a coating layer. Therefore, surface features should be created at sizes which are not heavily attenuated by the coating. This work helps to quantify those modified functional bandwidths of surface texture.

Chapter 6

Function

6.1 Overview

The aim of the work in this chapter was to develop a model to predict the visual appearance of packaging steel from surface texture data. The purpose of developing this model is to enable the prediction of visual appearance from simulated surfaces, in order to aid the design of novel surface textures that give better control over the visual appearance of tinplate products.

A microfacet approach was used, based off the previous success of other authors and the empirical results presented in earlier chapters of this thesis. Chapter 2 describes the work of other authors who have used the angular distribution of specularly reflecting planes to predict the visual appearance of surfaces and in Chapter 4, it was discovered that the slopes of surfaces correlate strongly with the visual appearance. From these evidences, along with the advantage of relative simplicity of implementation, it was decided that a microfacet approach would be used to model the visual appearance of packaging steel.

First a general overview of the theory is given, with some case studies in which this approach has been applied to real surfaces. Then a model is developed from the theory, the implementation of the model is described and some issues with model validation are discussed. Due to these issues, the model is modified using the approach of Landskroon, and is finally applied to packaging steel surfaces to show that the proportion of surface slopes reflecting into the gloss detector angles is a good predictor of measured gloss.

6.2 Microfacet theory

The function under consideration is the visual appearance of a surface. Microfacet models are used in the computer graphics industry to simulate realistic lighting of objects and environments [87–91]. Microfacet theory rests on two assumptions.

1. A surface can be represented as a collection of small planes known as microfacets.

2. each of these planes reflects any incident radiation into the specular angle.

From these two assumptions, the BRDF of a surface can be derived, which describes the angular dependence of the intensity of reflection from a surface. The BRDF

of the surface is computed by calculating the number of microfacets at the appropriate orientation to specularly reflect light from the source to the detector.

Microfacet theory gives the BRDF of a surface in the following form [90].

$$f(\mathbf{l};\mathbf{v}) = \frac{D(\mathbf{h})G(\mathbf{l},\mathbf{v},\mathbf{h})F(\mathbf{l},\mathbf{h})}{4\cos(\mathbf{l})\cos(\mathbf{v})} \tag{6.1}$$

Where $\mathbf{l}$ is the lighting vector, $\mathbf{v}$ is the viewing vector and $\mathbf{h}$ is the half-vector (bisector) between $\mathbf{l}$ and $\mathbf{v}$.

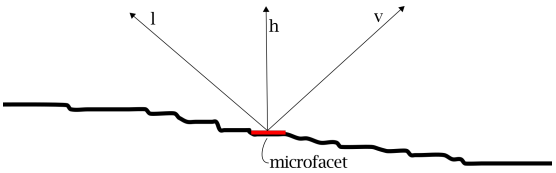

Figure 6.1: Only microfacets with a normal halfway between the lighting and viewing directions will reflect light from the lighting into the viewing direction.

The surface under investigation is taken to be composed of microfacets, oriented over a certain distribution. This orientation of a single facet is called the microfacet normal $\mathbf{m}$ and the distribution of all microfacets is called the normal distribution function (NDF). This is represented by $D(\mathbf{h})$ in Equation 6.1.

Assuming irradiation vector $\mathbf{l}$ and viewing vector $\mathbf{v}$ then only certain microfacets oriented to give a specular reflection from $\mathbf{l}$ into $\mathbf{v}$ will contribute to the BRDF term. This can be seen in Figure 6.1. Due to the specular assumption, these contributing microfacets are the ones with $\mathbf{m} = \mathbf{h}$.

The masking-shadowing function G is used to limit the space of possible surface/light interactions to only those that are physically possible. Due to the nature of the topography, there will be microfacets unable to receive light from the source (masked) and unable to reflect to the viewer (shadowed). Heitz has reviewed a number of choices for masking-shadowing functions [92]. However, the value of the masking-shadowing term is close to one except for near-grazing angles [71]. The geometry of the lighting/viewing angles for the measurement of gloss means that $G = 1$ for this application.

The Fresnel term F is used to model the reflectivity of the surface material. Modelling the Fresnel term can be achieved via the Schlick approximation [87]. However, this investigation is interested in the effects of topography on visual appearance, therefore the reflectivity will not be modelled and the Fresnel term will be set as $F = 1$.

To summarise, $D(\mathbf{h})$ models the topography, $G(\mathbf{l}, \mathbf{v}, \mathbf{h})$ models the visibility of certain regions of the topography, and $F(\mathbf{l}, \mathbf{h})$ models the material properties. $D(\mathbf{h})$ has by far the largest effect on the final modelled appearance and $G(\mathbf{l}, \mathbf{v}, \mathbf{h})$ and $F(\mathbf{l}, \mathbf{h})$ can be approximated using various methods. Most computer graphics applications use an a priori NDF, mathematically deriving it from certain starting assumptions, rather than deriving it from a measured surface [71, 90, 93–95].

Several investigators have taken microfacet theory from the realm of computer graphics and applied it to real world surfaces.

Leloup et al. compared BRDF measurements with gloss measurements [70]. To obtain the gloss of a surface, they integrated the BRDF over the cone angle of the detector, which gives good correlation only at the 20° geometry. They state that a fuller knowledge of the optical design of a gloss meter is necessary for a stronger correlation.

Obein et al. used microfacet theory to predict the BRDF of real surfaces and compared their predictions to measurements made with a goniophotometer [69]. They concluded that the facet hypothesis is reliable for predicting the BRDF.

Both of the above investigations considered relatively simple surfaces whereas Dong et al. developed a method of predicting the BRDF of surfaces created using surface texturing methods similar to those used in industry [71]. The NDF was derived from white light interferometry measurements of brushed metal surfaces. Locally-weighted linear least squares fitting was used to fit a plane at each point of the surface data. The normal of this plane is taken to be the normal of the surface at that point and a histogram of many such normals is built in order to estimate the effective NDF. Predictions of surface reflectivity were found to agree with goniophotometer measurements. Using this method, successful predictions of the appearance of highly anisotropic surfaces were made. When fitting a plane to the surface, Dong et al. used a linear least squares regression method with a Gaussian weighting factor. They suggest that the width of the Gaussian kernel acts as a filter which filters out high frequency surface content, which more accurately represents the true interaction of light with surface. They obtained the best results with a filter on the order of 1 $\mu\mathrm{m}$.

Compare this to Shipulski and Brown, who discovered that highest surface reflectivity occurs at 10 $\mu\mathrm{m}$ and above, with scattering increasing/reflectivity decreasing to a maximum/minimum level at 100 nm [11]. This accounts for the success of Dong et al. in using a 1 $\mu\mathrm{m}$ filter, filtering out the surface content which most scatters incident

light.

Landskroon simplified the microfacet approach further with an additional assumption [45]. When attempting to predict gloss, only those facets which reflect specularly into the gloss detection angles are relevant. The reasoning is that a surface with a higher proportion of facets oriented within that angular range will have higher gloss. This was used to make predictions of the visual appearance of tinplate surfaces. Landskroon used surface measurements with a sampling interval of 1 μm, with no filtering. The normal of each point was calculated using a 3-point neighbourhood. The number of surface points oriented at an angle which would reflect specularly into the gloss receptor angle was counted, to determine the percentage of surface area reflecting into the gloss detector. The assumption is that the greater this percentage, the higher the gloss. This can be shown visually by plotting the surfaces with points reflecting into the detector coloured white and all other points coloured black. An example of this is shown in Figure 2.6.

These investigations show that microfacet theory is capable of providing valuable insights when applied to real world surfaces.

6.3 Implementation

A microfacet model was developed in MatLab after the pattern laid down by Dong et al., with some differences. All code was written by the author. The model inputs are measurements of surface texture in the form of a heightmap and the outputs are reflection distribution curves (RDF). A measure of visual appearance can then be derived from the RDFs. As with the method of Dong et al, the RDFs are calculated from the surface data by determining the normal at every point of the surface, then counting the number of points that a reflect into a range of angles from a specific angle of incidence. The difference is in the way that the surface normals are calculated. Instead of fitting a Gaussian-weighted plane to each point using the width of the Gaussian kernel as a filter and the normal to the plane as the surface normal as per Dong et al., the surface is first filtered using a Gaussian filter, then the normal is calculated using the standardised formula described by Whitehouse and presented in Section 2.3.4 [4].

The model was used to replicate the 20° geometry found on the Rhopoint IQ, the input light is at 20° and detector is an array of diodes at $20^\circ \pm 7.5^\circ$. This is done by generating an incident vector at 20° from the vertical, then determining at each point

of the surface if the normal at that point is oriented in such a way that the ray reflected from that point will be directed into the area of the detector. The output of the model is a distribution that represents the intensity of the reflection at each angle (by counting the number of rays at each angle).

Several assumptions are made in the model. The first is that all reflections are specular, i.e. the angle of reflection is equal and opposite to the angle of incidence. Another assumption is that no masking or shadowing of surface reflection occurs, as this is only required at grazing angles [71]. A final assumption to note is that the model only considers topographical effects on surface reflections, and neglects effects of surface chemistry etc.

The general scope of the model can be seen in Figures 6.2 and 6.3. These figures show the input surface and a representation of the surface reflection for an input ray at 20°.

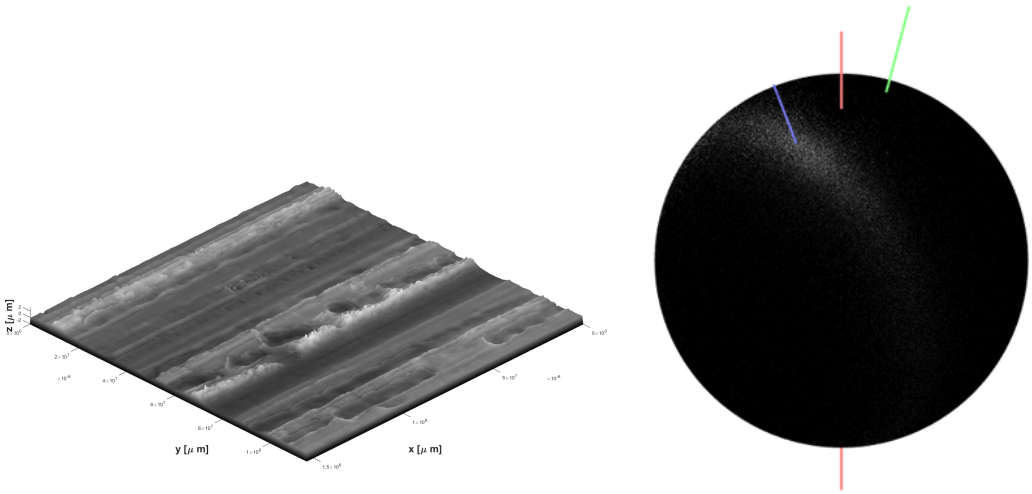

Figure 6.2: The figure on the left shows the surface used to generate the reflection distribution on the right. Each point on the sphere represents a reflection from the surface from an input angle of 20°, assuming specular reflection. The green line represents the incident angle and the blue line its specular reflection, with the white points showing the scatter of incident radiation.

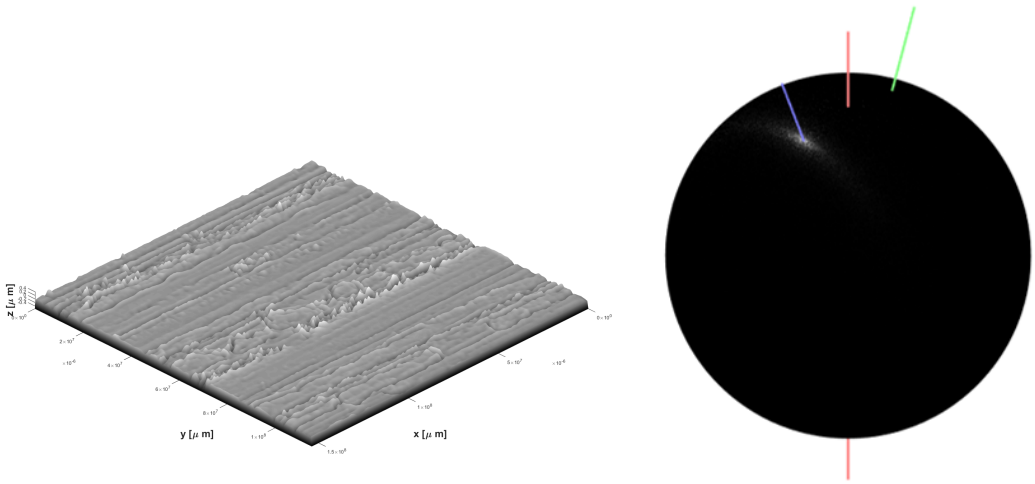

Figure 6.3: The figure on the left shows the same surface as in Figure 6.2 after filtering with a Gaussian band pass filter at a wavelength of 3 ± 1 µm. The figure on the right shows the reflection distribution from the surface.

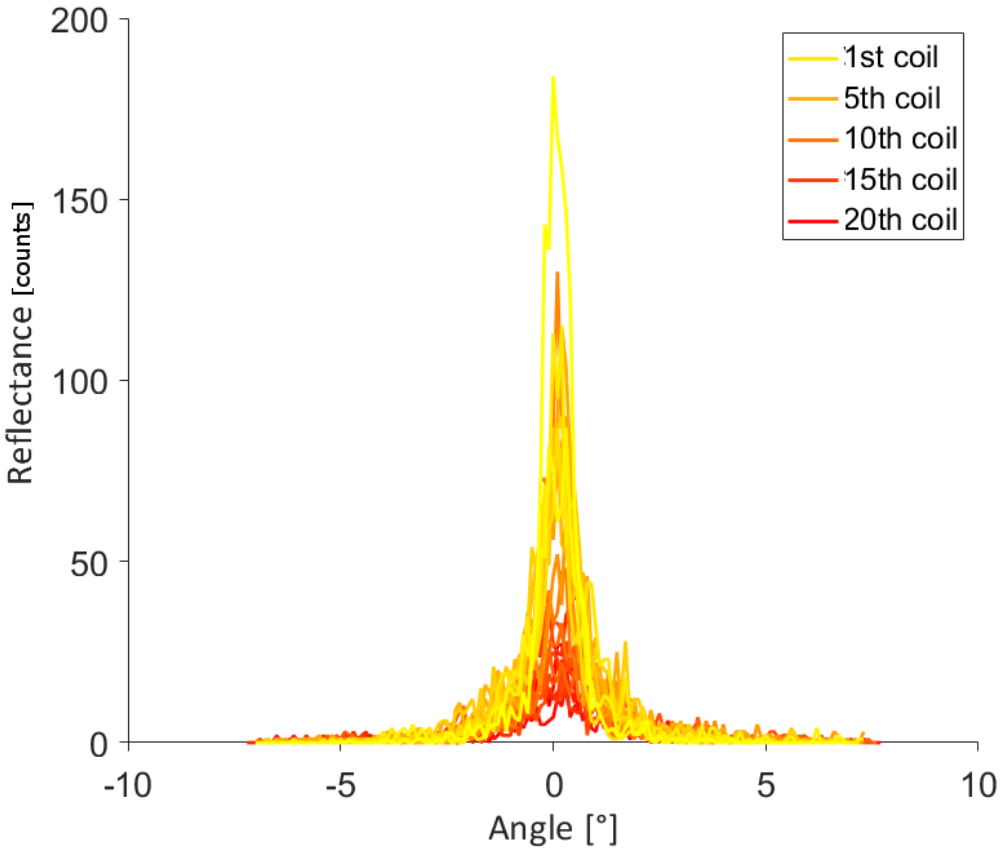

Figure 6.4: Reflection distributions of the surfaces of Sample Set 2, generated using a micro-facet approach.

The detector of the Rhopoint glossmeter lies in the same plane as the incident light. This was replicated by taking a slice of the overall hemispherical reflection from the surface in the same plane as the incident radiation across the same range of angles, to obtain a plot of reflection intensity across the detector angle. RDFs of the surfaces of

Sample Set 2 are shown in Figure 6.4. These can be compared to measured RDFs of the same sample set in Figure .

6.3.1 Validation

As described in the literature review, parameters characterising visual appearance are derived from the reflection distribution curves. Gloss is a measure of the specular reflection, haze is a measure of the off-specular reflection. The DOI is a measure of the ratio between the gloss and the haze. Figure 3.9 shows how these parameters are calculated from the RDF.

MatLab scripts were written to calculate visual appearance parameters from predicted RDFs. Some ambiguities in the knowledge of the exact method of calculating these parameters means a step to validate the custom built scripts is important. The implementation of these scripts and their validation are described here.

The implementation of calculations of gloss, haze and DOI are relatively simple. In each of these scripts the input is the RDF which is an array consisting of two columns, one of which is the angles across which the measurement has been made and the other is the reflectivity at each angle. Gloss is defined as the sum of the recorded reflectivity in the range $\pm 0.9^\circ$ around the specular angle. Therefore the script is a simple summation of the values of reflectivity found within that range. Haze is similar, but the summation is across the angles $-1.0^\circ \rightarrow -2.0^\circ$ and $1.0^\circ \rightarrow 2.0^\circ$. These definitions are taken from the Rhopoint user manual, which claims adherence to ISO .

These scripts were validated by running the scripts on RDFs for which the actual visual appearance parameters are known. Then the output of the scripts was compared to the known values. The measurements on which the validation was performed were taken from Sample Set 2.

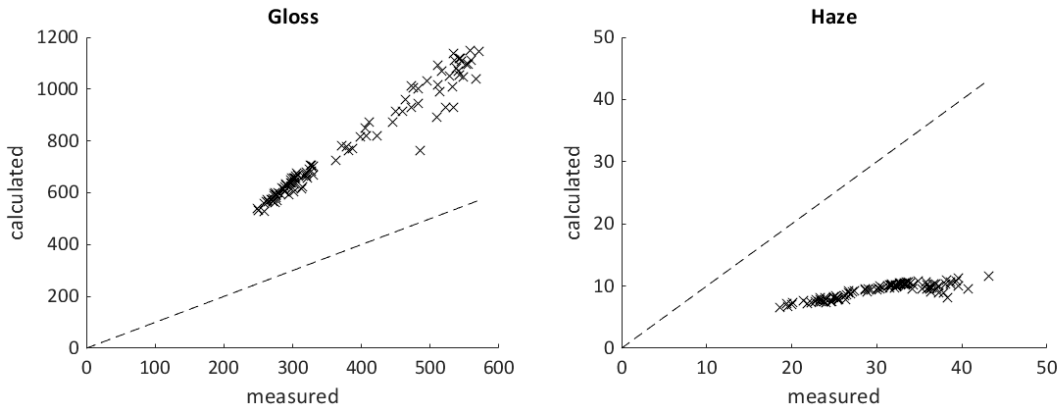

Figure 6.5: Figure showing visual appearance parameters measured directly by glossmeter compared with visual appearance parameters calculated from reflectance curves measured by glossmeter.

From Figure 6.5 it can be seen that gloss and haze parameters calculated from the reflectance curves according to the glossmeter manual (which comply with standards ISO 2813 and ASTM D523) do not match with the values measured directly by the glossmeter [68]. The gloss is over predicted and the haze is under predicted. This means it is not possible for the microfacet model to accurately predict the gloss or haze using the modelled reflectance curves (such as those in Figure 6.4) as an intermediary. A possible reason for this discrepancy is that the actual internal calculation carried out by the glossmeter to determine these parameters is not the same as the simple summation of reflectance curve valued described in the manual.

These same obstacles were encountered by Leloup et al., using a different gloss measurement system [70]. A fuller knowledge of the metrological systems of the glossmeter is necessary to make better predictions. Specifically, more knowledge about the calculation of parameters from the reflection distribution is needed.

As it is not possible to make direct predictions of gloss parameters from surface data, an alternate route was sought for. Landskroon had success in correlating the amount of surface slopes reflecting into the gloss receptor angle with the measured gloss [45]. This approach is identical to summing the values of the RDF across the gloss receptor angle. In other words, instead of predicting measured gloss values directly from surfaces, the percentage of surface slopes reflecting into the gloss angle is used as an intermediary. The proportion of surface slopes that reflect into the gloss detection angle can be described as the active surface area. The active surface area is the area of a surface that actively contributes toward the measured gloss of the surface.

6.4 Results

Figures 6.6 and 6.7 were created from surface texture measurements made on Sample Set 2. The surfaces measurements at x11 magnification were used, with a sampling interval of $0.9031\mu m$. Only the measurements made along the centre of strip were used for these plots, and each point is the mean of 3 measurements. The plots on the left of each figure show the proportion of surface points oriented to reflect into the gloss detector angle for every coil of the sample set. The plots on the right show the correlation between the proportion of the surface reflecting into the gloss detector and the measured gloss. The gloss measurements are the gloss at 20°, also taken from the centre of the strip. The mean of 5 measurements both along and across the strip was taken.

The difference between Figures 6.6 and 6.7 is in the filter settings applied to the surface measurements before the percentage of surface active in contributing to the measured gloss is calculated.

For Figure 6.6, the filter settings were determined by the results of Chapter 4.1. Results from that chapter show that the variation of the shortest wavelengths of surface texture is responsible for the variation in visual appearance parameters. The highest correlation between surface texture and visual appearance was found to occur at the $3 \pm 1\mu m$ band. The plots in Figure 6.6 were created from surface measurements filtered with those settings ($3\mu m$ centre wavelength, $2\mu m$ bandwidth).

For Figure 6.7, the filter settings were determined by results of Chapter 5. For the stone and light stone finishes, which are comparable to the fine stone finish of Sample Set 2, the MAF(MSa) for the 2.8 gsm coating weight is about 25% at $25\mu m$. This means that for a surface coating weight of 2.8 gsm, the majority of the substrate texture is still visible through the coating. The filter central wavelength was set at 25 μm and given a bandwidth of 20 μm to capture surface information around the scale of interest.

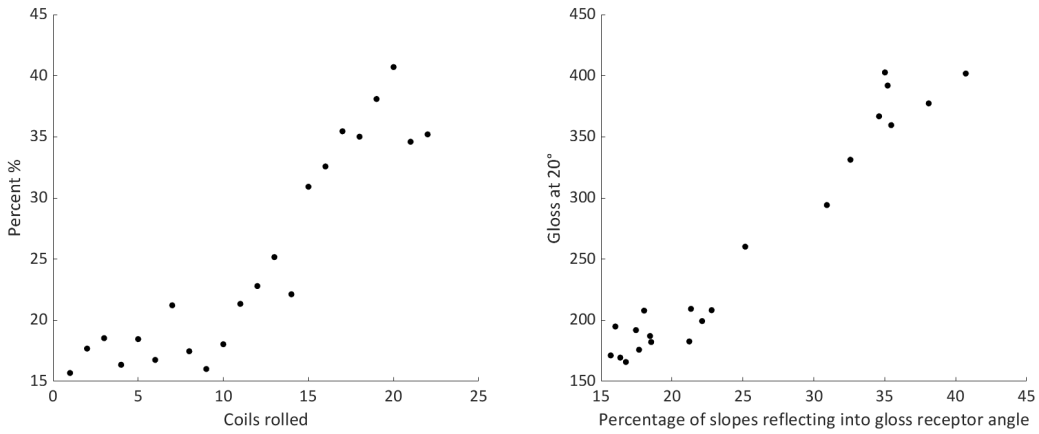

Figure 6.6: The surfaces of Sample Set 2 after filtering at $3 \pm 1\mu m$, showing the proportion of surface points that reflect into the gloss angle. The relationship between proportion of surface reflecting into gloss receptor and measured gloss. Rsqa = 0.95.

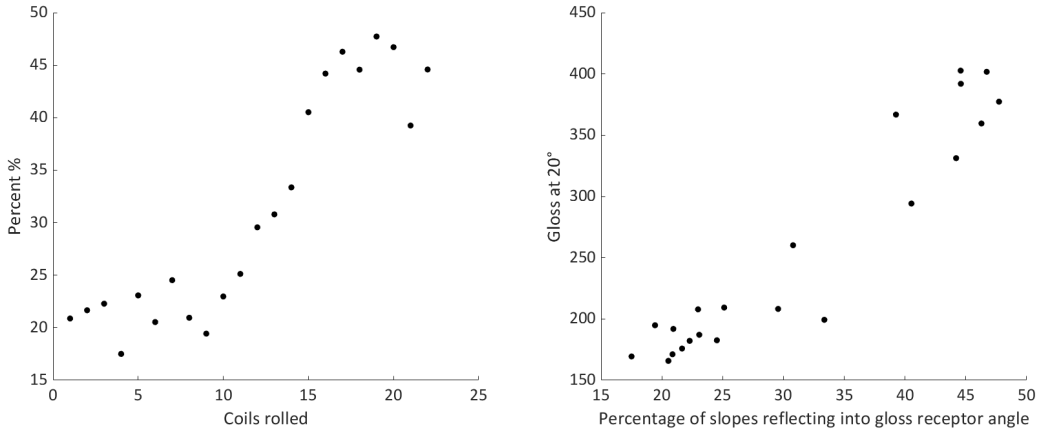

Figure 6.7: The surfaces of Sample Set 2 after filtering at $25 \pm 10\mu m$, showing the proportion of surface points that reflect into the gloss angle. The relationship between proportion of surface reflecting into gloss receptor and measured gloss. Rsqa = 0.91.

Figure 6.8 shows a comparison between the active surface area of two different finishes. Samples from each finish were taken from the 7th coil to be rolled. There is a slight difference between the measurements as one set was made at X11 magnification and the other at X10, meaning the sampling interval of the Stone finish samples is 0.97 μm and the sampling interval of the Fine Stone finish samples is 0.90 μm. These surfaces were also filtered with a central wavelength of 25 μm and a bandwidth of 20 μm.

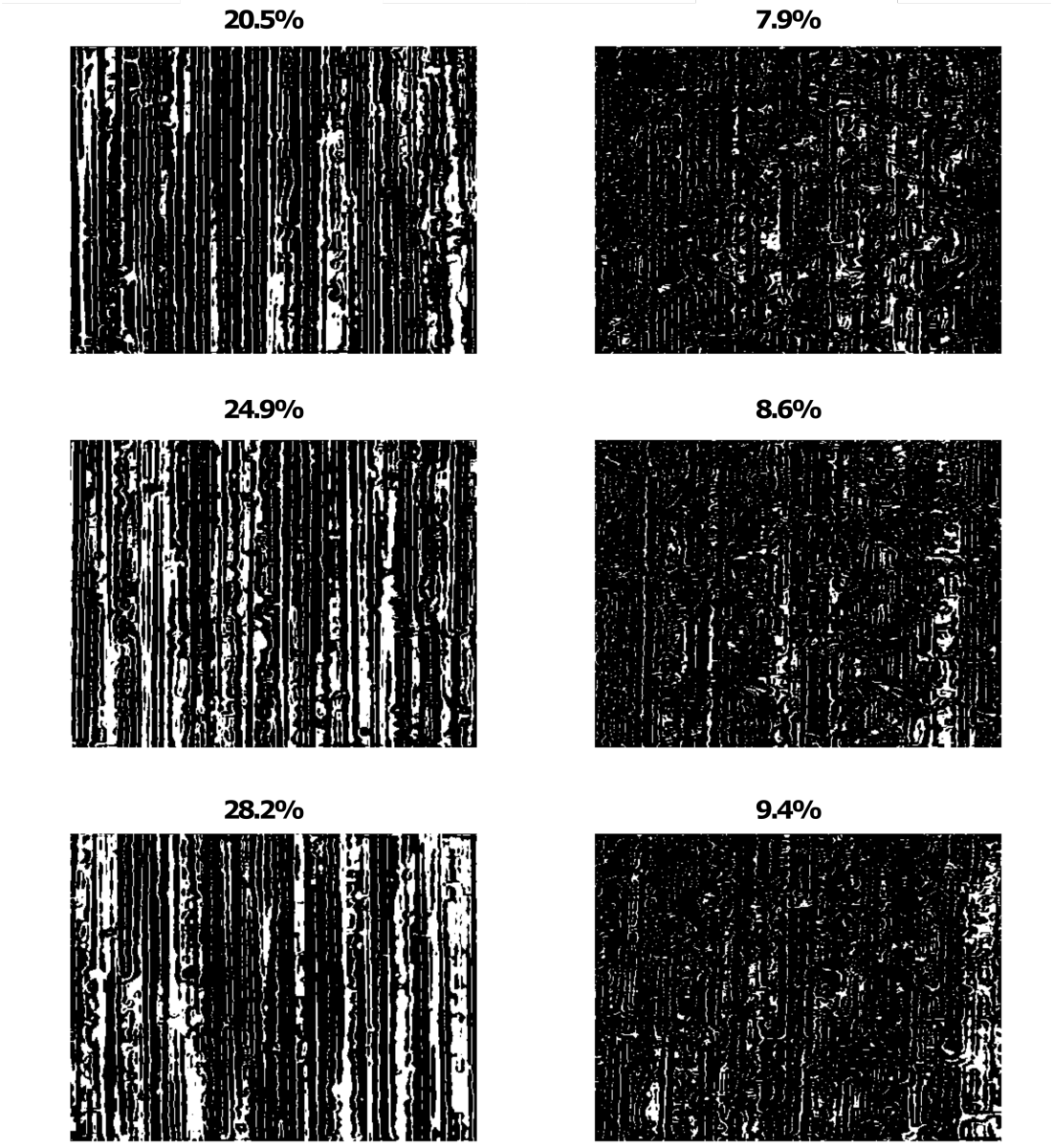

Figure 6.8: Comparison between the active surface area of fine stone and stone finish surfaces. The mean active area of the fine stone finish surfaces is 24.5%. The mean active area of the stone finish surfaces is 8.6%.

6.4.1 Discussion

Figure 6.6 shows that at the scales of surface texture that have greatest influence over visual appearance, as shown in 4.1, there is a large difference in the active surface area over the length of the roll campaign, with an increase from about 15% to about 40%. This same information can be seen in Figure 4.25. The discrepancy in values between Figure 6.6 and Figure 4.25 is explained by the different sets of measurements used in each figure. Figure 4.25 was generated using a set of measurements taken at X41 magnification and 6.6 was generated using a set of measurements at X11 magni-

fication. The X11 magnification was used in this section to enable better comparison with another set of measurements, seen in Figure 6.8, which will be discussed later in this section. However, although there is a difference in the magnitude of the results of Figures 6.6 and Figure 4.25, the proportional increase across the length of the roll campaign is similar for both sets of results, with the active surface area increasing by a factor of 2.6 for Figure 6.6 and 2.7 for Figure 4.25.

The effect that this increase in active surface area has on visual appearance can be seen in the right hand plot of 6.6. The strength of this correlation is Rsqa = 9.5. In fact, it can be observed that the gloss (at 20°) of a surface can be estimated from the active surface area by multiplication by a factor of 10.

The reasoning behind generating Figures 6.6 and 6.7 is to enable a comparison between different surface scales. This means a comparison can be made between the surface content with greatest influence over visual appearance and the surface content at longer wavelengths that will still be present after the strip has been coated. In comparing the strength of the correlation between active surface area and gloss measurements, it can be seen that the Rsqa drops from 0.94 to 0.91. This drop can be seen in the relative spread of values in the right-hand plot of Figure 6.7 compared to Figure 6.7, with a slight increase in the percentage of surface slopes reflecting into the gloss detection angle. The correlation at longer wavelengths is still strong enough for predictions of visual appearance to be made from the active surface area, however a simple multiplication by a factor of 10 will no longer suffice as an estimate of specular gloss.

Figure 6.8 shows a comparison between stone and fine stone finish surfaces. The surfaces were filtered with band pass filter, with a central wavelength of 25 μm and a bandwidth of 20 μm. The mean active area, for 3 measurements on 2 surfaces (only one measured surface shown in the Figure) was 22.1% for fine stone surfaces and 8.8% for stone surfaces. Surface texture disruption of the EDT texture surface can be clearly seen.

These results have implications for the design novel surface textures with enhanced control over visual appearance. When designing surfaces, although the shortest wavelengths of surface texture have greatest influence over visual appearance, it is sufficient to control the slopes at longer wavelengths. Controlling the slopes at longer wavelengths means that:

1. Modifications made to surface texture will not be attenuated by the coating layer.

2. It will be possible to manufacture discernable differences in visual appearance.

6.5 Conclusions

- A model of visual appearance of surfaces was developed, using a microfacet modelling approach.

- The model is unable to provide precise predictions of visual appearance parameters such as gloss and haze, due to a lack of information about the methods by which those parameters are measured.

- The active area, which is the proportion of the surface that reflects light into the gloss receptor angle, was investigated as a potential predictor of visual appearance.

- The active area of surfaces at two different scales was compared. The first scale was the scale of strongest correlation and the other was the scale at which surface features will retain prominence through the coating layer.

- The active area at scales which remain visible through the coating is a good predictor of visual appearance, as measured by the specular gloss at 20°. The strength of the correlation between these two parameters is $R^2 = 0.91$ for Sample Set 2.

Chapter 7

Design

7.1 Overview

Throughout this thesis, the focus has been on the effect of surface texture on visual appearance, to determine how visual appearance can be controlled in the manufacturing process of tinplate packaging steel. Reflectivity of the tin coating plays a major role in the visual appearance of packaging steel. Not only is there a difference in the magnitude of gloss before and after tin coating, but also the difference in gloss post-coating is greater than the difference in gloss pre-coating. This means that the coated surface brings out the difference in underlying surface texture. Subtle differences in visual appearance prior to tin coating become large differences after coating. This underscores the importance of controlling underlying substrate texture in order to control the visual appearance of the final coated product.

In this chapter, insights derived in previous chapters are used to design surface textures that give enhanced control over visual appearance. Each of the chapters gives useful information toward the design of these surface textures. These are as follows:

1. **Substrate** - variation in surface slopes at the smallest scales have greatest influence on visual appearance.

2. **Coating** - the tin coating attenuates the smallest scales of surface texture, up to a cross-over point, dependent on coating weight, at which the underlying substrate features are visible through the coating.

3. **Function** - the proportion of surface slopes reflecting into the gloss detection angle is a good predictor of surface gloss, even at the cross-over scale.

In Chapter 2, various methods of surface texturing were discussed. Among these were laser texturing processes. Laser texturing (LT) processes are able to achieve greater control over surface texture properties as tighter control over the dimensions of the individual unit event is possible. With EDT, the size of the unit event is determined by the pulse energy. This gives a crater of a certain size, however independent control of event depth and radius is not possible. With LT, independent control of event depth and event radius is possible. This is because the duration as well as the energy of the pulse can be controlled. The texturing systems are already realised in commercial applications such that by Pomini, which claims control over the mean amplitude of surface texture as well as control over the crater radius [96]. Laser systems also have

greater control over the placement of events, allowing deterministic distributions of unit events. In this chapter, the enhanced control of laser texturing is brought together with the insights of work carried out in this thesis to design surfaces which can be realised in a manufacturing environment.

First, models of conventional surface texturing processes are developed and combined to replicate conventional surface finishes as produced by the manufacturing process of tin plate packaging steel. These surface texture simulation models are then expanded to take into account the enhanced control offered by laser texturing. A series of potential surface textures are designed and simulated according to a set of constraints. The active area approach as described in Chapter 6.1 is used to assess the functionality of the surface texture designs.

7.2 Simulation of surface texture

In this section, methods of surface texture simulation are described, implemented and assessed. More specifically, two surface texturing processes are modelled, namely grinding and EDT. These are used to simulate two finishes often produced in the tinplate industry, and often sold into markets for which visual appearance is a critical function. These are stone and fine stone finishes. The EDT model is then used to simulate the LT texturing process and several novel surface finishes are developed.

7.2.1 Background

There many methods available for the simulation of surface texture. These methods fall largely into two categories: statistical/spectral modelling and physical modelling. A combination of the two approaches has been used in this project, with the physical method dominating and the statistical method being used to support it.

Statistical models simulate surface textures by describing the spectral properties of the surface then generating a distribution of surface heights according to that spectrum. These surfaces are defined by their statistical and spectral characteristics. For example, Newland, Hu and Tonder, Wu et al., among many others, have developed models using the Fast Fourier Transform (FFT) to generate surface topographies [97–99]. In general, these methods begin with defining the spectral content of the surface in frequency space then performing an inverse Fourier transform into xyz space to get the heights

(and their locations) of the surface.

Physical models replicate the actual physical processes that the surface undergoes to generate deterministic surfaces created by those processes. These techniques often utilise the unit event of the machining/texturing process. One advantage of these techniques is that the input parameters can be matched to process parameters making it possible to investigate the effect of process parameters on the surface texture

In this section, physical models of grinding and EDT processes are described, and a spectral modelling approach is used to model the grinding wheel surface. First, conventional surface textures are created and validated against measurements made on real surfaces. Then alternate surface textures are developed which give enhanced control over visual appearance.

7.2.2 Simulation of ground surfaces

Grinding is an abrasive machining process in which small abrasive particles are used to cut away material from a surface. A grinding wheel, made of hard particles embedded in an adhesive, is rotated at speed and forced into the surface. In the tinplate industry, grinding is used to create the surface texture of work and back-up rolls which are used in cold rolling the steel strip. The size and distribution of the particles, the feed rate and depth of cut are the primary process parameters for the creation of workpiece topography (as well as its initial topography). Grinding is one of the most well-established manufacturing processes and has been the subject of extensive research for many years. A more thorough description of the process can be found in Chapter 2.

Many models and simulations of the grinding process have been developed, based on both empirical and analytical methods. Brinksmeier et al. give a comprehensive review of the history and variety of grinding models [100]. Salisbury et al. offer an abridged review [101]. These models tend to have in common a three-step process:

1. Model the grinding wheel surface.

2. Model the workpiece surface.

3. Model the interaction between the grinding wheel and the workpiece.

For the first step, essentially two approaches are available. The grinding wheel surface can be obtained by measuring a real wheel or generated by an analytical model. These models often approximate the shape of a grain using simple shapes

such as spheres then distribute these shapes randomly across a plane [102]. Spectral approaches as described above are also used [103]. For the second step, the workpiece surface is often taken to be a plane. This assumption is made as the grinding process is a material removal process and the original workpiece surface is destroyed.

A number of approaches are available when modelling the interaction between wheel and the workpiece. These are kinematic-geometrical models, finite element models (FEM) and molecular dynamics (MD) models. Kinematic-geometrical models consider the relative motions of wheel and surface. The material removal of the wheel is determined by tracking the locations in space of each point on the wheel and workpiece surfaces and modelling every contact of those points. Most models assume total material removal, i.e. at each contact point, the material on the workpiece surface is removed by the wheel surface. This simplification is somewhat unrealistic as it neglects the effects of pile up and deformation, however it leads to good results. More sophisticated models extend this basic kinematic-geometric approach to include effects such as pile up, crushing of grains and plastic deformation of work piece material. Molecular dynamic models represent the surface as a collection of interacting atoms arranged on a crystal lattice. The resultant surface is created by modelling the motion imparted to each atom by the motion of a grit. This approach is inappropriate for the work in this thesis as it operates on the nanometre scale. FEM is used mainly to model the thermal dynamics of grit-surface interactions and also operates on a scale smaller than that required in this thesis, often modelling the interaction of only a single grit and the surface [100].

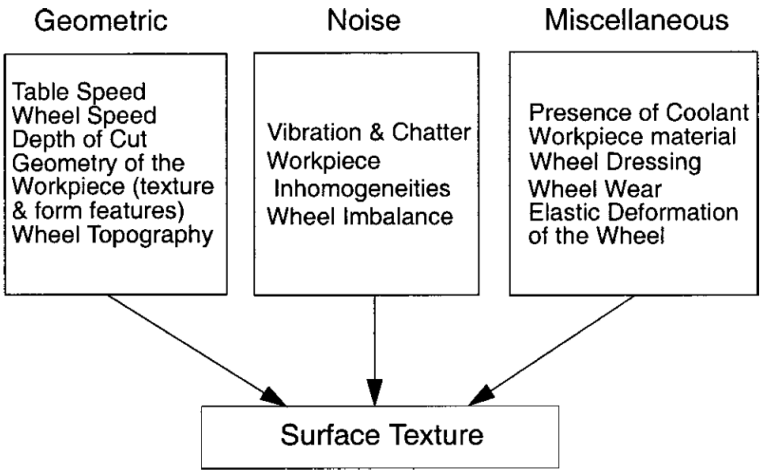

Figure 7.1: Factors affecting surface texture of ground workpiece in the grinding process.

For simplicity of implementation and macroscopic range, the kinematic approach

has been used in this project. The model used in this project is based off of the work of Salisbury et al. [101]. Their model generates a ground surface based on the cutting conditions, wheel topography and initial workpiece topography. The model calculates the motion of every point on the wheel surface with respect to the workpiece height points. If the motion of the wheel indicates contact between the points, the workpiece heights are updated to show their new position as workpiece material in contact with the cutting grains is completely removed. Only the primary parameters (called "geometric" in Figure 7.1) are considered, secondary parameters ("noise" and "miscellaneous" in Figure 7.1) such as vibration and wear are not considered. Predictions of surface roughness parameters such as Ra, Rz etc. from the simulated topography show good agreement with measured ground surfaces.

The grinding wheel surface was modelled after the approach of Cao et al., which was developed from that of Chen and Rowe [104, 105]. Grinding wheel surfaces are a mass of grains in a bonding agent, which gives a stochastic, isotropic surface, with grains presenting cutting points to the workpiece surface at random orientations and positions. The size of the grains of a grinding wheel are described by the grit number, which is related to the size of the mesh used to sort the grains. These are related in the following way: $d_g = 15.2M^{-1}$ where d_g is the grain dimension, or the aperture opening of the sorting mesh. Cao et al. model the grain height using a Gaussian distribution, controlled by d_g as follows

$$h = \sigma h' + d_g \tag{7.1}$$

where h is the protrusion height of a grain, h' is a number drawn randomly from the Gaussian distribution, with mean d_g and standard deviation σ. These heights are then distributed over a plane using a mesh as modelled by Chen and Rowe. They derived a formula for grain distribution by assuming uniform packing of spherical grains, giving grain interval

$$\Delta = d_g \sqrt[3]{\frac{\pi}{12(32 - S)}} \tag{7.2}$$

where S is the wheel structure number. A wheel surface is generated by distributing the heights of Equation 7.1 over the intervals determined by Equation 7.2. This model takes as its inputs the wheel structure number, grain size, number of surface points and root mean square roughness. The height distribution of the surface is then generated

across a grid with horizontal interval determine by the size of the grains. An example of such a surface can be seen in Figure 7.4.

The interaction was modelled using the kinematic-geometric approach, as described above, found in Salisbury et al. [101]. The inputs of the model are the grinding wheel radius, angular speed of the wheel, table speed, depth of cut, number of surface points and grid interval size. The workpiece surface was taken to be planar. The model outputs a heightmap representing the ground surface.

At any time, the position of any point on the grinding wheel surface can be described by the following equations and depicted in Figure 7.2.

$$x = i \tag{7.3}$$

$$y = y_0 - f \cdot \Delta t + (R + h_{ij}) \sin(\theta_{0j} - \omega \Delta t) \tag{7.4}$$

$$z = R - f - (R + h_{ij}) \cos(\theta_{0j} - \omega \Delta t) \tag{7.5}$$

with:

$i =$ wheel height array index in the radial direction,

$j =$ wheel height array index circumferential direction,

$h_{ij} =$ height of the grinding wheel surface array at element (i, j),

$\theta_{0j} =$ initial angle of the jth row of the grinding wheel array,

$y_0 =$ initial distance between the **O** and **W** origins in the Y direction,

$R =$ nominal radius of the wheel.

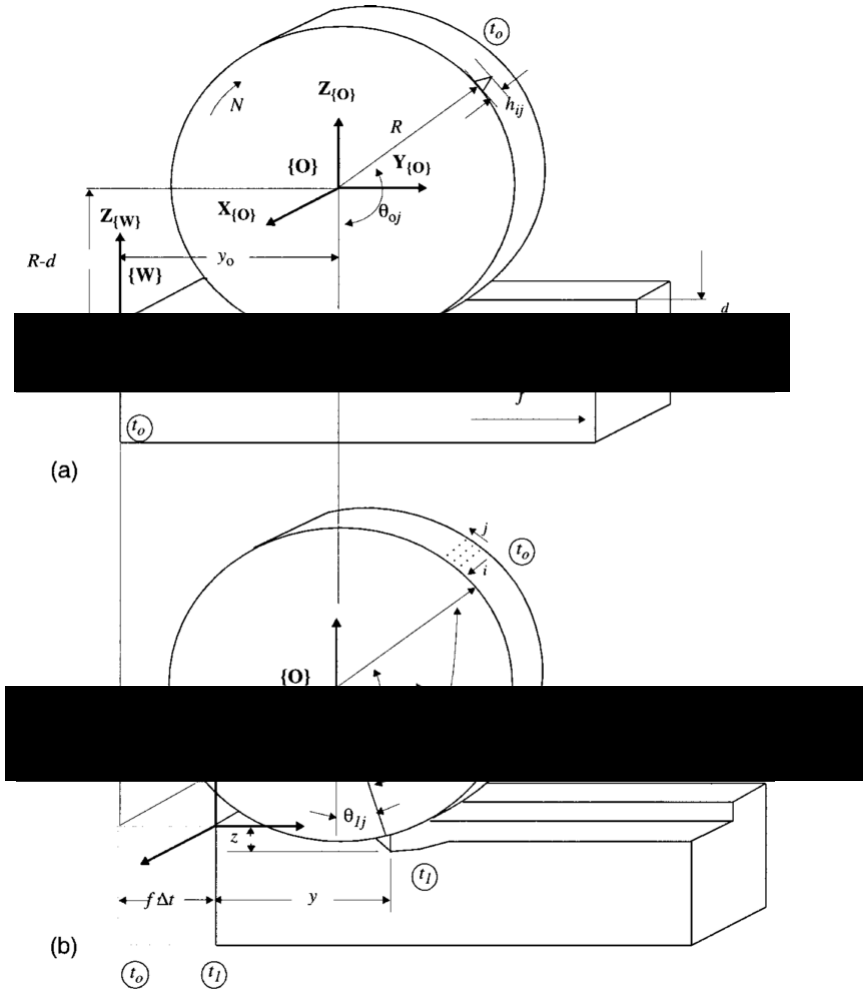

Figure 7.2: The grinding model process. Top is at time $t = t_0$, bottom is at time $t = t_0 + \Delta t$ [101].

The time t0 + dt is the instant at which point on the grinding wheel has the same y location as a point in the workpiece array. When this is zero, i.e. when the wheel and workpiece points have the same location in y, Equation 7.4 can be used to determine dt. Since Equation 7.4 is non-linear, a Newton-Raphson routine is used to estimate dt. In this routine, an initial guess value for time, dt, is specified, which is then used to iteratively estimate dt until the error in estimation approaches a predetermined limit. This dt is then used to find Z_{new}, the height of the wheel point according to Equation 7.5. The height of the workpiece surface height at the same (x,y) location, is then compared to Z_{new}. A point on the surface of the workpiece is altered by a grinding wheel point only if it has height less than the height of the workpiece at that same location. This is repeated for every (x,y) location and the ground surface is the new height, Z_{new}, at each location. This routine is shown in Figures 7.2 and 7.3 and was implemented in MatLab.

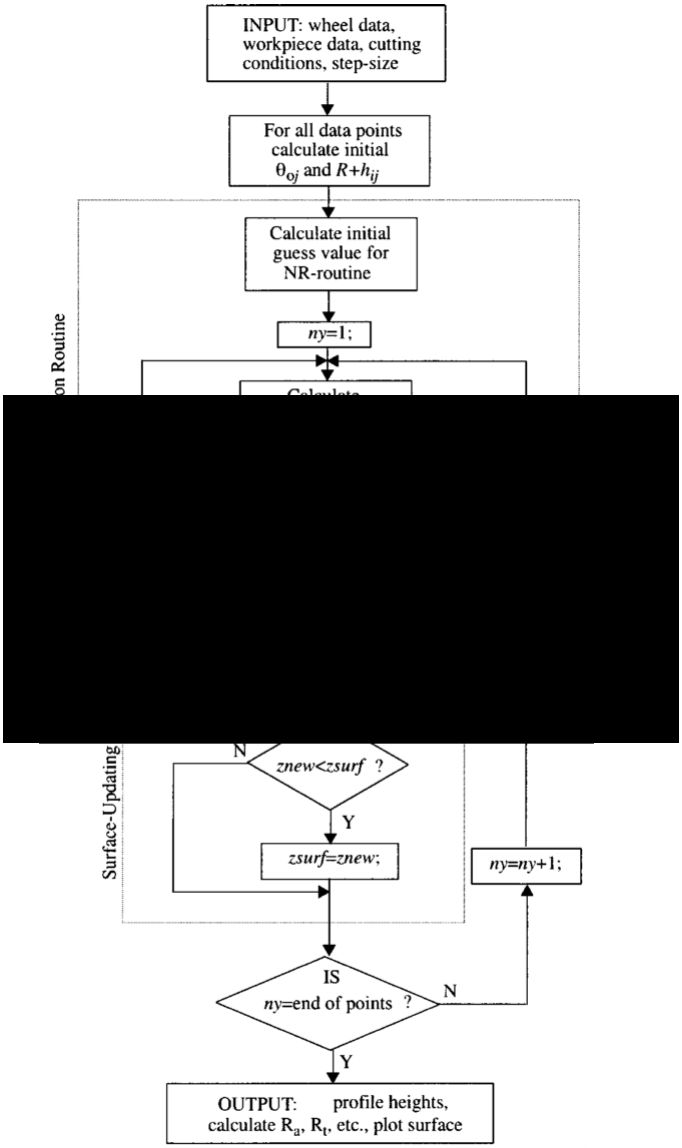

Figure 7.3: Flowchart showing the model routine [101].

7.2.2.1 Results

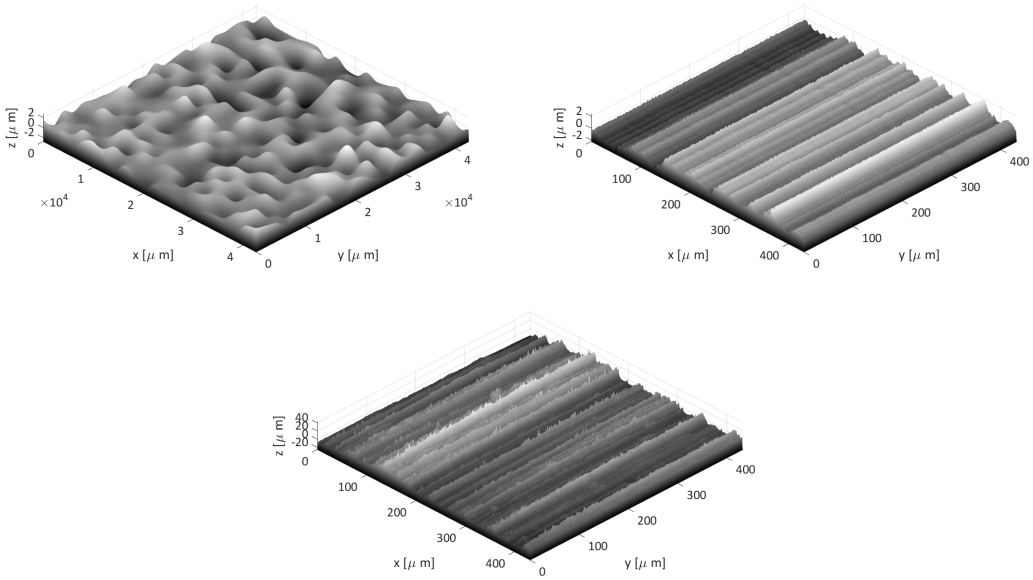

Figure 7.4: The figure on the top left is an example of a grinding wheel surface generated to simulate ground surfaces. The figure on the top right shows a simulated ground surface resulting from the grinding wheel surface. The third figure is a measured ground surface.

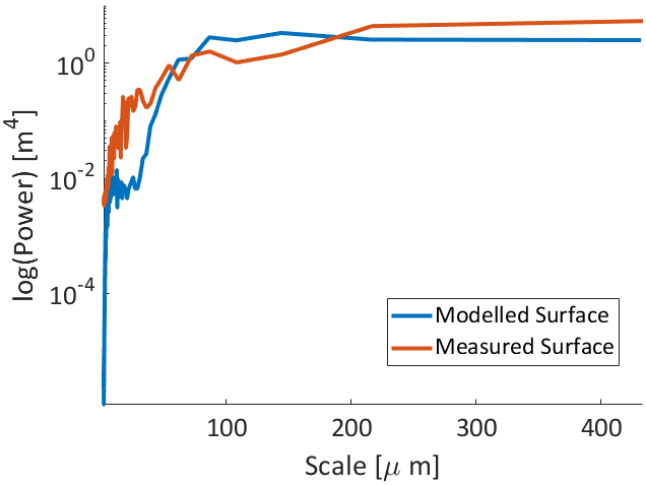

Figure 7.5: The mean PSDs of measured and modelled ground surfaces taken across the rolling direction.

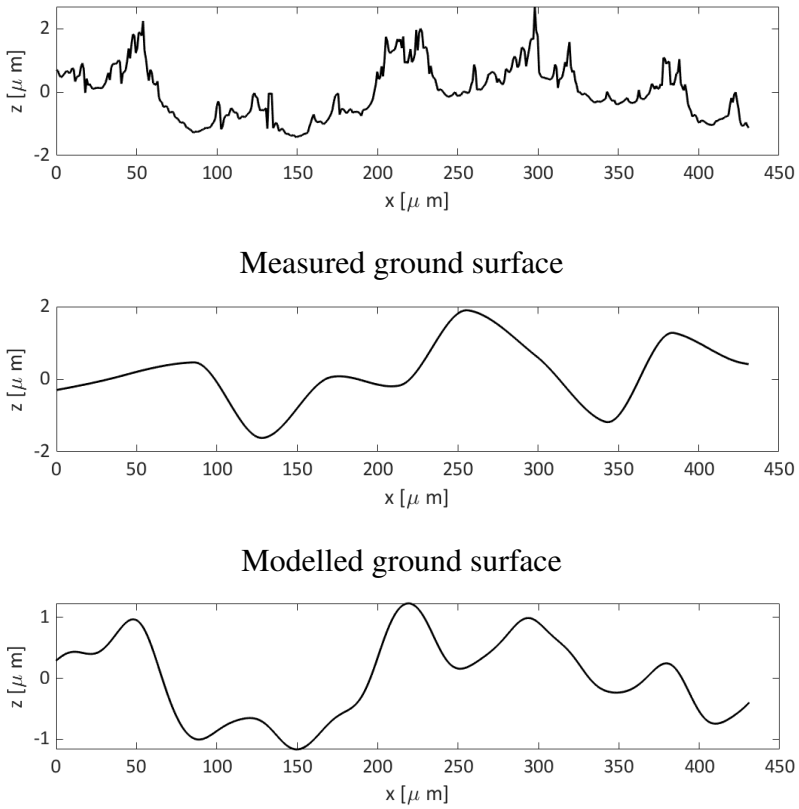

Figure 7.6: Three surface profiles, the first taken from a real ground surface, the second taken from a modelled ground surface and the third taken from a real ground surface, after filtering at a scale of strongest similarity as shown in Figure 7.5.

7.2.2.2 Discussion

Figure 7.4 shows the output of the Salisbury grinding model. The image on the left is the randomly generated grinding wheel surface used to obtain the simulated workpiece surface seen on the right. When compared to real, measured surfaces, it can already be observed that much surface information is missing, particularly in the high frequencies, as seen in Figure 7.5. However, the mean texture amplitudes show good agreement; The mean Sa of the modelled surfaces used here is 0.69 μm and the mean Sa of the measured surfaces is 0.67 μm.

Figure 7.5 was created using two sets of data, one taken from real, measured ground surfaces and the other from modelled ground surfaces. The real surface measurements were made on silicon replicas of ground work rolls. The orange line of Figure 7.5 is the mean 1D PSD taken across the rolling direction of three such measurements. The blue line is the mean 1D PSD taken across the rolling direction of 10 randomly generated ground surfaces. The mean Sa of the real, measured surfaces is 0.67 μm and the mean Sa of the modelled surfaces is 0.69 μm. This shows that the model can

accurately represent the average roughness of surfaces. However, Figure 7.5 shows that the spectral content of these surfaces is very different. The high frequency surface content is under-predicted and the low frequency surface content is over-predicted. The surfaces are only accurately predicted at a specific scale. Figure 7.6 shows this.

The content of the simulated workpiece surface is largely determined by the characteristics of the generated grinding wheel surface used to create it. The method of generating grinding wheel surface used to simulate these surfaces generates grinding wheel surfaces only at a specific scale, determined by the input parameter wheel grit, which determines the spacing between surface peak heights. In other words, the ground surfaces are accurately predicted only at the same scale as the grit of the wheel surface. Looking at Figure 7.1 it can be seen that only the "geometric" factors are taken into account in this model, with "wheel topography" dominating the results, and "noise" and "miscellaneous" factors are neglected. This would account for the missing higher frequency content. This model could be developed by generating multi-scale grinding wheel surfaces, giving multi-scale ground surfaces.

Salisbury et al. also developed a model of the grinding wheel surface [106]. They used a multi-scale empirical approach in which they used the inverse Fourier transform to convert the frequency data of a measured grinding wheel surface back into spatial data, at only specific spatial bandwidths of interest. They took areal measurements of a grinding wheel and determined the Fourier spectrum of that surface. They then divided that continuous Fourier spectrum into a number of discrete bands, summing the total power within each band and assigning it the frequency of the midpoint of that band. In other words, the variance in surface texture across a range of spatial frequencies is assigned to a single frequency representative of that band. These discrete bands create a simplified surface spectrum from which a surface can then be reconstructed using the inverse Fourier transform. Salisbury et al. found that this reconstructed surface is a good representative of the real surface, even though the frequency content of the surface has been simplified.

A model of the grinding wheel surface was developed, taking inspiration from both approaches described above. From Salisbury et al., the idea that surfaces can be efficiently reconstructed from limited frequency data was utilised, but simplifying the method further to make it amenable to modelling of the mechanisms of the manufacturing process. Whereas in the Salisbury grinding wheel model, 20 bands of surface frequencies were used, in the model developed here only three bands were used. These

three bands were chosen on the basis of Figure 7.1. One band was used to represent the surface texture created by the noise component, one to represent the texture created my the miscellaneous component and the final band to represent the geometric component. From Cao et al., the method of distributing Gaussian heights across a grid with intervals determined by grain spacing was used.

The model of the wheel surface is as follows. Instead of distributing heights across only one grid. Heights are distributed across three different grid intervals, one with a small interval to represent short-wavelength components (noise) one with a large interval to represent long-wavelength content (miscellaneous) and one in-between to represent mid-wavelength components (geometric). Each surface is then interpolated across the same grid such that they have the same spacing between points, with peaks still separated by the original spacing. The wheel surface is then assumed to be the sum of these three surfaces. The frequency content of the wheel surface is determined by the intervals between heights and their amplitudes. A wheel surface generated by this method can be seen in Figure 7.7.

This approach is valid as the miscellaneous factors, such as wheel deformation, and noise factors, such as vibration and chatter, would feed into the wheel surface as it is experienced by the workpiece. All the influences of the manufacturing process are summed up in the wheel surface as it is acted upon by the workpiece. In other words, the 'wheel surface' in the model is not just the wheel topography in isolation but is a representation of the interaction between the wheel and workpiece surfaces. Noise factors along the rolling direction were introduced to the Salisbury grinding model using a randomised variable which introduces a drift in the position of the wheel surface on the scale of a few microns to simulate chatter and vibrations. This is visible in the surface in Figure 7.7 but not in the PSDs of Figure 7.8 as they are taken across the rolling direction.

7.2.2.3 Multi-scale grinding model results

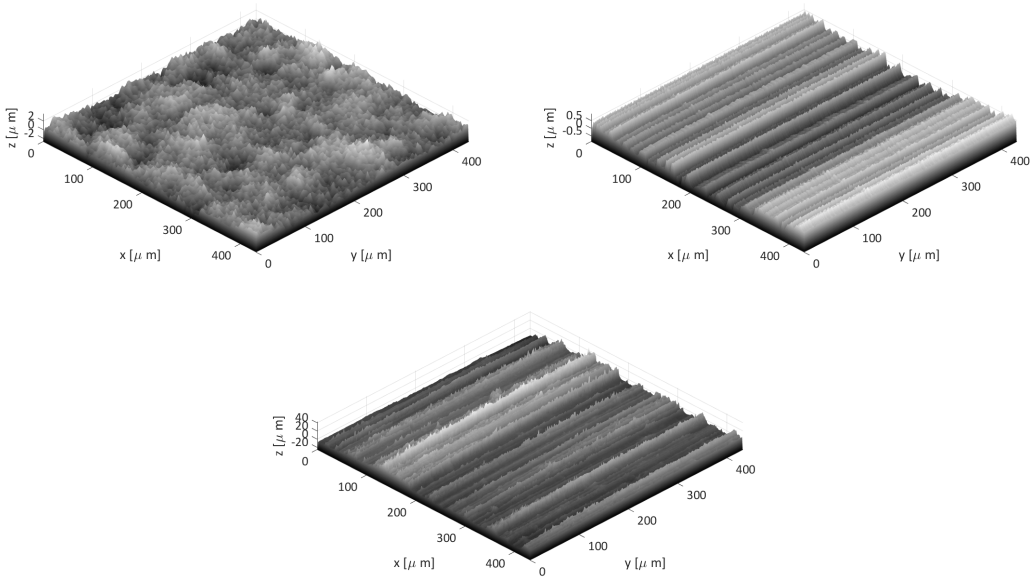

Figure 7.7: The figure in the top left is a multiscale modelled grinding wheel surface, the top right is a modelled multiscale ground workpiece surface, and the third figure is a measured real ground workroll surface.

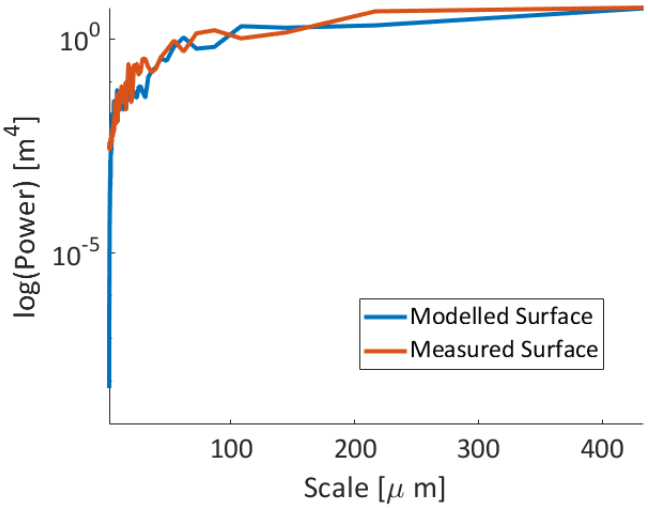

Figure 7.8: The mean PSDs of measured and modelled ground surfaces taken across the rolling direction, using the multi-scale model.

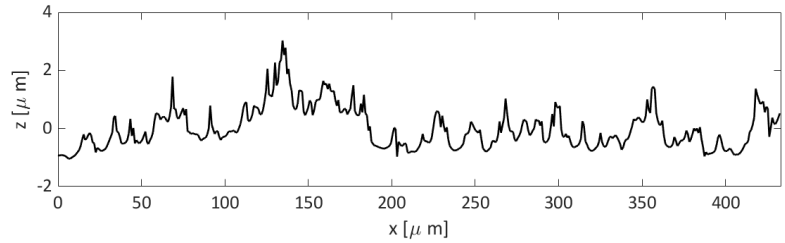

Measured ground surface profile,

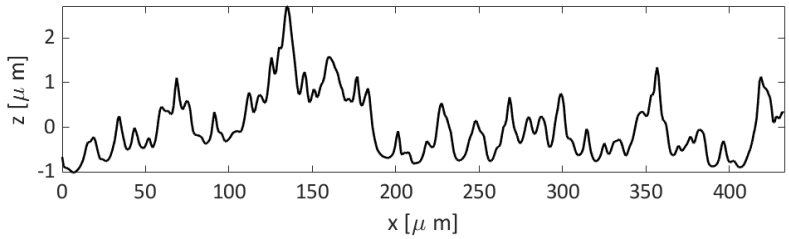

Measured, filtered ground surface

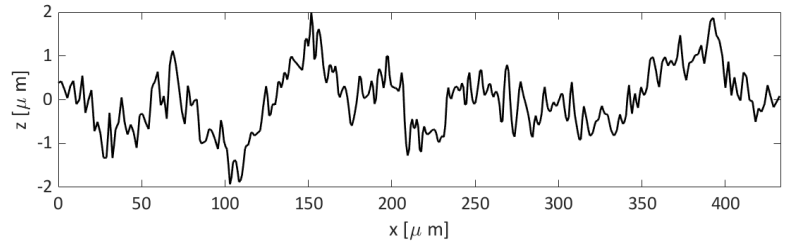

Modelled ground surface

Figure 7.9: Measured surface profiles, with and without measurement noise, compared to multi-scale modelled surface profile taken across the rolling direction. The missing high frequency content is now visible.

7.2.2.4 Discussion

Figure 7.8 shows the ability of the multiscale model to match the surface textures produced by the tinplate manufacturing process. There is a good match between the spectral content of the modelled and measured surfaces. To simulate the surfaces used to create this figure, the amplitudes and spacings of the three grinding wheel components were adjusted to match measurements. Therefore a necessary advance to this model would be to validate the wheel surfaces against measurements made on real wheel surfaces. An attempt was made to do this using silicon replicas, however due to the high roughness of the wheel surfaces, the replica could not accurately capture the surface and the whitelight interferometer could not capture data from the steep sides of the even the better replica surfaces. However, for modelling of surface function, it is sufficient to match the properties of the surfaces, without modelling the process phenomena.

Comparisons between Figures 7.5 and 7.8 shows that the model is now able to match the short wavelength components, however there is still some overestimation of long wavelength surface texture components. The mean Sa of the measured surfaces is 0.67 μm and the mean Sa of the modelled surfaces is 0.56 μm. There is still some discrepancy in power in the very highest frequencies, visible in Figure 7.5. This may be due to the presence of measurement noise, which is therefore missing from the modelled surfaces, rather than an accurate representation of physical surface features.

The intention behind this approach is to enable connection of the grinding wheel surface with the manufacturing process by development of separate models of each of the three discrete factors influencing the grinding process. Different phenomena govern the creation of small-scale noise content, midrange geometric content and large scale miscellaneous content. Separation of these into discrete frequency bands mean governing models could be developed for each of the different phenomena, using empirical or analytical methods, to determine the appropriate peak spacings and amplitudes.

7.2.3 Simulation of EDT surfaces

Electro-discharge texturing removes material from the surface of the work piece by vaporisation due to the action of electrical discharges between an electrode and the surface. A spark is created in the gap between the electrode and the workpiece which vaporises the material in that location, leaving a crater in the workpiece surface. The electrodes are scanned across the surface until the entire workpiece is textured. The size of the crater is controlled by the type of dielectric used, voltage pulse duration and the peak current of each pulse [27].

As described in Chapter 2, modelling of the surface topography created by the EDT process tends to be empirical and oriented toward determining correlations between process and surface parameters rather than generating representations of surface height maps. Models of the EDT process that do attempt to simulate the surface texture do so by first defining the unit event (in this case the EDT crater), then distributing multiple instances of the unit event across the x-y plane of the surface. Jithin et al. represent the crater as an inverted hemisphere [107]. Their approach gives good agreement between measured and simulated average amplitude of surface roughness. Wentink et al. represent the crater using an analytical function, defining the crater geometry in

terms of sine functions [32]. Their approach includes a description of the crater rim formed by material deposited from the interior of the crater which is missing from the approach of Jithin et al. This is essential for modelling the strip surface texture, as it is the inverse of the roll texture that creates the strip texture. Therefore it is the properties of the crater rims on the work roll that are essential to the texture of the strip.

The unit event is described by Equation 7.6 and is shown in Figure 7.10.

$$h(\lambda) = \begin{cases} -d\cos(\frac{\pi\lambda}{2\eta}) & 0 <= \lambda <= \eta \\ -\frac{2rd(\pi-2)\eta^2}{\pi(\eta^2-\omega^2)}\sin(\frac{\pi(\lambda-\eta)}{(\omega-\eta)}) & \eta < \lambda < \omega \\ 0 & \lambda >= \omega \end{cases} \tag{7.6}$$

with: d the depth at the centre of the crater, η, ω the inner and outer radii of the crater, r the ratio of material redeposited from the crater into the rim.

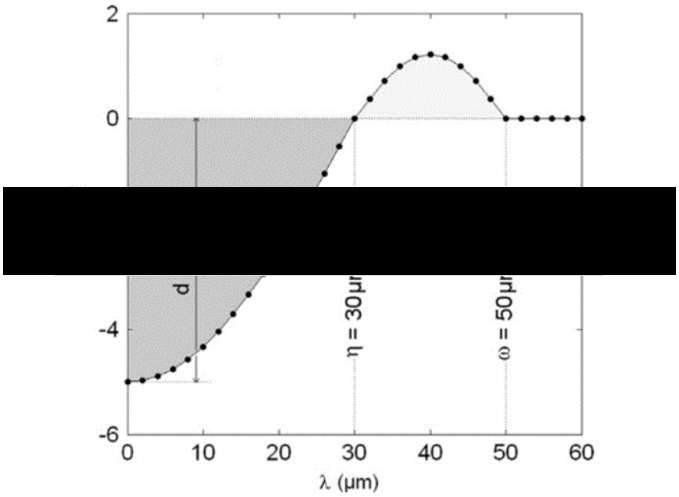

Figure 7.10: A diagram of the unit event described by Equation 7.6 [32].

The events can be distributed across a plane with a number of different distributions ranging from purely random through to purely deterministic. The MatLab code for the model was obtained directly from the authors and used to generate simulated EDT surfaces. An example is shown in Figure 7.11.

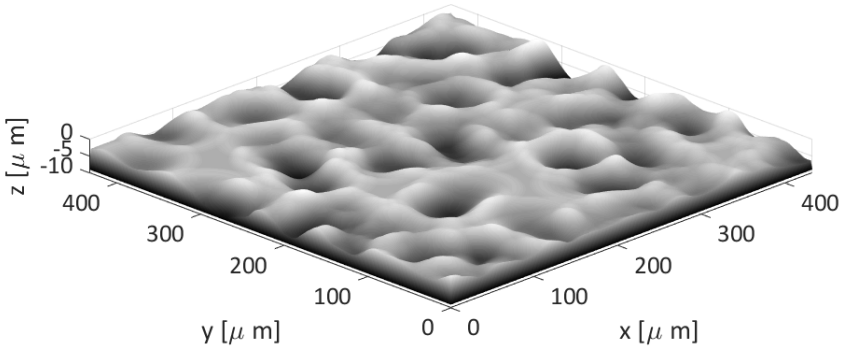

Figure 7.11: A simulated EDT surface, generated by the Wentink EDT model.

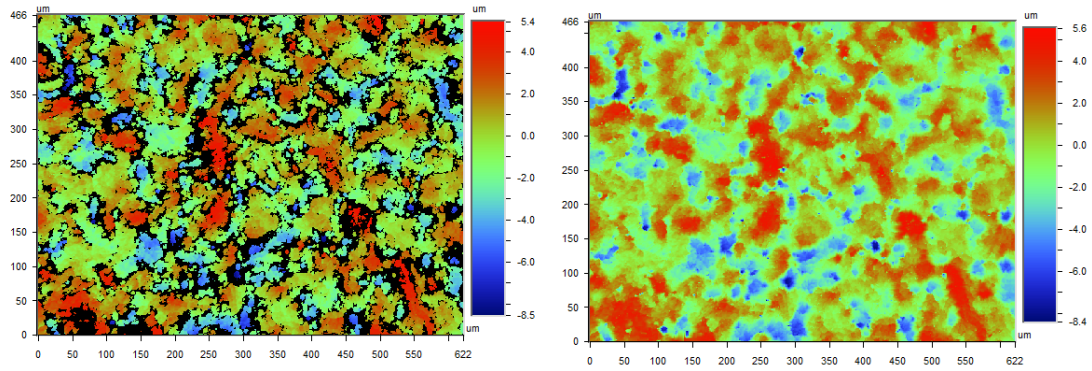

Figure 7.12: The figure on the left shows a white light interferometry measurement of a replica EDT surface, showing the missing data points. The figure on the right shows the same surface after interpolation of the missing data points.

Table 7.1: Surface texture parameters of measured EDT replica surfaces.

Parameter	Surface 1	Surface 1	Surface 3	Surface 4
Sa	2.32	2.42	1.90	2.41
Sq	2.90	3.03	2.31	2.82
Ssk	-0.25	-0.13	-0.84	0.11
Sku	2.93	2.91	3.70	2.82
Sdq	42.4	43.1	37.8	41.4

To validate the EDT model against measurements made on real surfaces, silicon replicas of an EDT work roll were made. Due to the high roughness of the surface, when measurements were made, the whitelight interferometer could not capture surface data from the steep sides of the surface features. This can be seen in Figure 7.12. In the figure on the left, every black point represents a missing data point. The figure on the right shows the same surface after interpolation with a data-restoration routine built into the Wyko software. In order to offset the uncertainty in these measurements, 5 measurements were made of the surface in the exact same location, then the mean of the 5 measurements was taken, in order to maximise the captured surface data. Table

7.1 shows a set of surface texture parameters calculated for the replica EDT surface. The surfaces show good agreement, as seen also in Figure 7.13, except for Surface 3 which is an outlier. It was assumed that this surface replica did not correctly capture the surface texture and was left out of all further analysis.

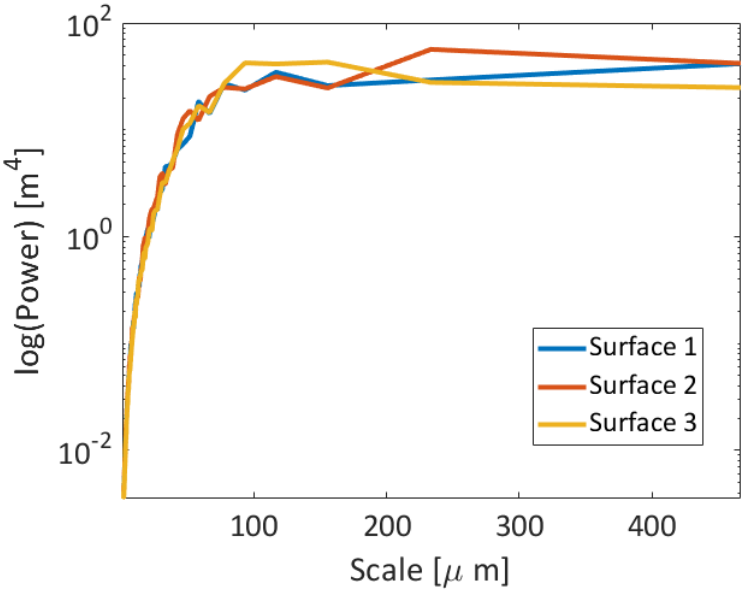

Figure 7.13: Measured PSDs of three replica EDT surfaces.

7.2.3.1 Multi-scale EDT model results

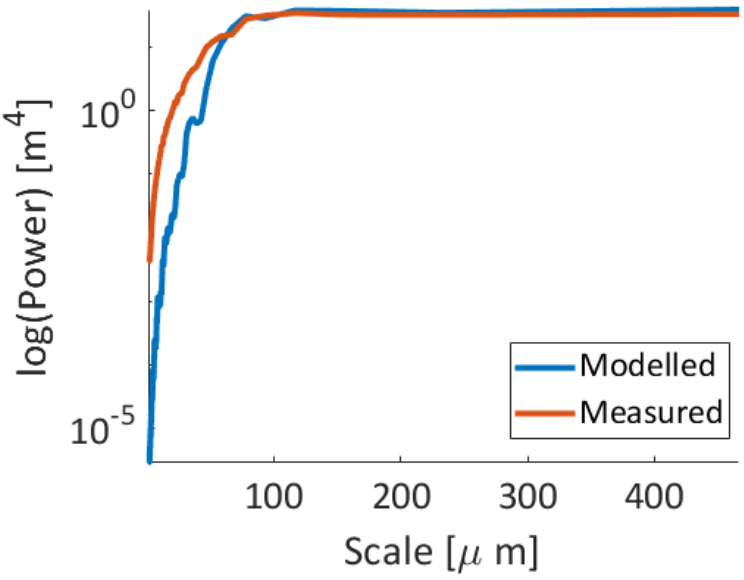

Figure 7.14: Comparison between modelled and measured PSDs of EDT surfaces.

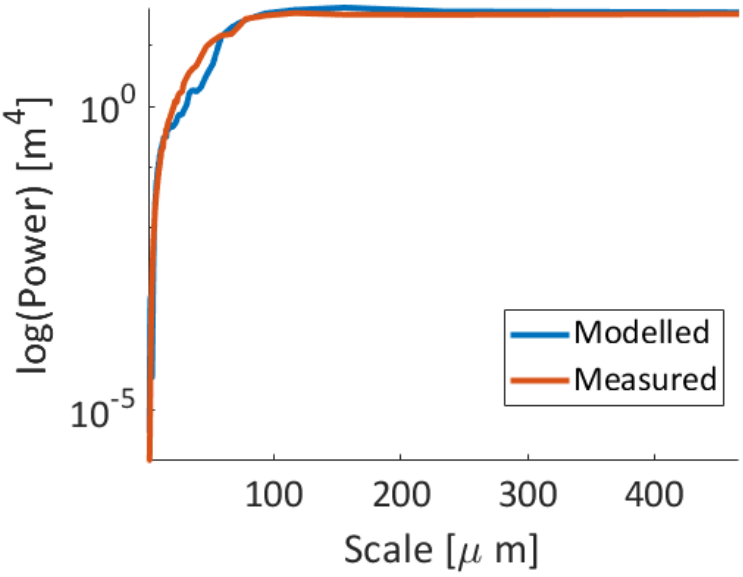

Figure 7.15: Comparison between PSDs of measured EDT surfaces and multi-scale modelled surfaces.

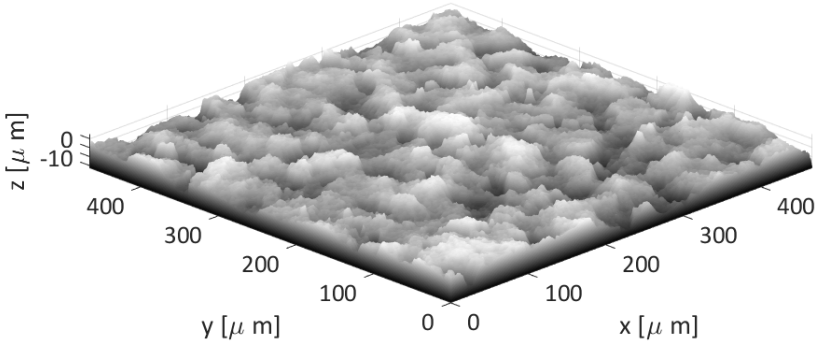

Figure 7.16: Measured EDT surface.

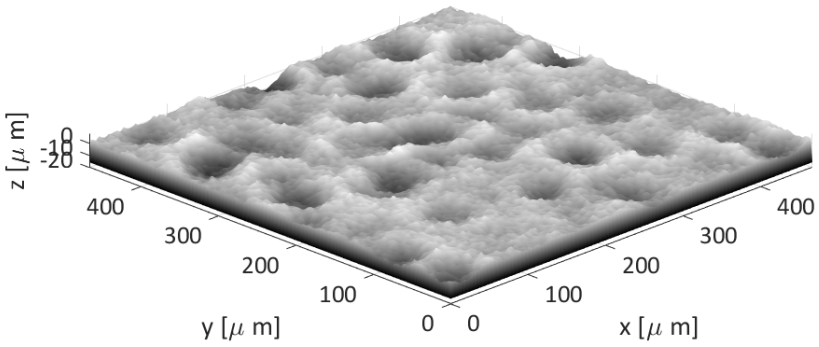

Figure 7.17: Multi-scale modelled EDT surface.

7.2.3.2 Discussion

Figure 7.14 shows a comparison between measured and modelled EDT surfaces. The PSD of the measured surfaces is the mean of the three measurements seen in Fig-

ure 7.13. The PSD of the modelled surfaces is the mean of 10 simulated surfaces, simulated by the EDT model described above, shown in figure 7.11. Much like with the grinding model, large discrepancies can be observed between the measured and modelled surface content, particularly at higher frequencies. Improvements in the prediction of the function of simulated surfaces texture could be had by increasing the realism of the unit event model. The model does not take into account the multi-scale nature of surfaces. The analytic form of the unit event results in simulated surfaces that exist at a very narrow band of spatial wavelengths, rather than a superposition of variations at multiple wavelengths giving a much broader spatial spectrum as found in real surfaces.

The EDT model was expanded to include higher frequency surface content using the same method as was used for the grinding model, by adding noise terms to the surface data. Scale and amplitude parameters were adjusted to match the surface content of measured surfaces. As before, future work should attempt to link these parameters to physical processes, however for the purposes of this thesis it is sufficient to match the textures. The multi-scale modelled surfaces can be seen in Figure 7.15. Again, the mean of ten simulated surfaces was used to produce this plot. In Figures 7.16 and 7.17 measured and modelled surface textures can be compared. By addition of further bands of surface information, a much closer match is obtained between simulated and measured surfaces.

7.2.4 Texture transfer model

A simple texture transfer model was developed to model the imprinting of roll texture on the strip surface. This model was based off the work of Kijima et al. who showed that the texture transfer of large rolls can be modelled as the vertical indentation of the roll roughness into the strip [36]. Therefore the texture transfer model works by inverting the roll surface (as it is the peaks of the roll that become the valleys of the strip and vice versa), then overlaying the roll surface and the strip surface. At every point at which the roll surface is less than the strip surface, the updated strip height at that point is set as the roll height. As it is unrealistic to assume that the full texture of the roll is imparted to the strip, the roll is given an offset so that only a proportion of the roll is imprinted into the strip. This offset parameter is adjusted for different surface finishes to ensure the roughness matches those set in the specifications.

7.2.5 Simulating surface texture

In this section, conventional surface finishes created by the manufacturing process of packaging steel are simulated using the above describes surface texture models. The surfaces chosen for modelling are surfaces created by the the temper mill, as these surfaces are often sold into markets for which visual appearance is a critical surface function. The aim is to model the outgoing strip surface of the temper mill. This is done by using the models described above to simulate the textures of every work roll that the strip experiences as it pass through the initial five-stand double reduction mill and then the two-stand temper mill, using a simple imprinting method to simulate the transfer of surface texture of each successive work roll.

Prior to rolling at the temper mill, the strip is rolled in a five-stand double reduction mill. Every roll in the five-stand DR mill has ground texture. A simulated work roll surface is generated for each roll using the grinding model described in the previous section, with average roughness set by the manufacturing process parameters. Assuming the incoming strip is a plane surface, the first roll texture is transferred to the plane surface, then the texture of the next roll in the series is transferred onto the new strip surface and so on with each successive roll texture being transferred onto the strip surface such that the outgoing strip is an accumulation of the textures of every roll in the series. A schematic of this process is shown in Figure, 7.18, with the average roughness specifications of each roll shown in Table 7.2. An example of simulated strip produced by the five-stand DR mill is shown in Figure 7.19. The average roughness of the modelled strip surface is $S_a = 0.39\mu\text{m}$, which is comparable to the specified average roughness of $R_a = 0.30 - 0.45\mu\text{m}$.

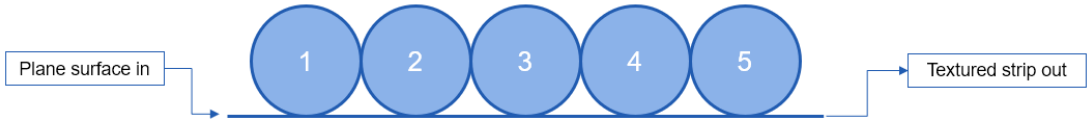

Figure 7.18: Simulation of textures produced by the five-stand DR mill prior to temper rolling.

Table 7.2: Surface texture parameters of each roll of the 5 stand DR mill. The outgoing strip average roughness is specified as $R_a = 0.30 - 0.45\mu\text{m}$.

Stand	**Min Ra [μm]**	**Max Ra [μm]**
1	1.50	2.00
2	1.25	1.45
3	0.75	0.90
4	0.65	0.75
5	0.55	0.65

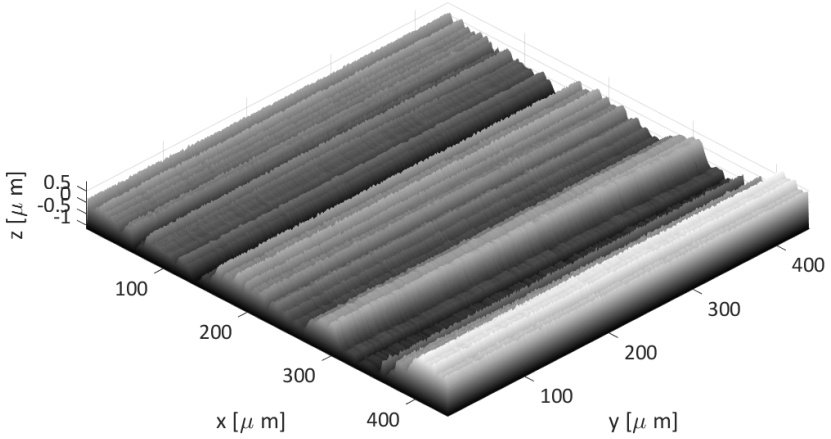

Figure 7.19: Simulated surface texture of strip coming out of the 5 stand mill, before further texturing at temper mill. Average roughness of this surface $S_a = 0.39\mu\text{m}$.

After rolling by the DR mill, the strip is then rolled at the temper mill. This section focuses on two surface finishes, namely stone and fine stone finish. Stone finish is produced with an EDT roll in stand 1 and a ground roll in stand 2, whereas fine stone finish is created with a ground roll in both stands, as shown in Figure 7.20. The outgoing strip surface is modelled in the same way as for the five-stand mill. The surfaces of both work rolls are simulated using the grinding and EDT models described above, with average roughness within manufacturing process specifications. These are shown in Figure 7.20. The incoming strip surface is the outgoing strip of the DR mill, and each successive roll texture is transferred to the strip surface using the texture transfer model. Simulated stone surface can be seen in Figure 7.22 and compared to a measured surface in Figure 7.21. Surface profiles of modelled and simulated stone finishes can be seen in Figure 7.23. An example simulated fine stone surface can be seen in Figure 7.25 and compared to a measured surface in Figure 7.24. Surface profiles of

modelled and simulated stone finished can be compared in Figure 7.26.

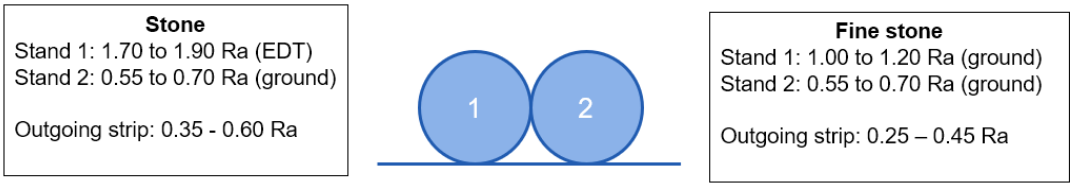

Figure 7.20: Simulation of textures created by the temper mill.

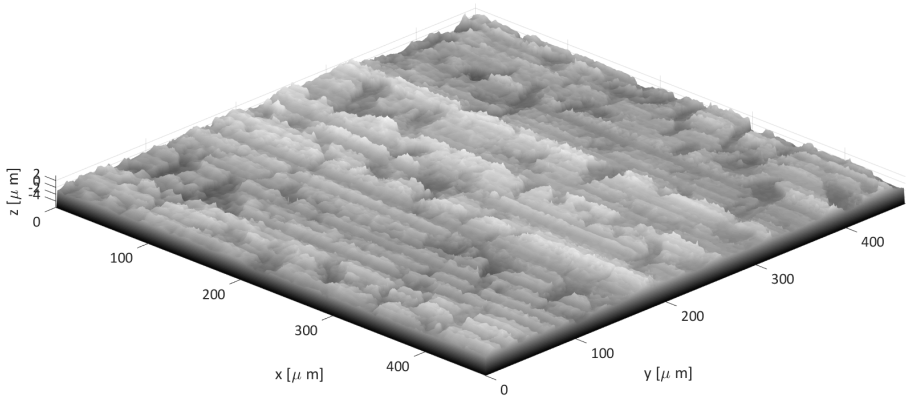

Figure 7.21: Measured stone surface, created with an EDT textured roll in stand 1, and a ground textured roll in stand 2 of a 2 stand temper mill. Sa $= 0.75\mu$m for this surface.

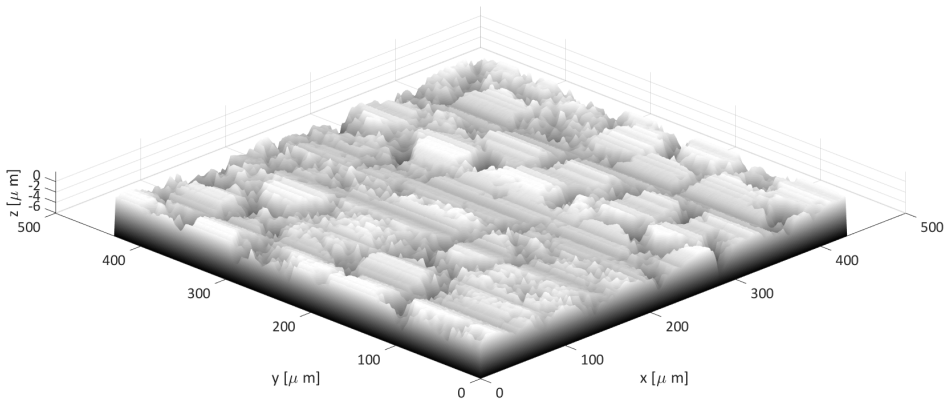

Figure 7.22: Simulated stone surface, created with an EDT textured roll in stand 1, and a ground textured roll in stand 2 of a 2 stand temper mill. Sa $= 0.86\mu$m for this surface.

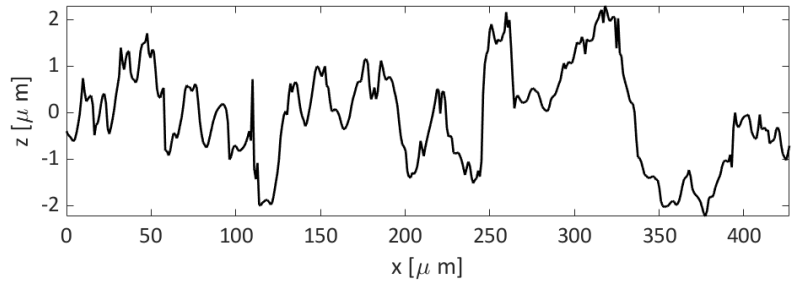

Measured stone surface profile

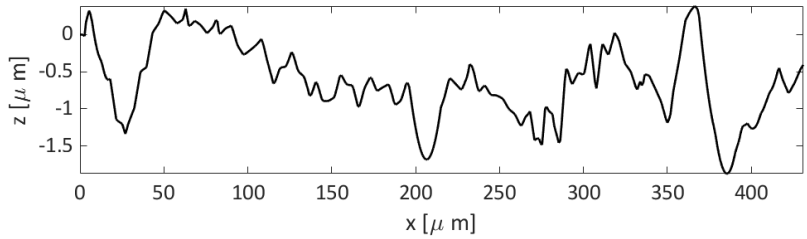

Modelled stone surface profile

Figure 7.23: Measured and simulated stone finish surface profiles.

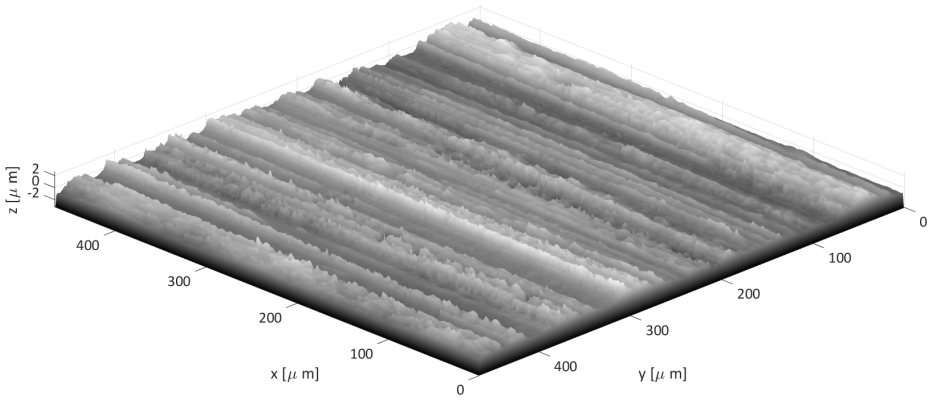

Figure 7.24: Measured fine stone surface, created with a ground textured roll in both stands of a 2 stand temper mill. Sa $= 0.52\mu$m for this surface.

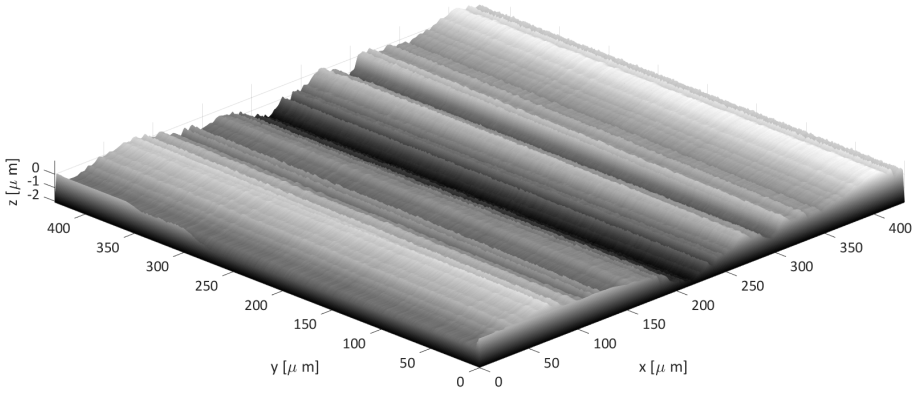

Figure 7.25: Simulated fine stone surface, created with a ground textured roll in both stands of a 2 stand temper mill. Sa $= 0.53\mu\mathrm{m}$ for this surface.

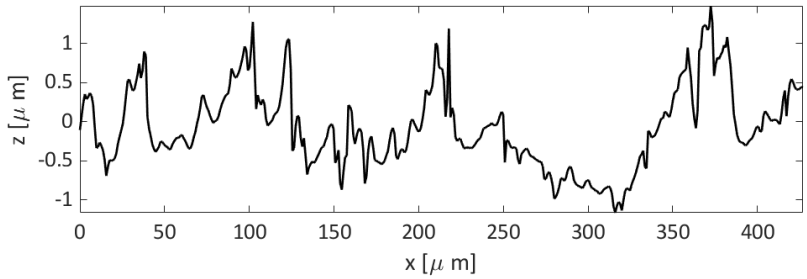

Measured fine stone surface profile

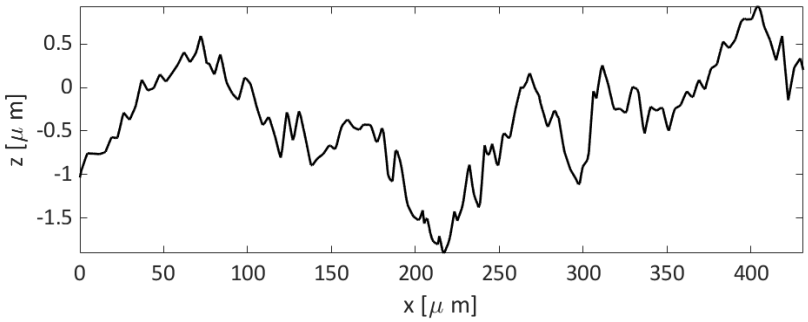

Modelled fine stone surface profile

Figure 7.26: Measured and simulated stone finish surface profiles.

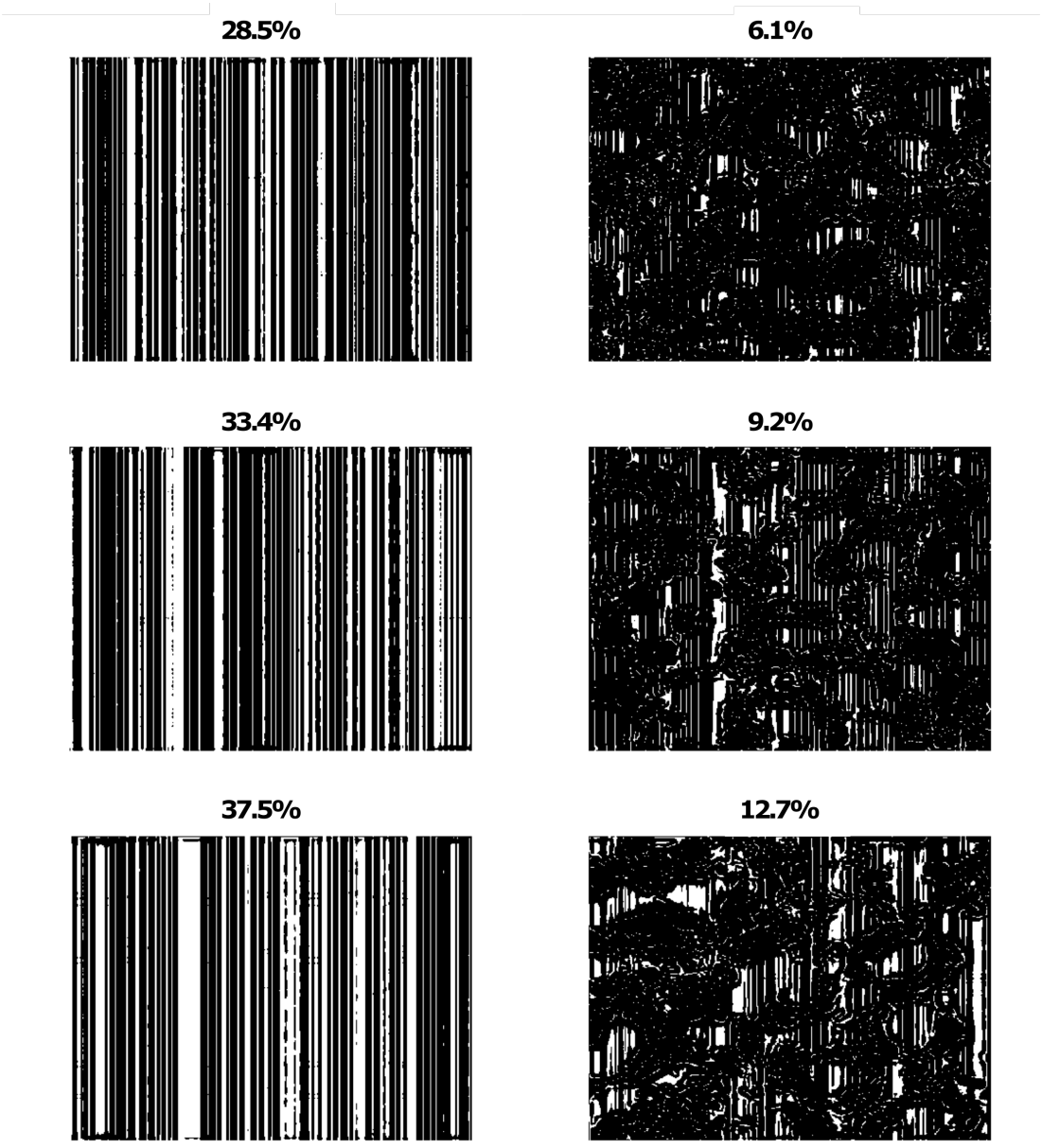

Figure 7.27: Simulated fine stone and stone finish surfaces, showing the proportion of surface facets reflecting into the gloss angle.

Comparison of Figures 6.8 and 7.27 show how well the surface texture simulations are able to replicate the active area of real world surfaces. For 10 simulated surfaces, the mean area reflecting into the gloss receptor was 32.3% for fine stone surfaces and 10.7% for stone surfaces. The active area of fine stone finish is over-predicted by $32.3 - 24.5 = 7.8\%$, however the stone finish is only $10.7 - 8.6 = 2.1\%$ over-predicted. The larger over-prediction of fine stone finish may be due to the lack of variation along the rolling direction in the simulated surfaces when compared to the measured surfaces.

7.3 Design constraints, decisions and justifications

It has been shown that surface slopes are responsible for surface gloss. Therefore the main purpose of this work was to design surfaces in which slopes are controlled, leading to control over visual appearance. It has also been shown that different scales have different effect on visual appearance and also are affected differently by a tin layer coating. These scale considerations fix the size of the surface features to be generated. The control over surface slopes needs to occur at scales small enough to actually affect visual appearance but not so small that their variation is obscured by the tin layer.

Other constraints were suggested by Tata Steel, in order to align surface texture designs with surface texture currently in production. The surface texture must be isotropic to match the current EDT surface textures, with roughness amplitudes at similar levels to the fine stone finish. The surfaces were modelled in the same way as the conventional surfaces described above, following the schematic shown in 7.28.

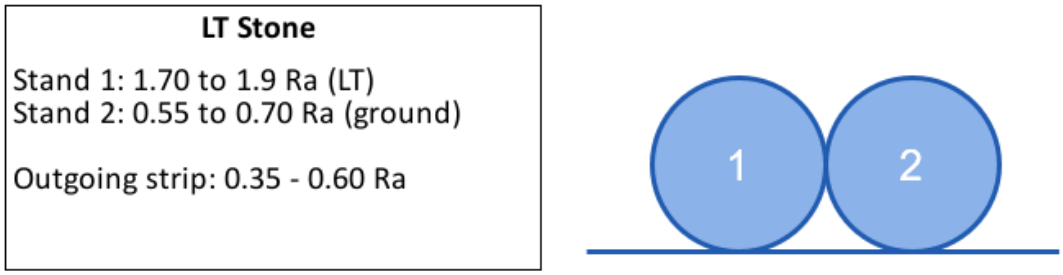

Figure 7.28: Simulation of novel surface textures, using a laser texture roll in Stand 1 of the temper mill.

Equation 7.6 defines a crater shaped unit event. The slopes of the sides of this crater can be controlled by fixing depth and varying radius. For the same depth event but larger radius, the surface slopes would be shallower. This is shown in Figure 7.29. The aim with these surfaces is to disrupt the image forming properties of surface. Smaller radii, therefore steeper slopes, should disrupt image more, i.e scatter light more, giving a relatively lower gloss finish.

For these surfaces, the crater depth was set such that accumulation of events would result in surfaces which have Ra within the specification of one of Tata Steel's products. The events were distributed randomly across the surface. The retention ratio of material in the rim was set at 0.6. This assumption is based on the fact that the majority

of surface material is not vaporised but melted and relocated to the event rim.

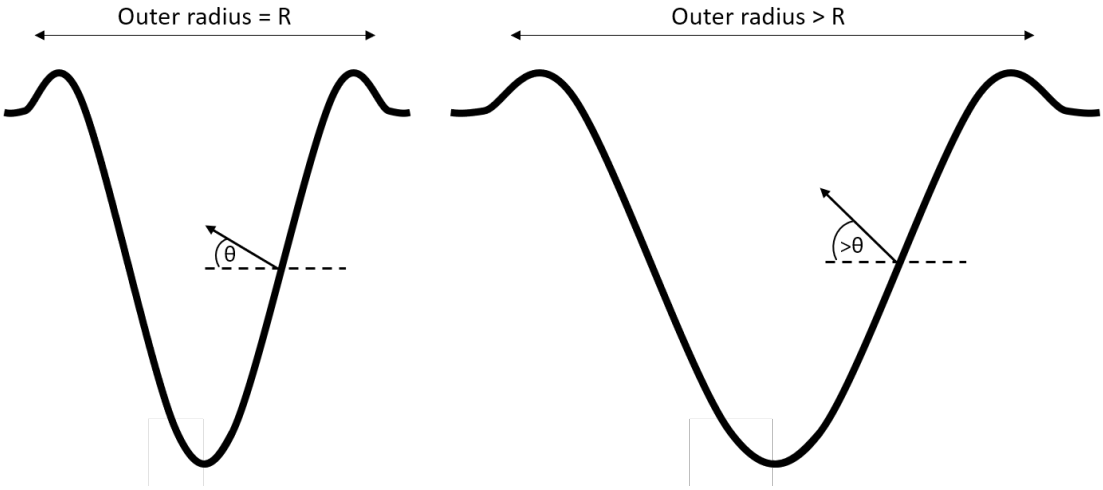

(a)

Figure 7.29: Controlling the slope of crater sides by varying the radius at fixed depth. Note that for illustrative purposes this figure is not to scale. Crater depth is much less than crater radius in reality.

7.4 Results

Three surfaces were generated using the model with parameters described above, using three event radii. These are shown in Figure 7.31. The dimensions of the events are listed in Table 7.3.

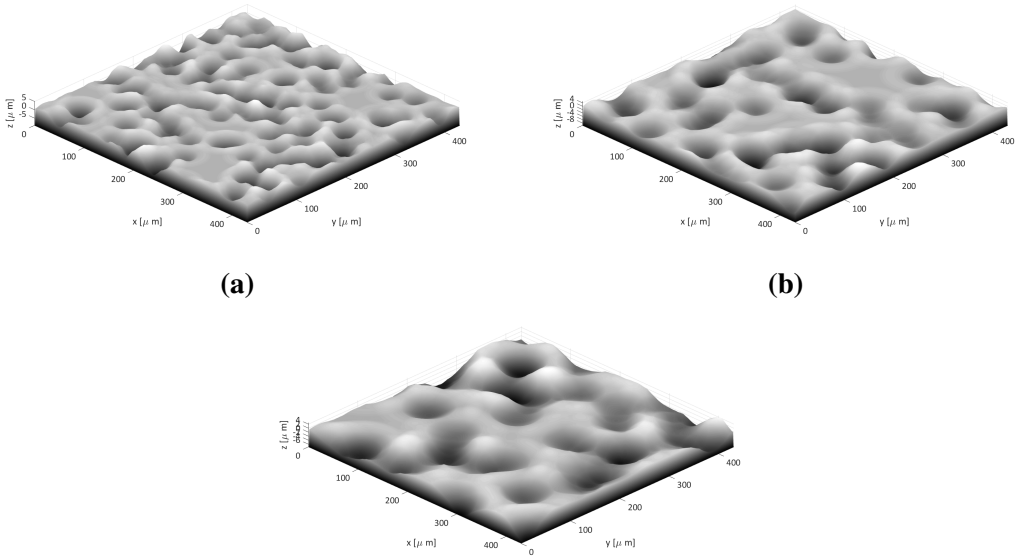

(a) **(b)**

(c)

Figure 7.30: Roll surfaces generated using three event radii, while maintaining a fixed depth, in order to control the surface slopes.

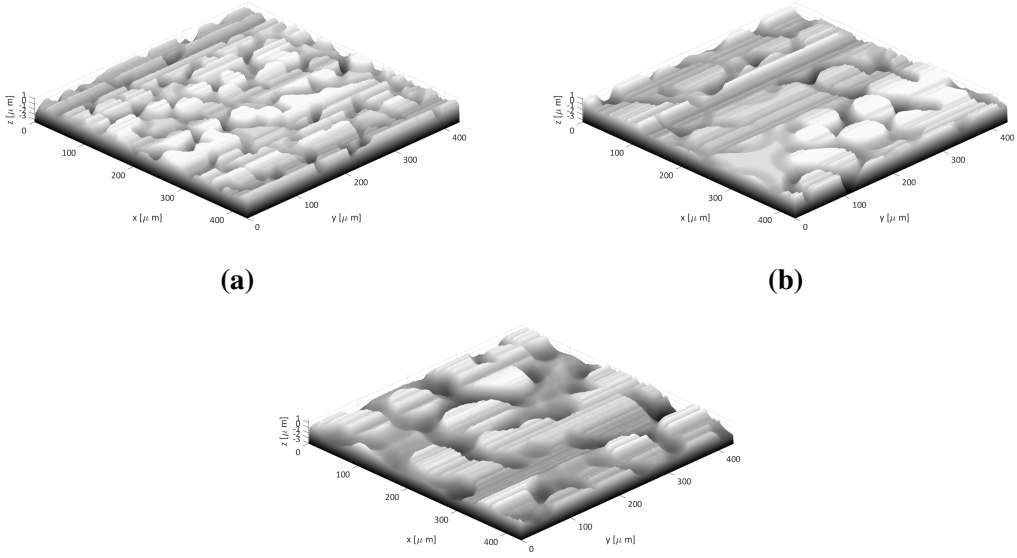

(a) **(b)**

(c)

Figure 7.31: Strip surfaces generated using three event radii, while maintaining a fixed depth, in order to control the surface slopes.

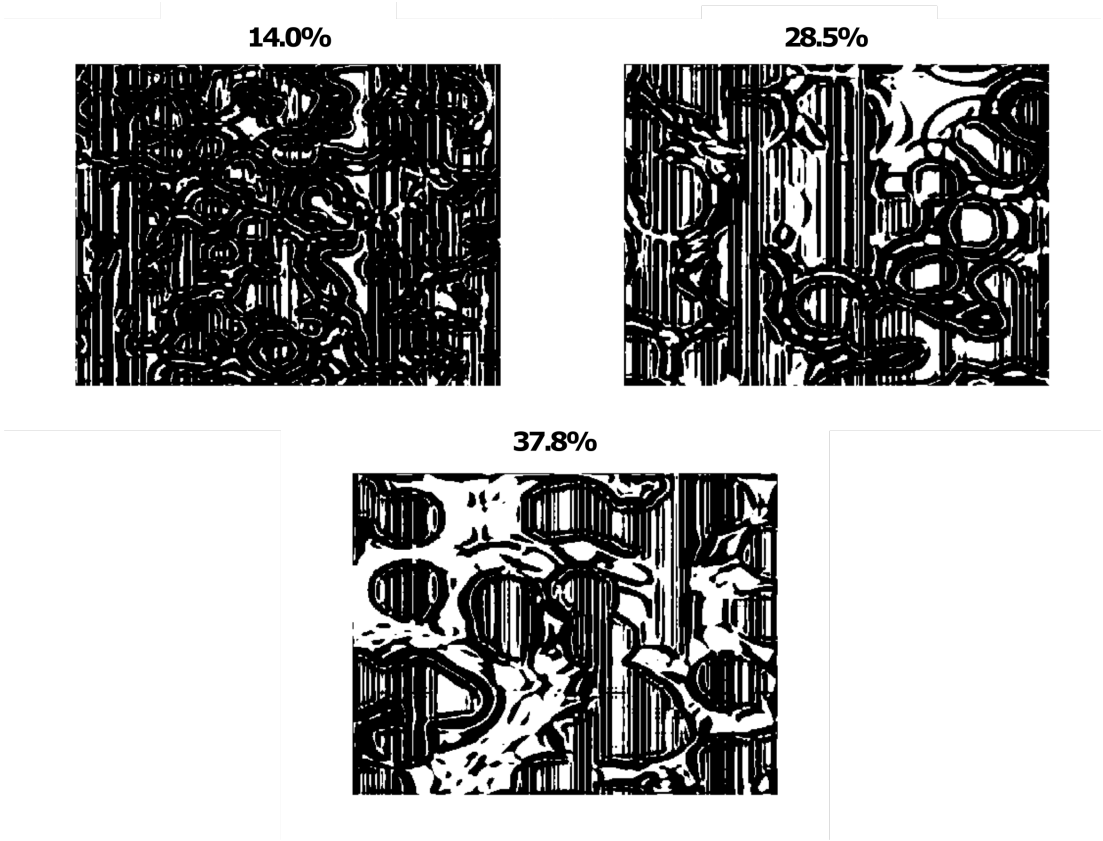

Figure 7.32: Simulated surfaces showing differing proportion of surface facets reflecting into the gloss receptor angle, after filtering at $25 \pm 10\mu\mathrm{m}$, with the surfaces maintaining an average roughness within specification.

Table 7.3: Values for the novel surface textures shown in Figure 7.32.

Event inner radius	**Surface Sa [μm]**	**Active area [%]**
20	0.59	14
30	0.56	29
40	0.64	38

In Chapter 6.1, it was shown that the proportion of the surface reflecting into the gloss receptor angle is strongly correlated with gloss. Therefore, Figure 7.32 shows that the simulated surface substrates would have clearly discernable differences in visual appearance. The features are large enough not to be totally obscured by surface coating. The slopes of the underlying substrate will influence the slopes of the coated surface, in turn influencing the visual appearance.

7.5 Non-conventional surface designs

Up to now, surfaces have been designed staying within the constraints of current standards and operating procedures. However, laser texturing provides several capabilities that enable movement outside the limited space of surfaces able to be realised with conventional processes. These capabilities include:

- The ability to accurately target event placement for the creation of deterministic structures.
- The ability to texture the strip directly.

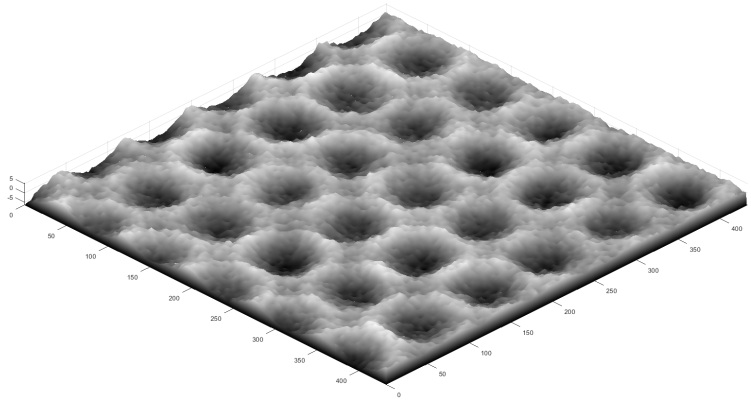

Figure 7.33: Simulated surface showing the possibilities to model regularly distributed events.

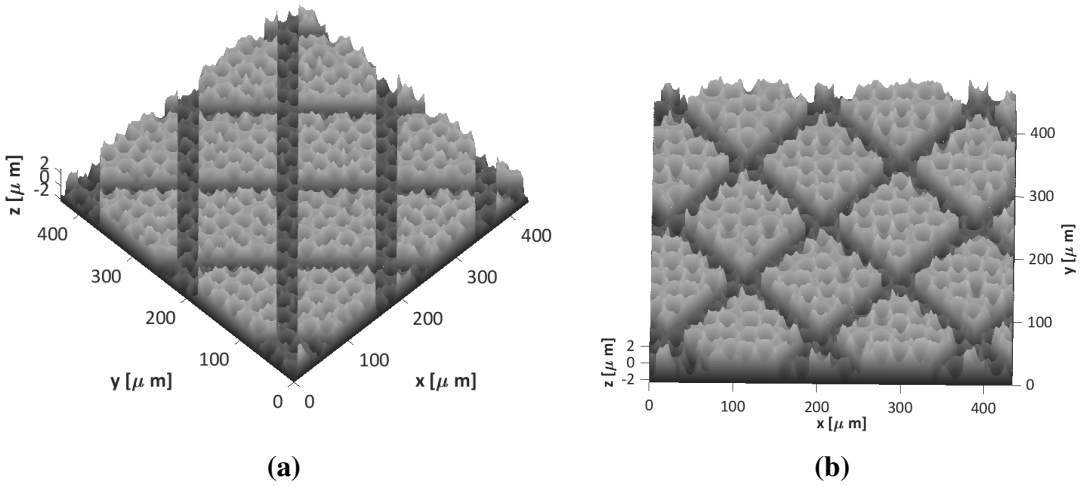

(a) **(b)**

Figure 7.34: Novel surface designs, using a combination of deliberate placement of unit events and texturing directly onto the strip.

Figure 7.33 shows the capabilities of the surface texturing model to generate regularly distributed events. Figure 7.34 shows a simulated surface created by utilising the advanced capabilities of laser texturing. The surface is created in a two stage process. The first stage is the laser texturing of work rolls to create a pattern of square depressions in the surface, separated by raised channels. When pressed into the strip, this would result in square protrusions, separated by sunken channels. The width of these squares and channels could be optimised to provide the optimal bearing area of the surface, thereby optimising the formation of alloy layer close to the surface after reflow of the tin layer. This would in turn provide optimal scratch resistivity of the coated surface. The second stage is laser texturing of the strip directly, to give a secondary texture of a grid of small craters, overlaid on the square protrusions. The slopes of these craters could be controlled to give the desired appearance properties of the strip. One of the major influences on variation in visual appearance is the wear of work rolls. The ability to texture the strip directly would mitigate this effect and allow for the production of a more consistent surface finish.

7.6 Conclusions

- A model of the grinding texturing process was implemented.
- The grinding model was developed to provide multi-scale simulations of surface texture.

- A model of the EDT process was also developed to provide multi-scale simulations of surface texture.
- These models were used to simulate surface finishes created by the packaging steel manufacturing process.
- The visual appearance of these surfaces was modelled using the active area approach.
- The active area of simulated fine stone finishes was over-predicted by 7.8%.
- The active area of simulated stone finishes was over-predicted by only 2.1%.
- A series of surface textures were designed, that offer enhanced control over the visual appearance of packaging steel.
- A model of visual appearance, developed in Chapter 6, was used to demonstrate the effectiveness of the surface texture designs.

Chapter 8

Conclusions and Discussion

8.1 Conclusions

In this section, the conclusions of the previous chapters are collated for reference. In the following section, these conclusions are discussed and placed in context.

8.1.1 Chapter 4 - Substrate

A standard analysis of the surface texture of packaging steel substrates showed that:

- There is a coupling between the amplitude of surface roughness and the rms slope parameter for all surfaces.
- Across the length of the roll campaign, the deviation of mean roughness amplitude Ra remains within the 0.25 μm window determined by the product specification.
- However, analysis of the same sample set showed a large deviation in the Sdq parameter across the same range.
- The wear processes involved in surface rolling have a significant effect on surface texture, both across the strip and along the length of the roll campaign.

Multi-scale analysis of the surface texture of packaging steel substrates showed that:

- Most surface finishes have a characteristic wavelength around 40μm.
- For Sample Set 1, all finishes show a region of low amplitude but high variation in the the highest frequency bands.
- Analysis of Sample Set 2 also showed a characteristic wavelength around 40 μm, however the prominence of the material at this wavelength reduces over the length of the roll campaign.
- The high frequency band of low amplitude but high variation is the band most heavily affected by the wear process.
- Measurements of the visual appearance of Sample Set 2 revealed that the visual appearance change over the course of a roll campaign, with specular gloss doubling after 20 coils.

- Specular gloss is strongly correlated with Sdq, with $R^2 = 0.86$ for gloss at $20°$ and $R^2 = 0.87$ for RSpec.
- When this analysis was expanded to a multi-scale analysis, the correlation strength between Sdq and gloss at $20°$ increased to $R^2 = 0.91$, at a wavelength band of $3 \pm 1\mu m$.
- At the same spatial wavelength band, the correlation strength between gloss at $20°$ and Sa increased from 0.56 to 0.88.
- The wear process causes variations in surface slopes at the smallest of scales, which causes the change in visual appearance of the packaging steel substrate.

8.1.2 Chapter 5 - Coating

- The modification of the surface texture of packaging steel by a tin coating process has been quantified across multiple scales.
- The functional bands of surface texture, at scales $< 30\mu m$, with low amplitude but high variation in surface slope, are most heavily attenuated by the surface coating.
- The application of tin coating to packaging steel substrate reduces the amplitude and flattens the slopes of short wavelength surface content.
- For 2.8 gsm the minimum attenuation is at different wavelengths for different finishes, varying from $24.5\mu m$ to $54\mu m$ for anisotropic finishes - this quantifies the scale at which surface features retain prominence through the coating layer.
- These occur at wavelengths much lower than those quantified by the waviness parameter, therefore controlling the waviness parameter would not aid in controlling the visual appearance of tinplate packaging steel.

8.1.3 Chapter 6 - Function

- A model of visual appearance of surfaces was developed, using a microfacet modelling approach.

- The model is unable to provide precise predictions of visual appearance parameters such as gloss and haze, due to a lack of information about the methods by which those parameters are measured.

- The active area, which is the proportion of the surface that reflects light into the gloss receptor angle, was investigated as a potential predictor of visual appearance.

- The active area of surfaces at two different scales was compared. The first scale was the scale of strongest correlation and the other was the scale at which surface features will retain prominence through the coating layer.

- The active area at scales which remain visible through the coating is a good predictor of visual appearance, as measured by the specular gloss at 20°. The strength of the correlation between these two parameters is $R^2 = 0.91$ for Sample Set 2.

8.1.4 Chapter 7 - Design

- A model of the grinding texturing process was implemented.

- The grinding model was developed to provide multi-scale simulations of surface texture.

- A model of the EDT process was also developed to provide multi-scale simulations of surface texture.

- These models were used to simulate surface finishes created by the packaging steel manufacturing process.

- The visual appearance of these surfaces was modelled using the active area approach.

- The active area of simulated fine stone finishes was over-predicted by 7.8%.

- The active area of simulated stone finishes was over-predicted by only 2.1%.

- A series of surface textures were designed, that offer enhanced control over the visual appearance of packaging steel.

- A model of visual appearance, developed in Chapter 6, was used to demonstrate the effectiveness of the surface texture designs.

8.2 Discussion

In Chapter 1, the work of this thesis was set in the larger context of some general trends in the packaging steel industry. These are:

1. The increasing value (and competitiveness) of markets for which visual appearance is a critical function.

2. The increasing scrutiny given by customers of packaging steel to the visual appearance of their products.

In order to remain competitive and meet customer needs, manufacturers of packaging steel need to increase their understanding of and control over the visual appearance of their products. It is helpful to reconsider Figure 8.1, as the work of this thesis aimed at elucidating the two relationships between the three domains represented in the diagram.

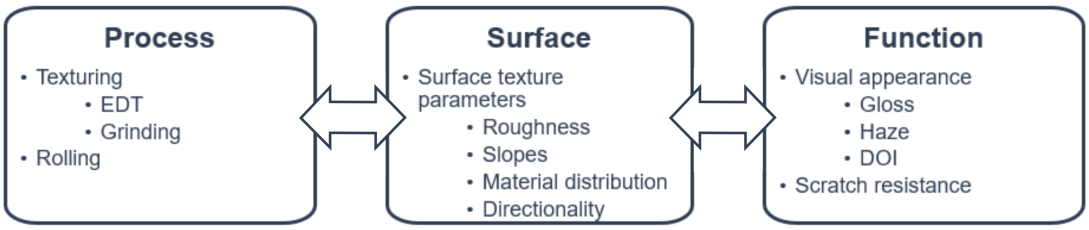

Figure 8.1: The three domains considered in this thesis, and the relationships between them.

These considerations gave rise to a set of overarching aims that guided the work of this thesis. These aims were:

- Determine the relationship between the manufacturing process and surface texture of packaging steel.

- Determine the relationship between surface texture and visual appearance of packaging steel.

- Utilise discovered relationships to develop methods of controlling visual appearance of packaging steel.

In this section, the work of this thesis is again discussed in the light of this larger context. The conclusions presented earlier are assessed against these aims to determine the extent to which they have been fulfilled. From these discussions, suggestions are made as to how the work of this thesis could be further developed.

8.2.1 Process to texture

The relationship between the manufacturing process and the surface texture has been described using models of the texturing processes that create the surface texture of packaging steel. Models for the grinding and EDT processes, the two most widely used texturing processes in the packaging steel industry, were implemented off of the basis of the work of others. The model of ground surface was taken from the work of Salisbury et al. and the EDT model was taken from the work of Wentink et al.. It has been shown throughout this thesis that when investigating the functionality of surface texture it is critical to consider the multi-scale nature of surfaces. Surfaces are multi-scale because the processes that create them operate across a broad range of spatial wavelengths. Therefore, these two models were further developed to account for the multi-scale properties of surfaces, resulting in the ability to simulate surface textures that closely resembled measured surfaces across the spatial spectrum. The EDT model was also used to model laser texturing process, under the assumption that the unit events for each process are similar. This enabled the design of surface textures with enhanced control over visual appearance. Although the literature on laser texturing is growing, there still appears to be space for a description of the laser texturing process using the unit event approach.

The multi-scale modelled processes were matched to real surfaces, however they were not linked empirically or analytically with the process parameters of the grinding or EDT processes. Prior to the work described in this thesis, there was no in-depth description of the creation of surface textures in the packaging steel manufacturing process. The work described in this thesis has made it possible to accurately simulate surface texture of products manufactured in the packaging steel industry, however, there is still work to be done on linking the simulated surfaces to process parameters. These simulated surfaces were used to make predictions about the visual appearance of packaging steel products, however there is the potential to use the surface texture models in combination with other models of texture-dependent functions such as fric-

tion, wear, lubrication, wetting, adhesion and surface transfer phenomena. The work described in this thesis has also generated knowledge in the field of steel packaging, more specifically knowledge of the relationship between texture and appearance at specific wavelength scales, as well as the way in which those scales are modified by the addition of a coating.

8.2.2 Texture to function

The relationship between the surface texture and the visual appearance of packaging steel has been investigated and described using the techniques of multi-scale surface analysis. Prior to the work carried out in this thesis, there were large gaps in the knowledge of this relationship due to the lack of appropriate surface metrology as described by the work of Muralikrishnan in Chapter 2. This gap was filled by again taking into account the multi-scale nature of surfaces, for both substrate and coated surfaces.

For uncoated substrate, measurements were made of surface function and correlated against measurements of surface texture decomposed across surface scale to determine the functional bandwidths of surface texture. It was found that variations of surface slopes in the short-wavelength bands of surface texture were strongly correlated with variation in visual appearance parameters. A multi-scale analysis of coated surfaces quantified the amount by which these variations in surface slopes in the short-wavelength bands are attenuated by the addition of a tin coating. Visual appearance was modelled using the slopes of surface texture at the appropriate scales and used to design surface textures which give enhanced control over visual appearance.

Modelling the visual appearance of packaging steel could be developed further on two fronts. First, the BRDF model could be developed by the integration of the Fresnel term and the masking-shadowing function into the prediction of the BRDF. This would give a more realistic model of surface/light interaction, allowing for modelling of surface chemistry as well as surface topography. Second, increased knowledge of gloss measurement systems is needed. The predictions of visual appearance were handicapped by the lack of knowledge about the operation of the glossmeter. Predictions could be improved by determining more accurately the methods of light detection and parameter calculation used by glossmeters. This would enable predictions of visual appearance parameters directly from substrate textures, instead of relying on the in-

termediary parameter of surface slopes. Better predictions of visual appearance of surfaces would support the development of functional surfaces. The standardisation of gloss measurement may need to be improved as a prerequisite to the development of modelling of surface gloss.

To summarise, this work has made known what surface parameters, at what scale, must be controlled in order to control the visual appearance of packaging steel. This enabled the development of functional surfaces, currently being trialled by a manufacturer of packaging steels.

8.3 Future work

The above discussion has described the achievements of the work presented in this thesis as well as areas into which the work could be further developed. Laser texturing holds great potential as a surface texturing process to enable greater control over surface function. For this reason it should be thoroughly investigated for its potential applications in the steel packaging industry. A possible program for further work would be as follows:

- Develop multi-scale model of surface function.
  - Measure surface texture.
  - Measure surface function.
  - Decompose surface texture across multiple scales.
  - Correlate function with texture at each scale to determine functional bandwidths of surface texture.
- Develop model of surface texture.
  - Full multi-scale characterisation of the laser texturing unit event.
    - Measure topography of single events.
    - Measure topography of interacting events.
  - Develop multi-scale model of the unit event.
    - Separate overall process into multiple processes, each affecting different bands of spatial frequencies.

  - Simulate novel surfaces using different distributions and dimensions of unit events.

- Assess surface function of simulated surfaces using surface function model.

This process could be carried out to develop surfaces which fulfil the specific needs of certain customers. For example, surface adhesive, tribological, damage resistive properties could be optimised depending on the end product of the material. Adhesive properties could be optimised if surface coating is crucial, tribological properties could be optimised if can forming takes precedence and damage resistivity could be optimised if product longevity is critical.

In addition to the above, there are opportunities to develop the metrology of industrial surfaces. The considerations of the multi-scale nature of surfaces and the necessity of multi-scale analyses mean that the Sdq parameter is inherently flawed. A fuller description of the flaws of the Sdq parameter is given in Section 4.2. In this thesis, filtering was used to overcome this limitation of the Sdq parameter. However, a downsampling method of calculating surface slopes would give the ability to tune the scale of the Sdq parameter, without requiring filtering the surface thereby avoiding the manipulation of surface data that occurs with filtering. Such a parameter would have several advantages over the filtering method. During the work carried out in this thesis, such a parameter was developed, however due to some inherent mathematical difficulties, the work was not completed. However, there is still the opportunity for such a parameter to be developed, and a simple, easily understood and easily implemented parameter could aid in the utilisation of slope-scale analysis in industry, and overcome some of the limiting factors discovered by Muralikrishnan. This could lead to the discovery of functional correlations between surface slopes and surface functions that have up to now been obscured by the lack of scale-sensitivity of the parameter.

8.4 Summary

Overall, the work presented in this thesis brings together empirical analysis and computer modelling to characterise packaging steel products from the manufacturing process, through substrate and coating, to function. The work has resulted in the ability to model surface texture and predict the visual appearance of packaging steel, resulting in surface designs offering enhanced control over visual appearance. The two rela-

tionships shown in Figure 8.1 have been described and suggestions have been made as to how these descriptions could be further developed. The work done was specific to the packaging steel industry and limited to the surface function of visual appearance, however the approach taken could be generalised to other industries and other surface functions. The work provides a pathway for the discovery of functional bandwidths of surface texture, and the design of surface textures which offer enhanced control over those surface functionalities. This process is shown in Figure 8.2. A similar process could be carried out to design substrate textures for other surface functions, to develop differentiated products for high value markets. A range of surface finishes could be developed each with a different functionality for a specific market.

The work also provides a method for securing intellectual property rights over surface designs for differentiated products in specific industries. It is not possible to secure protection over any surface design in general, however it is possible to secure protection if it can be shown that the surface design fulfils a certain function in a specific industry. The roadmap from process to function provides this justification. The work described in this thesis, if generalised, will allow for the creation, and protection, of value-added products for packaging steel manufacturers.

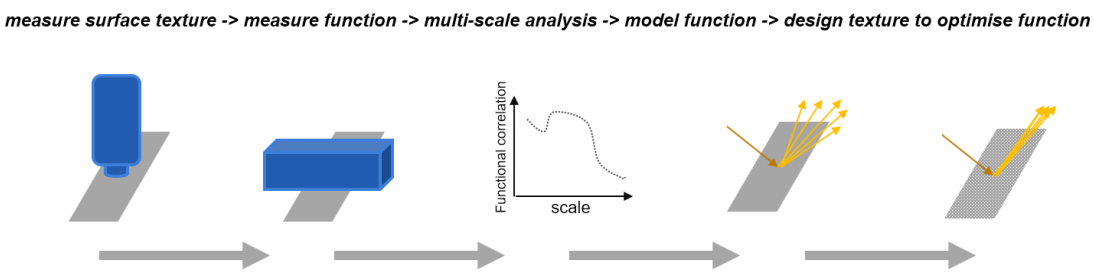

Figure 8.2: A pathway from substrate texture to function for high value, differentiated products.

Bibliography

[1] R. W. Fleming, "Visual perception of materials and their properties.," *Vision research*, vol. 94, pp. 62–75, jan 2014.

[2] Bloomberg, "China's Lethal Milk Scandal Revereberates a Decade Later." `https://www.dairyherd.com/article/chinas-lethal-milk-scandal-reverberates-decade-later`, 2015. Accessed: 10-09-2020.

[3] E. G. Piwoz and S. L. Huffman, "The Impact of Marketing of Breast-Milk Substitutes on WHO-Recommended Breastfeeding Practices," no. August 2015, 2016.

[4] D. J. Whitehouse, *Handbook of surface and nanometrology*. IOP Publishing, 2003.

[5] R. Leach, "Characterisation of areal surface texture," *Characterisation of Areal Surface Texture*, vol. 9783642364, pp. 1–353, 2013.

[6] D. J. Whitehouse, "Surfaces and their Measurement," 2002.

[7] C. A. Brown, H. N. Hansen, X. J. Jiang, F. Blateyron, J. Berglund, N. Senin, T. Bartkowiak, B. Dixon, G. Le Goïc, Y. Quinsat, W. J. Stemp, M. K. Thompson, P. S. Ungar, and E. H. Zahouani, "Multiscale analyses and characterizations of surface topographies," *CIRP Annals*, 2018.

[8] H. Davies, "Reflection of electromagnetic waves from a rough surface," *Journal of Applied Physics*, 1954.

[9] H. Bennett and J. Porteus, "Relation between surface roughness and specular reflection at normal incidence," 1961.

[10] D. J. Whitehouse, "A philosophy of linking manufacture to function— an example in optics," *Proceedings of the Institution of Mechanical Engineers, Part B: Journal of Engineering Manufacture*, vol. 207, no. 1, pp. 31–42, 1993.

[11] M. Shipulski and C. Brown, "A Scale-based model of reflectivity," 1994.

[12] H. Li, K. E. Torrance, C. Graphics, and R. Hall, "An experimental study of the correlation between surface roughness and light scattering for rough metallic surfaces," vol. 5878, pp. 1–15, 2005.

[13] B. Linke and J. Das, "Aesthetics and Gloss of Ground Surfaces: A Review on Measurement and Generation," *Journal of Manufacturing Science and Engineering*, vol. 138, no. 6, p. 064501, 2016.

[14] BS EN 10202, "BSI Standards Publication Cold reduced tinmill products," 2015.

[15] I. O. P. C. Series and M. Science, "How to Select the most Relevant Roughness Parameters of a Surface : Methodology Research Strategy How to Select the most Relevant Roughness Parameters of a Surface : Methodology Research Strategy," 2018.

[16] G. T. Smith, *Industrial Metrology*. 2002.

[17] Morgan, *Tinplate*.

[18] ITRI, "Guide To Tinplate," no. April, 2009.

[19] D. Llewellyn, "Steels: Metallurgy and Applications," 1992.

[20] J. Simao, D. Aspinwall, M. Wise, and K. Subari, "Surface texture transfer in simul," *Journal of Materials Processing Technology*, vol. 0136, 1996.

[21] J. G. Lenard, "Flat Rolling – A General Discussion," *Primer on Flat Rolling*, pp. 17–35 and 315, 2007.

[22] H. R. Le and M. P. F. Sutcliffe, "Analysis of surface roughness of cold-rolled aluminium foil," *Wear*, vol. 244, no. 1-2, pp. 71–78, 2000.

[23] B. Griffiths, *Manufacturing Surface Technology*. Kogan Page Science, 2001.

[24] W. B. Rowe, "Introduction," *Principles of Modern Grinding Technology*, no. Chapter 7, pp. 1–14, 2014.

[25] A. Darafon, A. Warkentin, and R. Bauer, "International Journal of Machine Tools & Manufacture Characterization of grinding wheel topography using a white chromatic sensor," *International Journal of Machine Tools and Manufacture*, vol. 70, pp. 22–31, 2013.

[26] J. Webster and M. Tricard, "Innovations in abrasive products for precision grinding," *CIRP Annals - Manufacturing Technology*, vol. 53, no. 2, pp. 597–617, 2004.

[27] J. McGeough and H. Rasmussen, "A theoretical model of electrodischarge texturing," *Journal of Materials Processing Technology*, vol. 68, no. 2, pp. 172–178, 1997.

[28] J. Terpák, L. Dorčák, and J. Revaj, "Quality control of the electro-discharge texturing," *Metalurgija*, vol. 49, no. 1, pp. 19–22, 2010.

[29] S.-K. Kim, M.-K. Kim, and E.-C. Jeon, "A study on the characteristics of electro-discharge texturing for temper mill work roll," *KSME International Journal*, vol. 12, no. 1, pp. 153–159, 1998.

[30] G. P. Petropoulos, N. M. Vaxevanidis, and M. Radovanovi, "Morphological - Functional Aspects of Electro-Discharge Machined Surface Textures," vol. 55, pp. 95–103, 2009.

[31] A. V. Gorbunov, V. K. Belov, and D. O. Begletsov, "Texturing of rollers for the production of auto-industry sheet," *Steel in Translation*, vol. 39, no. 8, pp. 696–699, 2009.

[32] D. J. Wentink, D. Matthews, N. M. Appelman, and E. M. Toose, "A generic model for surface texture development , wear and roughness transfer in skin pass rolling," *Wear*, vol. 328-329, pp. 167–176, 2015.

[33] F. Clarysse and M. Vermeulen, "Aesthetic surfaces created with the Electron Beam texturing technology," no. 1.

[34] Z. T. Wang and M. J. Yang, *Laser-guided discharge surface texturing*. Elsevier Ltd., 2014.

[35] R. Bünten, K. Steinhoff, W. Rasp, R. Kopp, and O. Pawelski, "Development of a FEM-model for the simulation of the transfer of surface structure in cold-rolling processes," *Journal of Materials Processing Technology*, vol. 60, no. 1-4, pp. 369–376, 1996.

[36] H. Kijima, "Influence of roll radius on roughness transfer in skin-pass rolling of steel strip," *Journal of Materials Processing Technology*, vol. 214, no. 5, pp. 1111–1119, 2014.

[37] C. Wu, L. Zhang, P. Qu, S. Li, and Z. Jiang, "A simple approach for analysing the surface texture transfer in cold rolling of metal strips," *International Journal of Advanced Manufacturing Technology*, vol. 95, no. 1-4, pp. 597–608, 2018.

[38] B. Çolak and N. Kurgan, "An experimental investigation into roughness transfer in skin-pass rolling of steel strips," *International Journal of Advanced Manufacturing Technology*, vol. 96, no. 9-12, pp. 3321–3330, 2018.

[39] F. Plouraboué and M. Boehm, "Multi-scale roughness transfer in cold metal rolling," *Tribology International*, vol. 32, no. 1, pp. 45–57, 1999.

[40] H. Kijima and N. Bay, "Skin-pass rolling I-Studies on roughness transfer and elongation under pure normal loading," *International Journal of Machine Tools and Manufacture*, vol. 48, no. 12-13, pp. 1313–1317, 2008.

[41] H. Kijima and N. Bay, "Skin-pass rolling II-Studies of roughness transfer under combined normal and tangential loading," *International Journal of Machine Tools and Manufacture*, vol. 48, no. 12-13, pp. 1308–1312, 2008.

[42] H. Kijima, "Influence of roll radius on contact condition and material deformation in skin-pass rolling of steel strip," *Journal of Materials Processing Technology*, vol. 213, no. 10, pp. 1764–1771, 2013.

[43] K. Hilgenberg and K. Steinhoff, "Texturing of skin-pass rolls by pulsed laser dispersing," *Journal of Materials Processing Technology*, vol. 225, pp. 84–92, 2015.

[44] M. Aarnts, J. Miedema, A. Wise, B. Vos, D. V. Eerden, E. Jasperse, J. Duizer, M. Litz, D. Matthews, H. V. D. Weijde, and J. Collingham, "Effect of substrate roughness on tin layer performance after reflow Surface investigation on the so

called Roughness Matrix – TSP IJW trial P0514 Reference Source number : Project number : Date of issue : Security Code : 30 October 2015 Author (s): Joos," 2015.

[45] J. Landskroon, "Tin gloss and roughness," *Ref Source 109053*, 2003.

[46] Y. Luo, "Design of A Paint Simulation and Visualization Tool for Automotive Surfaces,"

[47] R. Leach, A. Weckenmann, J. Coupland, and W. Hartmann, "Interpreting the probe-surface interaction of surface measuring instruments, or what is a surface?," *Surface Topography: Metrology and Properties*, vol. 2, no. 3, 2014.

[48] B. Muralikrishnan, "Advanced Surface Texture Analysis for Process Diagnostics and Functional Correlation," 2003.

[49] G. Le Goic, C. A. Brown, H. Favreliere, S. Samper, and F. Formosa, "Outlier filtering: A new method for improving the quality of surface measurements," *Measurement Science and Technology*, vol. 24, no. 1, 2013.

[50] I. O. for Standardization, *ISO 16610-31 Geometrical Product Specifications (GPS)— Filtration, Part 31: Robust profile filters: Gaussian regression filters*. International Organization for Standardization.

[51] B. Muralikrishnan and J. Raja, "Gaussian Regression Filters," *Computational Surface and Roundness Metrology*, pp. 67–76, 2009.

[52] J. Berglund, C. A. Brown, B. G. Rosén, and N. Bay, "Milled die steel surface roughness correlation with steel sheet friction," *CIRP Annals - Manufacturing Technology*, vol. 59, no. 1, pp. 577–580, 2010.

[53] G. Le Goïc, M. Bigerelle, S. Samper, H. Favrelière, and M. Pillet, "Multiscale roughness analysis of engineering surfaces: A comparison of methods for the investigation of functional correlations," *Mechanical Systems and Signal Processing*, vol. 66-67, pp. 437–457, 2015.

[54] C. Xia, X. Zhang, J. Zhang, H. Li, and S. Jia, "Evolution on Topography of Textured Work Rolls and Steel Strips during Cold Rolling and Temper Rolling," *Steel Research International*, vol. 88, no. 9, pp. 1–9, 2017.

[55] N. Nagase, S. Shido, and I. Yarita, "The Effect of Lubricant on Microwear of Dull Rolls in Temper Rolling by 4 Hi Rolling Mill," *ISIJ International*, vol. 49, no. 6, pp. 874–880, 2009.

[56] S. Manuel and O. Tavares, "Analysis of surface roughness and models of mechanical contacts," 2005.

[57] E. Sidick, "Power Spectral Density Specification and Analysis of Large Optical Surfaces," *Modeling Aspects in Optical Metrology II, Proc. SPIE*, vol. 7390, p. 73900L, 2009.

[58] B. Ma, A. K. Tieu, C. Lu, and Z. Jiang, "An experimental investigation of steel surface characteristic transfer by cold rolling," *Journal of Materials Processing Technology*, vol. 125-126, pp. 657–663, 2002.

[59] T. D. B. Jacobs, T. Junge, and L. Pastewka, "Quantitative characterization of surface topography using spectral analysis," *arXiv*, p. 1607.03040, 2016.

[60] E. L. Church, "Surface Scattering," *Chapter 7*, pp. 10–16, 1996.

[61] H. Li, "A study on wear and surface roughness of work roll in cold rolling," 2008.

[62] F. Ticconi, L. Pulvirenti, and N. Pierdicca, "Models for scattering from rough surfaces," *Electromagnetic Waves*, 2011.

[63] A. C. Chadwick and R. W. Kentridge, "The perception of gloss : A review," *Vision Research*, vol. 109, pp. 221–235, 2015.

[64] P. J. Marlow, J. Kim, and B. L. Anderson, "The perception and misperception of specular surface reflectance," *Current Biology*, vol. 22, no. 20, pp. 1909–1913, 2012.

[65] R. W. Fleming, "Human perception: Visual heuristics in the perception of glossiness," *Current Biology*, vol. 22, no. 20, pp. R865–R866, 2012.

[66] N. Frankhuizen, "What is the level of confidence in measuring gloss?." `https://www.pcimag.com/articles/100528-what-is-the-level-of-confidence-in-measuring-gloss`, 2015. Accessed: 14-10-2019.

[67] F. B. Leloup, G. Obein, M. R. Pointer, and P. Hanselaer, "Toward the soft metrology of surface gloss: A review," *Color Research and Application*, vol. 39, no. 6, pp. 559–570, 2014.

[68] D. Solutions, "Operating Instructions Rhopoint IQ," *Power*.

[69] G. Obein, T. Leroux, and F. Viénot, "Bi-directional Reflectance Distribution Factor and Gloss Scales," vol. 4299, no. 2, pp. 279–290, 2001.

[70] F. Leloup, P. Hanselaer, and S. Forment, "BRDF and gloss measurements," *CIE Expert Symposium on . . .*, pp. 1–6, 2007.

[71] Z. Dong, B. Walter, S. Marschner, and D. P. Greenberg, "Predicting Appearance from Measured Microgeometry of Metal Surfaces," *Siggraph*, vol. 1, no. 212, pp. 1–12, 2014.

[72] M. Bigerelle, J. Marteau, and C. Paulin, "Brightness versus roughness: a multiscale approach," *Surface Topography: Metrology and Properties*, 2015.

[73] T. Bartkowiak, J. Berglund, and C. A. Brown, "Establishing functional correlations between multiscale areal curvatures and coefficients of friction for machined surfaces," *Surface Topography: Metrology and Properties*, vol. 6, no. 3, 2018.

[74] H. S. Ho, M. Bigerelle, R. Vincent, and R. Deltomb, "Correlation modeling between process condition of sandblasting and surface texture: A multi-scale approach," *Scanning*, vol. 38, no. 3, pp. 191–201, 2016.

[75] Y. Yang and R. O. Buckius, "Surface length scale contributions to the directional and hemispherical emissivity and reflectivity," *Journal of Thermophysics and Heat Transfer*, vol. 9, no. 4, pp. 653–659, 2008.

[76] K. Vessot, P. Messier, J. M. Hyde, and C. A. Brown, "Correlation between gloss reflectance and surface texture in photographic paper," *Scanning*, vol. 37, no. 3, pp. 204–217, 2015.

[77] S. Mezghani, H. Zahouani, and J. Piezanowski, "Multiscale characterizations of painted surface appearance by continuous wavelet transform," *Journal of Materials Processing Tech.*, vol. 211, no. 2, pp. 205–211, 2011.

[78] J. Berglund, C. Agunwamba, B. Powers, C. A. Brown, and B. G. Rosén, "On discovering relevant scales in surface roughness measurement-an evaluation of a band-pass method," *Scanning*, vol. 32, no. 4, pp. 244–249, 2010.

[79] D. J. Whitehouse, D. K. Bowen, V. C. Venkatesh, P. Lonardo, and C. A. Brown, "Gloss and Surface Topography," *CIRP Annals - Manufacturing Technology*, vol. 43, no. 2, pp. 541–549, 1994.

[80] K. B. Smith, "A sharper look at gloss," *JOCCA - Surface Coatings International*, vol. 80, no. 12, pp. 573–576, 1997.

[81] P. Beckmann and A. Spizzichino, "The scattering of electromagnetic waves from rough surfaces," *USSR Computational Mathematics and Mathematical Physics*, vol. 4, pp. 247–249, 1964.

[82] E. Heitz, "Understanding the Masking-Shadowing Function in Microfacet-Based BRDFs ppt," *Inria*, vol. 3, no. February, p. 50, 2014.

[83] J. Kumar and M. S. Shunmugam, "A new approach for filtering of surface profiles using morphological operations," *International Journal of Machine Tools and Manufacture*, vol. 46, no. 3-4, pp. 260–270, 2006.

[84] B. Muralikrishnan and J. Raja, "Process diagnostics and functional correlation in surface metrology: Novel techniques, case studies and analysis system development," *Measurement: Journal of the International Measurement Confederation*, vol. 36, no. 2, pp. 175–183, 2004.

[85] X. J. Jiang and D. J. Whitehouse, "Technological shifts in surface metrology," *CIRP Annals - Manufacturing Technology*, vol. 61, no. 2, pp. 815–836, 2012.

[86] S. Lou, X. Jiang, and P. J. Scott, "Application of the morphological alpha shape method to the extraction of topographical features from engineering surfaces," *Measurement: Journal of the International Measurement Confederation*, vol. 46, no. 2, pp. 1002–1008, 2013.

[87] N. Hoffman, A. Martinez, B. Snow, and Y. Gotanda, "Physically-Based Shading Models in Film and Game Production," *Media*, 2010.

[88] B. Walter, Z. Dong, S. Marschner, and D. P. Greenberg, "The Ellipsoid Normal Distribution Function - GOOD FOR SHADOW/MASK," vol. 2014, no. August, 2014.

[89] J. Dupuy, E. Heitz, J. C. Iehl, P. Poulin, and V. Ostromoukhov, "Extracting Microfacet-based BRDF Parameters from Arbitrary Materials with Power Iterations," *Computer Graphics Forum*, vol. 34, no. 4, pp. 21–30, 2015.

[90] M. Ashikmin, S. Premože, and P. Shirley, "A Microfacet-based BRDF Generator," *Proceedings of the 27th annual conference on Computer graphics and interactive techniques*, pp. 65–74, 2000.

[91] M. Ashikhmin and S. Premoze, "Distribution-based brdfs," *University of Utah–Technical Report*, 2007.

[92] E. Heitz, "Understanding the Masking-Shadowing Function in Microfacet-Based BRDFs," vol. 3, no. 2, pp. 48–107, 2014.

[93] B. T. Phong, "Illumination for computer generated pictures," *Communications of the ACM*, vol. 18, no. 6, pp. 311–317, 1975.

[94] J. F. Blinn, "Models of Light Reflection for Computer Synthesized Pictures," *ACM SIGGRAPH Computer Graphics*, vol. 11, no. 2, pp. 192–198, 1977.

[95] R. Cook and K. Torrance, "A Reflectance Model for Computer Graphics," *ACM SIGGRAPH Computer Graphics*, vol. 15, no. 3, pp. 307–316, 1981.

[96] R. Mcwhirter, M. Cavallari, and C. Trevisan, "Pomini digital texturing – pdt ®,"

[97] J. Newland and J. C. Arnold, "Influence of production parameters on surface energy of tinplate," *Ironmaking & Steelmaking*, vol. 36, no. 6, pp. 456–461, 2009.

[98] Y. Z. Hu and K. Tonder, "Simulation of 3-D random rough surface by 2-D digital filter and fourier analysis," *International Journal of Machine Tools and Manufacture*, vol. 32, no. 1-2, pp. 83–90, 1992.

[99] J. J. Wu, "Simulation of rough surfaces with FFT," *Tribology International*, vol. 33, no. 1, pp. 47–58, 2000.

[100] E. Brinksmeier, J. C. Aurich, E. Govekar, C. Heinzel, H. W. Hoffmeister, F. Klocke, J. Peters, R. Rentsch, D. J. Stephenson, E. Uhlmann, K. Weinert, and M. Wittmann, "Advances in modeling and simulation of grinding processes," *CIRP Annals - Manufacturing Technology*, vol. 55, no. 2, pp. 667–696, 2006.

[101] E. J. Salisbury, K. V. Domala, K. S. Moon, M. H. Miller, and J. W. Sutherland, "A Three-Dimensional Model for the Surface Texture in Surface Grinding, Part 1: Surface Generation Model," *Journal of Manufacturing Science and Engineering*, vol. 123, no. 4, p. 576, 2001.

[102] X. Chen, W. Rowe, B. Mills, and D. Allanson, "Analysis and simulation of the grinding process. Part III: Comparison with experiment," *International Journal of Machine Tools and Manufacturing*, vol. 36, no. 8, pp. 897–906, 1996.

[103] T. A. Nguyen and D. L. Butler, "Simulation of surface grinding process, part 2: Interaction of the abrasive grain with the workpiece," *International Journal of Machine Tools and Manufacture*, vol. 45, no. 11, pp. 1329–1336, 2005.

[104] Y. Cao, J. Guan, B. Li, X. Chen, J. Yang, and C. Gan, "Modeling and simulation of grinding surface topography considering wheel vibration," *International Journal of Advanced Manufacturing Technology*, vol. 66, no. 5-8, pp. 937–945, 2013.

[105] X. Chen and W. B. Rowe, "Analysis and simulation of the grinding process. Part I: Generation of the grinding wheel surface," *International Journal of Machine Tools and Manufacture*, vol. 36, no. 8, pp. 871–882, 1996.

[106] E. J. Salisbury, K. V. Domala, K. S. Moon, M. H. Miller, and J. W. Sutherland, "A Three-Dimensional Model for the Surface Texture in Surface Grinding, Part 2: Grinding Wheel Surface Texture Model," *Journal of Manufacturing Science and Engineering*, vol. 123, no. 4, p. 582, 2001.

[107] S. Jithin, U. V. Bhandarkar, and S. S. Joshi, "Analytical Simulation of Random Textures Generated in Electrical Discharge Texturing," *Journal of Manufacturing Science and Engineering*, vol. 139, no. 11, p. 111002, 2017.